DEVELOPMENT OF ECO-FRIENDLY BIO-NANOCOMPOSITES BASED ON POLYCAPROLACTONE, POLY (LACTIC ACID) AND THEIR BLENDS WITH NANOCELLULOSE EXTRACTED FROM *SACCHARUM OFFICINARUM* FOR ADVANCED APPLICATIONS

Mbongeni Ngwenya

Thesis submitted in fulfilment of the requirements for the degree

DOCTOR OF PHILOSOPHY: ENVIRONMENTAL HEALTH

in the

Department of Life Sciences

Faculty of Health and Environmental Sciences

at the

Central University of Technology, Free State

Supervisor: Dr TP Gumede, PhD (Polymer Science)
Co-supervisor: Dr RA Pérez Camargo, PhD (Applied Chemistry and Polymeric Materials)
Co-supervisor: Dr B Motloung, PhD (Chemistry and Polymer Science)

Bloemfontein

September 2025

DECLARATION OF INDEPENDENT WORK

DECLARATION WITH REGARD TO
INDEPENDENT WORK

I, MBONGENI NGWENYA, identity number _____ and student number _____, do hereby declare that this research project submitted to the Central University of Technology, Free State, for the Doctor of Philosophy: Environmental Health, is my own independent work; and complies with the Code of Academic Integrity, as well as other relevant policies, procedures, rules and regulations of the Central University of Technology, Free State; and has not been submitted before to any institution by myself of any other person in fulfilment (or partial fulfilment) of the requirements for the attainment of any qualification.

_____ 26 September 2025

SIGNATURE OF STUDENT DATE

ACKNOWLEDGEMENTS

First and foremost, praise and thanks to God, the Almighty, for His showers of blessings throughout my studies and in completing this research successfully.

I would like to thank my family, friends and colleagues for their support, friendship and guidance throughout this period.

Special thanks must be made to the following people:

My supervisors, Dr TP Gumede, Dr RA Pérez Camargo and Dr B Motloung for their guidance, leadership, kindness and support throughout the course of study. It has been a privilege to be your student.

My loving family, my father (Jabulani Ngwenya), my mother (Solani Ngwenya), and my brothers and sisters. Your love, guidance, support and patience over the years are the reasons I am here today. If it was not for you, I would not have had this opportunity.

ABSTRACT

This thesis presents the development and characterization of biodegradable nanocomposites based on poly(lactic acid) (PLA), poly(ε-caprolactone) (PCL), and their blends reinforced with cellulose nanocrystals (CNCs) extracted from sugarcane bagasse. The research aimed to enhance the structural, thermal, morphological, and biodegradation performance of these polymers, thereby advancing sustainable alternatives to petroleum-based plastics. The work was organized in two parts: effects of CNCs on the individual matrices, i.e., neat PLA and PCL, and on the blended materials, i.e., PLA/PCL.

In the first study, CNCs were incorporated into neat PLA and PCL to investigate their individual responses to reinforcement. The addition of CNCs promoted crystallinity and significantly increased the biodegradation rate of both polymers. 1 wt.% CNCs loading doesn't show any impact on the biodegradation of PLA. 3 wt.% CNCs slightly increased the biodegradation rate of PLA with the weight loss of 8% at day 112, while 5 wt.% CNCs sped up the degradation of PLA and a wight loss 82.2% in the same period, although it reduced thermal stability and disrupted crystal ordering at higher loadings. In contrast, PCL showed minimal thermal changes but exhibited progressively faster biodegradation with increasing CNCs content. PCL/CNCs nanocomposites with 1, 3 and 5wt.% CNCs respectively exhibited a weight loss of 6.3, 12.1 and 36.4% at day 112, while neat PCL exhibited a weight loss of 5.4% at the same time.

In the second study, PLA/PCL blends (70/30 and 30/70 wt.%) were reinforced with CNCs (1, 3, and 5 wt.%) and evaluated for their structure–property relationships. CNCs enhanced crystallinity, interfacial adhesion, and biodegradation. The incorporation of CNCs to PLA/PCL (30/70) increased the biodegradation rate with increasing CNCs content in the composite. The incorporation of CNCs to PLA/PCL (70/30); 1, 3 wt.% CNCs has no impact on the biodegradation, while the incorporation of 5 wt.% CNCs to PLA/PCL (70/30) sped up the biodegradation, achieving 100% mass loss within 112 days, compared to only 0.3% for neat PLA. Thermal stability improved slightly at a 1 wt.% CNCs loading but declined at higher concentrations. Tensile testing confirmed superior strength of neat PLA compared to PCL and PLA/PCL blends, although CNCs-reinforced nanocomposites could not be mechanically tested due to sample brittleness.

The findings show that CNCs derived from agricultural waste can improve the biodegradation and structural performance of PLA, PCL, and their blends. This thesis highlights the potential of sugarcane bagasse-derived CNCs as sustainable reinforcements for biopolymer systems, supporting the development of eco-friendly materials for packaging, biomedical, and other advanced applications.

Keywords: poly(ε-caprolactone) (PCL), poly(lactic acid) (PLA), PLA/PCL blends, cellulose nanocrystals (CNCs), sugarcane bagasse, biodegradable nanocomposites, thermal and structural properties, biodegradation

Central University of Technology, Free State

TABLE OF CONTENTS

Central University of Technology, Free State

LIST OF FIGURES

LIST OF TABLES

LIST OF ABBREVIATIONS AND ACRONYMS

%	Percentage
I_a	Area under amorphous phases
I_c	Area under crystalline peaks
X_{cx}	WAXS crystallinity
ΔH_m	Melting enthalpy
µm	Micrometer
θ	Theater
λ	Wavelength
Å	Angstrom
CaAlg	Calcium alginate
cm	Centimeter
CNCs	Cellulose nanocrystals
CNFs	Cellulose nanofibrils
Cr_2O_3	Chromium(III) oxide
DSC	Differential scanning calorimetry
FTIR	Fourier transform infrared spectroscopy
g	Gram
h	Hour
H_2SO_4	Sulphuric acid
J	Joules
keV	Kiloelectronvolt
kPa	Kilopascal
kV	Kilovolt
L	Long period
M	Molar
µm	Micrometer
MCC	Microcrystalline cellulose
mg	Milligram
mL	Milliliter

mm	Millimeter
MMT	Montmorillonite
MPa	Megapascal
N	Newton
NaOH	Sodium hydroxide
NC	Nanocellulose
nm	Nanometer
O.MMT	Organophilic montmorillonite
^{o}C	Degrees Celsius
PBAT	Poly(butylene adipate-*co*-terephthalate)
PCL	Poly(ε-caprolactone)
P-CNCs	Phosphorylated cellulose nanocrystals
pH	Potential of Hydrogen
PLA	Poly(lactic acid)
q	Scattering vector
q_{max}	Maximum Scattering vector
ROP	Ring-opening polymerization
rpm	Revolutions per minute
rROP	Radical ring-opening polymerization
SAXS	Small angle X-ray scattering
SEM	Scanning electron microscopy
SFNPs	Silk fibroin nanoparticles
TAIC	Triallyl isocyanurate
T_c	Crystallization temperature
T_{cc}	Cold crystallization temperature
TEM	Transmission electron microscopy
TEMPO	2,2,6,6-tetramethylpiperidine-1-oxyl
T_g	Glass transition temperature
TGA	Thermogravimetric analysis
T_m	Melting temperature
T_{max}	Maximum degradation temperature
TOBC	(TEMPO)-oxidized bacterial cellulose

T_{onset}	Onset degradation temperature
V	Volume
v/v	Volume/Volume
w	Weight fraction
WAXS	Wide angle X-ray scattering
$W_{residue}$	Residual weight
$W_{residue}$	Residual weight
wt.%	Weight percentage
X_c	Degree of crystallinity
ʎ	Voiced palatal lateral approximant
α	Alpha
α'	Alpha prime
ΔH_c	Crystallization enthalpy
ΔH_{cc}	Cold crystallization enthalpy
ΔH_m^o	Melting enthalpy of 100% crystalline polymer

Chapter 1

INTRODUCTION

1.1 Background and context

In recent years, the extensive use of synthetic polymers has significantly contributed to environmental pollution. This poses substantial challenges to global sustainability efforts. Traditional petroleum-based plastics, like polyolefins, are non-biodegradable, and they lead to persistent waste disposal problems and high labor costs for environmental cleanup. In response, biodegradable polymers have gained interest as a possible alternative (Abhilash and Thomas, 2017). Biodegradable polymers degrade fully when exposed to microbes such as *bacillus subtilis* and *pseudomonas lipolytica*. They also fully degrade under aerobic (industrial composting, soil, and marine environments or anaerobic (sewage sludge digesters, oxygen-free soil) processes, providing a solution to waste disposal challenges (Abhilash and Thomas, 2017; Chamas et al., 2020; Zeenat et al., 2021). The deterioration can be either spontaneous or under controlled conditions, for instance industrial conditions, of these materials help to maintain environmental stability and prolong landfill life by reducing the volume of waste.

The polyester family is a remarkable class of biodegradable polymers, distinguished by hydrolysable ester linkages that can degrade in alkaline and acidic conditions (Rydz et al., 2015). Among these polymers, poly(ε-caprolactone) (PCL) and poly(lactic acid) (PLA) are potential alternatives due to their desirable properties, including biodegradability and processability (Farah et al., 2016; Jia et al., 2017; Mofokeng et al., 2012). PCL is a semi-crystalline aliphatic polyester that has outstanding processability, low melting point, and exceptional mechanical properties, making it suited for use in tissue engineering and load-bearing tissues (Amokrane et al., 2018; Luyt and Malik, 2018). PLA originates from renewable resources such as sugarcane and maize starch. It is commonly utilized in packaging, textiles, and biomedical applications due to its high strength, stiffness, and melting temperature. However, its low toughness and brittleness restrict its use in applications requiring plastic deformation at greater stress levels (Jia

et al., 2017; Zhang et al., 2022). Blending PLA with more flexible and tough polymers such as PCL can help in overcoming these limitations. This includes combining their respective benefits to achieve enhanced mechanical properties and flexibility.

Despite these advantages, PCL/PLA blends pose severe immiscibility issues. This immiscibility further causes uneven dispersion and poor interfacial interactions, reducing the overall performance of the blend (Shin and Han, 2017; Zhu et al., 2020). To address these issues, the introduction of a third component, such as compatibilizers or organic/inorganic fillers, has been proposed to improve the compatibility and mechanical properties of the blend. Several studies have proved the efficiency of different compatibilizers and fillers in improving the mechanical properties, phase adhesion, and overall performance of PCL/PLA blends (Chen et al., 2023; Kalita et al., 2020; Rao et al., 2019; Rytlewski et al., 2022; Zhu et al., 2020).

Nanocellulose, generated from plant cell walls and agricultural waste, has recently attracted substantial attention as a reinforcing filler in polymer composites without compromising biodegradable properties. It provides distinct mechanical, thermal, and barrier properties, as well as potential for functionalization and surface modification, allowing the production of tailored features for specific applications (Motloung et al., 2020; Salmani et al., 2024). Agricultural plant waste, such as sugar cane bagasse (*Saccharum officinarum*), provides an abundant and low-cost source of nanocellulose, making it an attractive option for sustainable material development.

1.2 Problem statement

Despite the potential of PLA/PCL blends and nanocellulose reinforcement, there are still difficulties in attaining uniform dispersion, enhanced interfacial bonds, and optimal performance. Furthermore, such reinforcement might influence the crystallization behavior of these mixes, resulting in various characteristics. This underlines the importance of studying aspects like thermal behavior, structure, morphology, mechanical capabilities, and biodegradation to better understand how nanocellulose affects these systems.

1.3 Research aim

The aim of this study was to investigate the fabrication, characterization, and performance of PLA, PCL, and PLA/PCL blend nanocomposites reinforced with cellulose nanocrystals extracted from sugar cane bagasse (*Saccharum officinarum*). It focused on thermal, structural, morphological, mechanical and biodegradation properties.

1.4 Research objectives

1. To extract cellulose nanocrystals (CNCs) from South African sugarcane bagasse using alkaline treatment, bleaching, and sulfuric acid hydrolysis.
2. To purify the nanocellulose through centrifugation, dialysis, ultra-sonication, and freeze-drying.
3. To characterize the isolated CNCs in terms of morphology, structure, and thermal analysis using techniques such as scanning electron microscopy, Fourier transform infrared spectroscopy (FTIR), and thermogravimetric analysis (TGA).
4. To prepare neat PLA, neat PCL, PLA/PCL blends, and nanocomposites with varying CNCs content using melt blending.
5. To ensure uniform dispersion of CNCs within the polymer matrices.
6. To investigate the thermal, structural, and morphological properties of neat polymers, blends, and CNCs-reinforced nanocomposites using differential scanning calorimetry (DSC), TGA, SEM, wide-angle X-ray scattering (WAXS), small-angle X-ray scattering (SAXS), and FTIR.
7. To assess the dispersion and integration of CNCs within the polymer matrices.
8. To evaluate the biodegradation behavior of neat polymers, blends, and nanocomposites through soil burial tests.
9. To assess the tensile properties of neat PLA, neat PCL, and PLA/PCL blends.

1.5 Structure of the thesis

Chapter 1: Introduction – This chapter provides the background and context of the study. It highlights the significance of nanocellulose-reinforced biodegradable polymers. It

presents the problem statement, clearly defines the research aim and objectives, and outlines the scope of the study. Additionally, the chapter describes the overall structure of the thesis, guiding the reader through the subsequent chapters.

Chapter 2: Literature review – This section provides a comprehensive review of the fabrication of nanocellulose-reinforced PLA, PCL, and their blends, with particular focus on the potential of CNCs and cellulose nanofibrils (CNFs). It examines nanocellulose extraction methods and surface modification strategies, followed by an overview of processing approaches such as melt blending, solvent casting, and injection molding. Emphasis is placed on how these techniques affect composite morphology, mechanical performance, thermal stability, and biodegradability, thereby highlighting structure–property relationships and their implications for sustainable material development.

Chapter 3: Experimental paper titled *The effect of sugarcane bagasse-derived cellulose nanocrystals on the thermal, structural, morphological, and biodegradation properties of poly(ε-caprolactone) and poly(lactic acid)*. This chapter presents an experimental investigation into the influence of CNCs on neat PCL and PLA. All experimental procedures, including material preparation, nanocrystal incorporation, and characterization methods, are described within the article itself. The study focuses on understanding how the addition of CNCs affects thermal behavior, morphology, structural properties, and biodegradability of polymers.

Chapter 4: Experimental paper titled *Thermal, structural, morphological, and biodegradation properties of poly(ε-caprolactone), poly(lactic acid) nanocomposites reinforced with sugarcane bagasse-derived cellulose nanocrystals*. This chapter extends the experimental work to PLA/PCL blend systems. Similar to Chapter 3, all methodology details are included within the article. The chapter examines the combined effects of CNCs reinforcement on the thermal, structural, morphological, and biodegradation properties of the biodegradable blend nanocomposites.

Chapter 5: Conclusions – This chapter summarizes the key findings and outcomes of the research, emphasizing the contributions made to the field of biodegradable nanocomposites. It also discusses the implications of the results and provides perspectives for future research directions.

References

Abhilash, M. and Thomas, D. (2017) 'Biopolymers for Biocomposites and Chemical Sensor Applications', in *Biopolymer Composites in Electronics*. Elsevier Inc., pp. 405–435. Available at: https://doi.org/10.1016/B978-0-12-809261-3.00015-2.

Amokrane, G., Falentin-Daudré, C., Ramtani, S. and Migonney, V. (2018) 'A Simple Method to Functionalize PCL Surface by Grafting Bioactive Polymers Using UV Irradiation', *IRBM*, 39(4), pp. 268–278. Available at: https://doi.org/10.1016/j.irbm.2018.07.002.

Chamas, A., Moon, H., Zheng, J., Qiu, Y., Tabassum, T., Jang, J.H., Abu-Omar, M., Scott, S.L. and Suh, S. (2020) 'Degradation Rates of Plastics in the Environment', *ACS Sustainable Chemistry and Engineering*, 8(9), pp. 3494–3511. Available at: https://doi.org/10.1021/acssuschemeng.9b06635.

Chen, Y., Lu, T., Li, L., Zhang, H., Wang, H. and Ke, F. (2023) 'Fully biodegradable PLA composite with improved mechanical properties via 3D printing', *Materials Letters*, 331. Available at: https://doi.org/10.1016/j.matlet.2022.133543.

Farah, S., Anderson, D.G. and Langer, R. (2016) 'Physical and mechanical properties of PLA, and their functions in widespread applications — A comprehensive review', *Advanced Drug Delivery Reviews*. Elsevier B.V., pp. 367–392. Available at: https://doi.org/10.1016/j.addr.2016.06.012.

Jia, S., Yu, D., Zhu, Y., Wang, Z., Chen, L. and Fu, L. (2017) 'Morphology, crystallization and thermal behaviors of PLA-based composites: Wonderful effects of hybrid GO/PEG via dynamic impregnating', *Polymers*, 9(10). Available at: https://doi.org/10.3390/polym9100528.

Kalita, N.K., Bhasney, S.M., Mudenur, C., Kalamdhad, A. and Katiyar, V. (2020) 'End-of-life evaluation and biodegradation of Poly(lactic acid) (PLA)/Polycaprolactone (PCL)/Microcrystalline cellulose (MCC) polyblends under composting conditions', *Chemosphere*, 247. Available at: https://doi.org/10.1016/j.chemosphere.2020.125875.

Luyt, A.S. and Malik, S.S. (2018) 'Can biodegradable plastics solve plastic solid waste accumulation?', in *Plastics to Energy: Fuel, Chemicals, and Sustainability Implications*. Elsevier, pp. 403–423. Available at: https://doi.org/10.1016/B978-0-12-813140-4.00016-9.

Mofokeng, J.P., Luyt, A.S., Tábi, T. and Kovács, J. (2012) 'Comparison of injection moulded, natural fibre-reinforced composites with PP and PLA as matrices', *Journal of Thermoplastic Composite Materials*, 25(8), pp. 927–948. Available at: https://doi.org/10.1177/0892705711423291.

Motloung, M.P., Ojijo, V., Bandyopadhyay, J. and Ray, S.S. (2020) 'Morphological characteristics and thermal, rheological, and mechanical properties of cellulose nanocrystals-containing biodegradable poly(lactic acid)/poly(ε-caprolactone) blend composites', *Journal of Applied Polymer Science*, 137(19). Available at: https://doi.org/10.1002/app.48665.

Rao R.Umamaheswara, Venkatanarayana, B. and Suman, KN.S. (2019) *ScienceDirect Enhancement of Mechanical Properties of PLA/PCL (80/20) Blend by Reinforcing with*

MMT Nanoclay. Available at: https://doi.org/https://doi.org/10.1016/j.matpr.2019.06.280.

Rydz, J., Sikorska, W., Kyulavska, M. and Christova, D. (2015) 'Polyester-based (bio)degradable polymers as environmentally friendly materials for sustainable development', *International Journal of Molecular Sciences*, 16(1), pp. 564–596. Available at: https://doi.org/10.3390/ijms16010564.

Rytlewski, P., Gohs, U., Stepczyńska, M., Malinowski, R., Karasiewicz, T. and Moraczewski, K. (2022) 'Electron-induced structural changes in flax fiber reinforced PLA/PCL composites, analyzed using the rule of mixtures', *Industrial Crops and Products*, 188. Available at: https://doi.org/10.1016/j.indcrop.2022.115587.

Salmani, M.R., Shirazi, F., Goodarzi, K., Noormohammadi, F. and Nourany, M. (2024) 'Improving Phase Compatibility of PLA-PCL Matrix-Droplet Blend Using CNC/PCL-PEG-PCL Triblock Copolymer to Prepare Porous 3D Osteoinductive Scaffolds', *Journal of Polymers and the Environment* [Preprint]. Available at: https://doi.org/10.1007/s10924-024-03392-5.

Shin, B.Y. and Han, D.H. (2017) 'Viscoelastic properties of PLA/PCL blends compatibilized with different methods', *Korea Australia Rheology Journal*, 29(4), pp. 295–302. Available at: https://doi.org/10.1007/s13367-017-0029-8.

Zeenat, Elahi, A., Bukhari, D.A., Shamim, S. and Rehman, A. (2021) 'Plastics degradation by microbes: A sustainable approach', *Journal of King Saud University - Science*. Elsevier B.V. Available at: https://doi.org/10.1016/j.jksus.2021.101538.

Zhang, J., Hirschberg, V. and Rodrigue, D. (2022) 'Mechanical fatigue of biodegradable polymers: A study on polylactic acid (PLA), polybutylene succinate (PBS) and polybutylene adipate terephthalate (PBAT)', *International Journal of Fatigue*, 159. Available at: https://doi.org/10.1016/j.ijfatigue.2022.106798.

Zhu, B., Wang, Y., Liu, H., Ying, J., Liu, C. and Shen, C. (2020) 'Effects of interface interaction and microphase dispersion on the mechanical properties of PCL/PLA/MMT nanocomposites visualized by nanomechanical mapping', *Composites Science and Technology*, 190. Available at: https://doi.org/10.1016/j.compscitech.2020.108048.

Chapter 2

LITERATURE REVIEW

This chapter has been published under the title:

Nanocellulose-Reinforced Poly(Lactic Acid) and Poly(ε-caprolactone) Bio-Nanocomposites: A Review and Future Outlook for Poly(Lactic Acid)/Poly(ε-caprolactone) Blend Systems

https://doi.org/10.3390/ma18225172

Mbongeni Ngwenya[1], Thandi P. Gumede[1], Ricardo Arpad Pérez Camargo[2] and Bennie Motloung[3*]*

[1]Department of Life Sciences, Faculty of Health and Environmental Sciences, Central University of Technology, Free State, Bloemfontein 9301, South Africa

[2]POLYMAT and Department of Polymers and Advanced Materials: Physics, Chemistry, and Technology, Faculty of Chemistry, University of the Basque Country UPV/EHU, Paseo Manuel de Lardizábal, 3, Donostia-San Sebastián 20018, Spain

[3]Department of Chemistry and Polymer Science, Faculty of Science, Stellenbosch University, Matieland 7602, South Africa

*Corresponding authors:

Thandi P. Gumede, tgumede@cut.ac.za and Bennie Motloung, motloung@sun.ac.za

Abstract

The growing demand for sustainable materials has intensified research on biodegradable polymers, particularly poly(ε-caprolactone) (PCL), poly(lactic acid) (PLA), and their blends. PLA and PCL offer biocompatibility and biodegradability, making them attractive for biomedical, packaging, and agricultural applications; however, their practical utility remains limited owing to intrinsic drawbacks. PLA has low impact strength and poor thermal resistance, while PCL suffers from low tensile strength and slow degradation kinetics. Blending PLA with PCL can complement their properties, providing a tunable balance of stiffness and flexibility. Further improvements can be achieved through the incorporation of micro- and nanocellulose (NC), which act as reinforcements, nucleating agents, as well as compatibilizers. We critically examine fabrication strategies for NC-reinforced PLA, PCL, and their blends, highlighting NC extraction, surface modification, processing strategies, and dispersion techniques that prevent agglomeration and facilitate uniform distribution. Comparative insights into composite and nanocomposite systems reveal that NC incorporation significantly enhances mechanical properties, thermal resistance, crystallization, and biodegradation kinetics, particularly at low filler loadings, owing to its high surface area, specific strength, and hydrophilicity. The review underscores the potential of PLA/PCL-based nanocomposites as eco-friendly biomaterials with tunable properties tailored for diverse sustainable applications.

Keywords: poly(ε-caprolactone); poly(lactic acid); nanocellulose; processing; PLA/PCL blends; nanocomposites; biodegradable; mechanical reinforcement

2.1 Introduction

Biodegradable polymers, including poly(lactic acid) (PLA) and poly(ε-caprolactone) (PCL), have gained significant attention. On one hand, PLA is derived from renewable resources such as corn starch, which provides degradation under specific conditions. On the other hand, PCL, despite being a synthetic polymer, also offers biodegradable characteristics. These polymers offer an alternative to petroleum-based plastics and align with the increasing demand for sustainable materials. However, both PLA and PCL exhibit limitations that restrict their wide-scale use. As summarized in Table 2.1, PLA and

PCL exhibit contrasting properties. PLA, despite its high tensile strength and rigidity, is brittle and prone to fracture (Wang *et al.*, 2023; Widjaja *et al.*, 2025), while PCL, known for its flexibility, suffers from low mechanical strength (Kurakula, Rao and Yadav, 2020). The combination of these polymers in blends aims to balance these properties, though the immiscibility of the two remains a challenge (Fernández-Tena, Otaegi, *et al.*, 2023). To address these limitations, different kinds of fillers, such as inorganic nanoparticles, carbon-based fillers, metal and metal oxides, bio-based nanofillers, and cellulose-based nanofillers, have been explored for the enhancement of PCL and PLA properties (Ghanem et al., 2024; Hou et al., 2024; Soriano-Cuadrado et al., 2024; Vidakis et al., 2024; Wang et al., 2024; Xiao et al., 2024; Carotenuto et al., 2025; Ntrivala et al., 2025; Şen and Sever, 2025). In particular, nanocellulose (NC) has emerged as an attractive nanofiller for these polyesters and their blends in the development of fully biodegradable nanocomposites. Beyond its inherent biodegradability, biocompatibility, and non-toxicity, NC exhibits high specific strength and tunable surface chemistry, setting it apart from inorganic, carbon-based, and metal-based fillers that may pose potential health or environmental concerns. These features, combined with their renewable origin, make it a promising and sustainable alternative for designing high-performance bio-nanocomposites. Recent research has focused on reinforcing these polymers and their blends with NC, either in the form of cellulose nanocrystals (CNCs), cellulose nanofibrils (CNFs), or bacterial nanocellulose. In PLA-based systems, NC has been shown to enhance tensile strength, Young's modulus, and crystallinity (Pracella et al., 2014; Gond and Gupta, 2020; Gond et al., 2022; Wu et al., 2022; Ahmad et al., 2023; Khoo, Chow and Ismail, 2023). This is due to its ability to act as a nucleating agent and reinforce the polymer structure at the nanoscale. For instance, studies have reported up to 40–60% improvement in tensile strength with the addition of well-dispersed CNCs at low loadings (1–5 wt.%), along with improved thermal stability (Gond *et al.*, 2022). Similarly, PCL-based systems exhibited increased stiffness and biodegradation rate (Rashtchian et al., 2020; Qiao et al., 2022; Chen et al., 2023), especially when surface-modified NC is used to improve interfacial adhesion with the more hydrophobic PCL matrix (Xu, Chen and Wu, 2018). Beyond individual matrices with NC, research has also focused on PLA/PCL blend-based nanocomposites, where NC plays a dual role: reinforcing the polymer network (Rytlewski *et al.*, 2022) and acting as a compatibilizer (Rao et al., 2019; Dadras

et al., 2020; Zhu et al., 2020; Salmani et al., 2024; Haghgoo et al., 2025; Nourany et al., 2025). Generally, in immiscible polymer blends, nanocellulose localizes at the interface between PLA and PCL phases, reducing interfacial tension and promoting stress transfer across both phases. This results in finer phase morphologies and an improvement in the mechanical synergy and dimensional stability. In some studies, the use of NC has yielded PLA/PCL blend composites with balanced toughness and strength, improved elongation at break and enhanced thermal behavior (Malinowski, 2016; Dadras et al., 2020; Rytlewski et al., 2022; Chen et al., 2023). Moreover, techniques such as melting extrusion and blending, solvent casting, injection molding and 3D printing have been used to optimize dispersion and alignment of NC within the matrix, directly influencing composite performance (Malinowski, 2016; Dadras et al., 2020; Kalita et al., 2020; Slouf et al., 2020; Rytlewski et al., 2022; Chen et al., 2023). Table 2.1 presents the summary of some of the PCL and PLA properties, such as tensile strength, elongation at break, melting temperature and glass transition temperature. It also presents the processing methods, approximate degradation under different composting conditions and applications of PCL and PLA.

This review provides a comprehensive overview of the synthesis and properties of PCL, PLA, and their blends, with a particular focus on the incorporation of different forms of NC as reinforcements to enhance their mechanical, thermal, and biodegradation performance. It is structured to first discuss the individual characteristics of PCL and PLA, followed by NC extraction and characterization, and then details the preparation, properties, and applications of PCL/NC, PLA/NC, and PLA/PCL blend-based bio-nanocomposites, including hybrid reinforcements.

Table 2.1. Comparison of properties of poly(ε-caprolactone) and poly(lactic acid) (Woodruff and Hutmacher, 2010; Hassan *et al.*, 2012; Luzi *et al.*, 2015; Ruz-Cruz *et al.*, 2022).

Polymer	Tensile Strength (MPa)	Elongation at Break (%)	Melting Temperature (°C)	Glass Transition (°C)	Processing Method	Approximate Degradation Time Under Composting Conditions (Months)	Applications
PCL	10–40	200–600	58–64	−65 to −60	Extrusion, injection molding, compression molding, solvent casting, electrospinning	>24	Drug delivery sutures
PLA	50–70	3–6	173–178	60–65	Extrusion, injection molding, compression molding, solvent casting	6 to 12	Orthopedic surgery, oral and maxillofacial surgery

2.2 Synthesis and Properties of Poly(ε-caprolactone)

Poly(ε-caprolactone) (PCL) is an aliphatic polyester that is widely recognized for its biodegradability, biocompatibility, and ease of processing, making it a material of interest in both biomedical and environmental applications. According to literature, PCL is synthesized via (i) ring-opening polymerization (ROP) (ionic- or metal-catalyzed, and coordination insertion method) of the cyclic monomer ε-caprolactone, (ii) cyclic ketene acetals using radical ring-opening polymerization (rROP), and (iii) 6-hydroxycaproic acid polycondensation, as shown in Figure 2.1 (Guarino *et al.*, 2017). ROP remains the most widely used method due to its high efficiency, ability to control molecular weight, and compatibility with large-scale production. Moreover, the ROP of ε-caprolactone process is highly sensitive to the choice of catalysts, which include stannous octoate, aluminum alkoxides, as well as zinc-based and tin-based complexes. The choice of a catalyst

affects the molecular weight distribution of the resulting PCL, which in turn influences its mechanical and thermal properties (Chaipakdee *et al.*, 2025). For example, the zinc–cobalt double-metal cyanide complex [Zn-Co(III) DMCC] produced higher molecular weight PCL, which exhibits better tensile strength and elongation at break, but may compromise processability due to its increased viscosity (Liu *et al.*, 2020). The recent literature has increasingly focused on alternative synthesis routes, including enzyme-catalyzed and organo-catalytic polymerization, to address concerns about the residual toxicity of tin-based catalysts such as stannous octoate in biomedical applications (Gong et al., 2021; Dias et al., 2022; Fernández-Tena et al., 2023). In one study, the role of steric hindrance in the catalytic efficacy during polymerization was investigated. For this purpose, tin(IV)-based catalysts such as tetramethyltin, dimethyldiphenyltin, triphenyltin chloride and tetraphenyltin were utilized and compared. The latter was reported to be effective in promoting propagation and thus produce PCL with high molecular weight, narrow dispersity, and low oligomer content. The resulting polymer exhibited superior tensile strength and elongation at break compared to the PCL synthesized using other catalysts (Gong *et al.*, 2021).

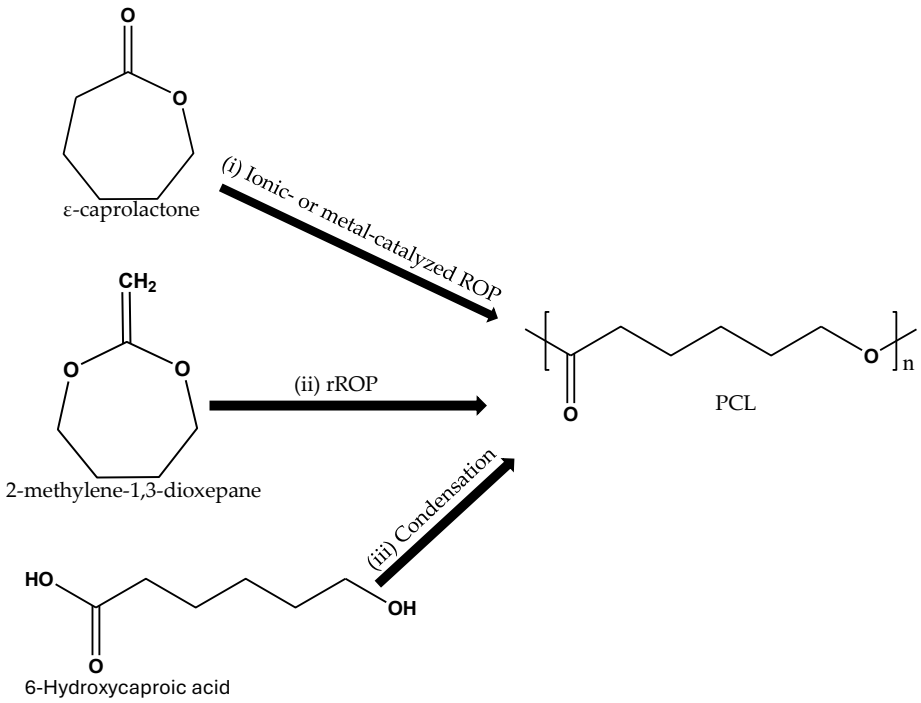

Figure 2.1. Various synthetic routes for the production of PCL (Adapted from (Meneses *et al.*, 2022), Open Access).

In terms of properties, PCL is semi-crystalline, with spherulites consisting of lamellae oriented in parallel and separated by amorphous regions with a reported degree of crystallinity of *ca*. 40%, a melting temperature in the range of 58–64 °C, and a glass transition temperature in the range of −65 to −60 °C (see Table 2.1) (Woodruff and Hutmacher, 2010; Selikane et al., 2024; Kumalo et al., 2025). These thermal properties contribute to its high flexibility and low-temperature processability. Mechanical studies have shown that PCL typically exhibits moderate tensile strength (10–40 MPa) and remarkable elongation at break (up to 600%), depending on the molecular weight, degree of crystallinity, and the processing conditions (Chen et al., 2023; Ikhtiarini et al., 2025). While its mechanical properties are suitable for applications requiring ductility, the softness of the materials and low modulus have motivated the use of PCL in blends or composites to improve structural performance. From a degradation standpoint, PCL undergoes slow hydrolytic degradation of its ester linkages, followed by microbial action, especially under composting or enzymatically active conditions (Guarino *et al.*, 2017). PCL degrades quickly, within months, under conditions such as warm temperature (~30–40 °C), active microbial community, moisture, and slightly acidic conditions (pH ~5–7). However, it takes years to degrade under conditions such as limited microbial activity and low temperature. High crystallinity and hydrophobicity of PCL also slow the degradation rate (Ghanem *et al.*, 2024; D'Amario *et al.*, 2025). While this slow degradation rate is beneficial for long-term biomedical uses such as scaffolds and drug delivery systems, it limits the effectiveness of PCL in short-lifespan packaging or agricultural applications unless it is blended with polymers with fast biodegradation kinetics or reinforced with hydrophilic fillers. The literature also highlights the limited polarity and hydrophobic nature of PCL, which often leads to poor compatibility with polar fillers and polymers. This has driven a considerable amount of research into surface modification, grafting, and compatibilization strategies to enhance its interfacial interactions in composites. Recent efforts include the functionalization of PCL chains and incorporation of nanofillers, such as NC, to improve both the mechanical and thermal performance of PCL-based materials while retaining biodegradability (Xu, Chen and Wu, 2018).

2.3 Synthesis and Properties of Poly(Lactic Acid)

Poly(lactic acid) (PLA) is one of the most extensively studied biodegradable aliphatic polyesters due to its bio-based origin, good mechanical strength, and biocompatibility. According to (Farah et al., 2016; Luyt and Malik, 2018), PLA is primarily synthesized via (i) direct polycondensation of lactic acid, (ii) azeotropic dehydrative condensation, and (iii) ROP of lactide, as illustrated in Figure 2.2. The ROP method is more favorable industrially due to the ability to achieve high molecular weight polymers and control over stereochemistry (Luyt and Malik, 2018). The synthesis process is typically catalyzed by tin(II) octoate, which allows for tuning of the molecular architecture of the polymer (Yamane and Sasai, 2003; Widjaja *et al.*, 2023).

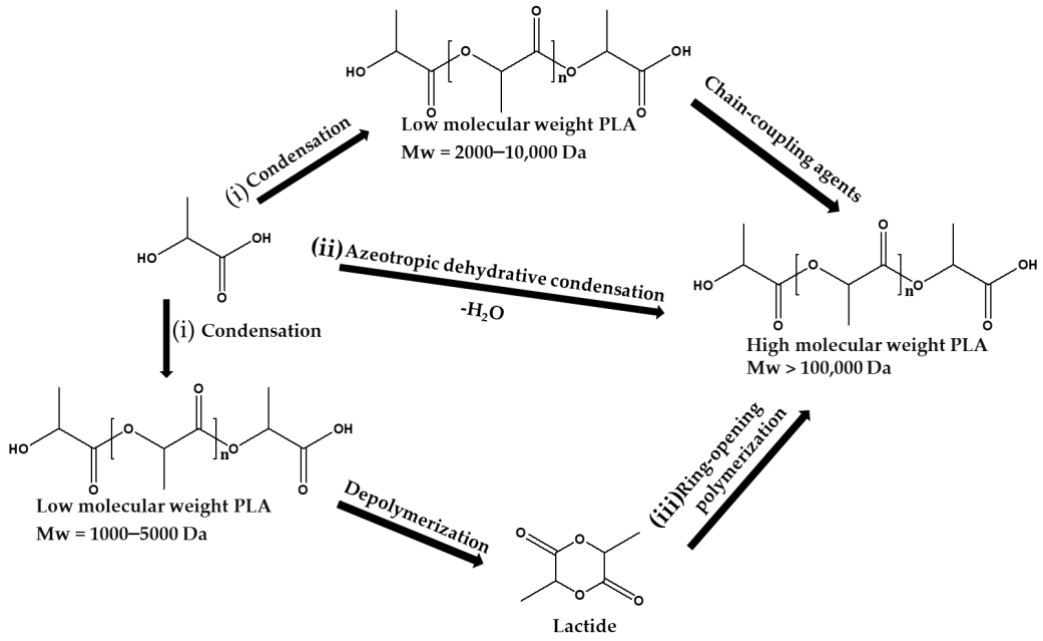

Figure 2.2. Different synthetic methods for the production of PLA (Adapted from (Refinetti *et al.*, 2014), Open Access).

In general, PLA consists of crystalline domains formed by thin plate-like stacks of folded polymer chains, connected to amorphous zones by chain folds and tie molecules (Saeidlou *et al.*, 2012). However, its physicochemical properties are closely linked to its stereochemistry. Research highlights that poly(L-lactic acid) is semi-crystalline with the degree of crystallinity of ca. 20–40% and exhibits a higher melting point (~170–180 °C), while poly(D,L-lactic acid) is mostly amorphous with the degree of crystallinity of ca. 0–10% and is more ductile (Yamane and Sasai, 2003). These differences influence

mechanical and thermal performance, with poly(L-lactic acid) showing higher tensile strength and modulus, whereas poly(D,L-lactic acid) offers better flexibility. The mechanical properties of PLA are well-established. (Woodruff and Hutmacher, 2010) reported tensile strengths in the range of 50–70 MPa. However, the inherent brittleness and low impact resistance of PLA are frequently cited drawbacks, prompting research into plasticization, copolymerization, and blending with more ductile polymers such as PCL or poly(butylene adipate–*co*–terephthalate) (PBAT). PLA is biodegradable, primarily via hydrolysis followed by microbial action. However, it is worth noting that biodegradation rates are significantly influenced by crystallinity, molecular weight, and environmental conditions. While industrial composting can achieve efficient biodegradation, PLA tends to persist under ambient conditions, raising concerns about its suitability in certain applications without additional modifications (Yamane and Sasai, 2003; Karpova *et al.*, 2024).

2.4 Nanocellulose: Extraction Methods and Characterization Techniques

Nanocellulose (NC) is a renewable and biodegradable nanomaterial typically derived from lignocellulosic biomass (Sikhosana et al., 2023). It has emerged as a promising reinforcing agent in biopolymer composites due to its high mechanical strength, low density, and ease of surface modification. Studies in the literature have identified three main types of NC, namely cellulose nanocrystals (CNCs), cellulose nanofibrils (CNFs), and bacterial nanocellulose (BNC), each with distinct structural and physical characteristics (Hassan et al., 2012; Qiao et al., 2022; Chen et al., 2023). Extraction typically begins with chemical pre-treatments of the starting biomass, such as alkaline delignification and bleaching to remove lignin and hemicellulose, yielding purified cellulose suitable for nanoscale processing. Figure 2.3 provides extraction methods, highlighting how they lead to different types of NC, namely CNCs (Figure 2.3a) and CNFs (Figure 2.3b). Each method has distinct effects on the properties of the resulting NC, which can further influence the performance of the final bio-nanocomposites. CNCs (Figure 2.3a) are mainly obtained via acid hydrolysis, with sulfuric acid being the most commonly used reagent. It breaks the amorphous cellulose regions and crystallizes the cellulose into highly ordered crystalline structures. However, this method can compromise thermal stability, prompting interest in alternative acids or enzymatic

hydrolysis to mitigate such effects. CNFs (Figure 2.3b), on the other hand, are extracted through mechanical fibrillation methods including high-pressure homogenization and grinding, often aided by chemical or enzymatic pre-treatments such as 2,2,6,6-tetramethylpiperidine-1-oxyl (TEMPO)-mediated oxidation to enhance fibrillation efficiency and reduce energy demand (Chitbanyong et al., 2020; Mokhena and John, 2020; Motloung et al., 2024). In contrast, BNC is biosynthesized by microbial fermentation and is valued for its ultrafine network structure, high purity, and superior water-holding capacity, which make it especially suitable for biomedical applications (Chen et al., 2023). The characterization of NC has been reported in the literature, with various studies highlighting how morphological, structural, and thermal properties influence their performance in polymer nanocomposites (Chitbanyong *et al.*, 2020; Mokhena and John, 2020; Kurniawan *et al.*, 2023). Transmission electron microscopy (TEM) and scanning electron microscopy (SEM) are frequently used to evaluate NC dimensions and morphology. According to the literature, sulfuric acid-derived CNCs typically appear as rigid, rod-like particles with lengths ranging from 100 to 300 nm and diameters between 5 and 20 nm, while CNFs exhibit entangled fibrillar structures several microns in length. X-ray diffraction provides insights into crystalline and polymorphic forms. CNCs extracted via acid hydrolysis typically exhibit higher crystallinity indices (ca. 60–90%) due to removal of amorphous regions (Kusmono *et al.*, 2020; Mohomane *et al.*, 2022). Such high crystallinity enhances stiffness and thermal resistance, making CNCs suitable for reinforcing semi-crystalline polymers such as PCL and PLA.

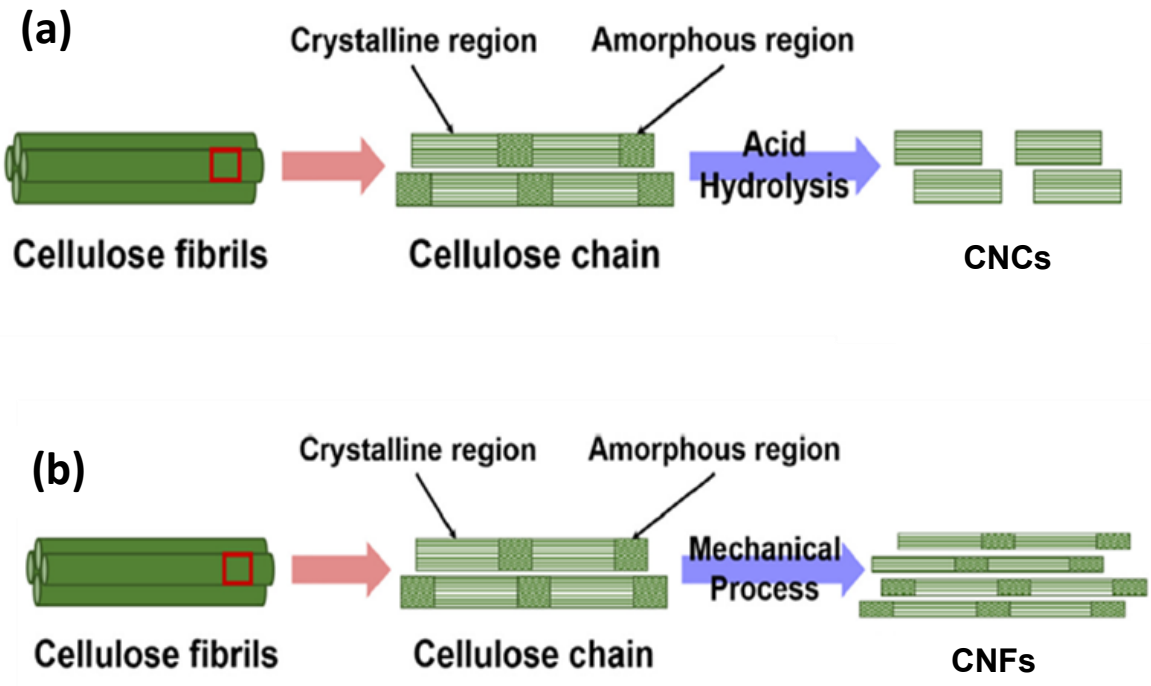

Figure 2.3. Schematic of the extraction of (a) CNCs and (b) CNFs from cellulose fibers via acid hydrolysis and mechanical process, respectively. The right-hand side represents a magnified view of the boxed region on the left to show cellulose at nanoscale (Adapted from (Phanthong *et al.*, 2018), Open Access).

Fourier transform infrared spectroscopy (FTIR) is widely used to confirm chemical composition and surface functional groups. The literature reports characteristic cellulose bands at ~3340 cm^{-1} (O–H stretching), ~2900 cm^{-1} (C–H stretching), and ~1050 cm^{-1} (C–O–C stretching), with additional peaks in modified NC, indicating successful surface functionalization (Xu et al., 2018; Motloung et al., 2024). For instance, esterification with citric acid or silanization with organo-silanes leads to peak shifts or the appearance of new bands, reflecting changed interfacial behavior. Thermogravimetric analysis (TGA) has been used to evaluate thermal stability, showing that CNCs produced via sulfuric acid hydrolysis degrade at lower temperatures (~180–250°C) due to the presence of sulfate ester groups (Gan and Chow, 2019). Differential scanning calorimetry (DSC) is used to observe transitions such as glass transition temperature (T_g) and to evaluate the influence of NC on the thermal behavior of polymer blends. The literature shows the importance of applying multiple complementary techniques to fully characterize NC and predict its behavior in specific composite

applications. Without such a comprehensive understanding, optimizing its reinforcing potential in PLA, PCL, and PLA/PCL blend matrices remains a challenge.

2.5 Poly(ε-caprolactone)/nanocellulose Bio-Nanocomposites: Preparation and Property Enhancements

The incorporation of NC into PCL matrices has gained significant attention in recent years. This is mainly because of its potential to address the limitations of neat PCL, such as low stiffness and moderate thermal resistance. The literature highlights various preparation techniques for PCL/NC bio-nanocomposites, with melt blending and solution casting being the commonly used (see Table 2.2). Melt blending offers the advantage of scalability and solvent-free processing, although achieving uniform NC dispersion remains a challenge due to its hydrophilic nature and tendency to agglomerate within the hydrophobic PCL matrix (Avella et al., 2022; Qiao et al., 2022). On the other hand, solution/solvent casting, often using chloroform or dichloromethane as solvents, facilitates better initial dispersion but is limited by environmental and processing drawbacks (Hassan et al., 2012; Xu et al., 2018; Rashtchian et al., 2020; Mondal et al., 2021; Li and Wu, 2022; Chen et al., 2023). Electrospinning has emerged as an effective technique for fabricating nanofiber-based PCL/CNCs scaffolds (Hivechi *et al.*, 2021). In these systems, CNCs were well-aligned within the fibers, contributing to anisotropic mechanical enhancement. For example, electrospun mats containing CNCs from cotton waste fiber demonstrated up to 50% tensile strength improvement at 1 wt.% CNCs loading. However, at concentrations beyond 4 wt.%, CNCs tend to agglomerate, adversely affecting elongation at break and reducing toughness. Therefore, an optimal loading of 2–3 wt.% is often recommended to balance strength and flexibility (Hivechi *et al.*, 2021). To overcome dispersion issues, research has shown that surface modification strategies such as acetylation, silanization, or surfactant treatment of NC can be useful. PCL-grafted CNCs, obtained via ring-opening polymerization of caprolactone monomer using the “grafting from” approach, have also been reported (Ye et al., 2025). For example, (Avella *et al.*, 2022) demonstrated that treated CNCs improved interfacial adhesion and dispersion within PCL, resulting in enhanced mechanical performance compared to unmodified fillers. In another study, grafting CNFs with PCL (CNFs-*g*-PCL) improved the dispersibility of CNFs in the PCL matrix, which led to improved mechanical

properties. Melting temperatures of the composites also increased, which improved the thermal processability of PCL (Ma *et al.*, 2024).

In terms of property enhancements, numerous studies confirm that the addition of NC significantly improves the mechanical performance of PCL. The tensile strength, Young's modulus, and elongation at break have all shown measurable increases at low NC loadings (typically < 5 wt.%) (Hassan et al., 2012; Luzi et al., 2015; Xu et al., 2018; Qiao et al., 2022; Chen et al., 2023). These improvements are attributed to the high aspect ratio and rigidity of NC, which contribute to effective stress transfer at the filler–matrix interface when dispersion is well controlled. In one study, (N'Gatta *et al.*, 2025) designed 3D-printed bioactive composite scaffolds for bone tissue engineering using fused deposition modeling, incorporating PCL, CNCs, and silver nanoparticles (AgNPs). The binary PCL/CNCs composite displayed significantly higher stiffness and ductility compared to the ternary PCL/CNCs/AgNps system, highlighting CNCs' role in enhancing the mechanical performance of the composite scaffolds. In another study, (Chanthavong *et al.*, 2025) fabricated green composites based on PCL and polyvinyl alcohol (PVA) blend reinforced with polyethylene oxide (PEO)-modified cellulose microfibers. Interestingly, the incorporation of just 1 wt.% cellulose into the PCL–PVA blend significantly increased the tensile strength (Khoshkava and Kamal, 2013). The observed enhancement in tensile strength underscores the reinforcing ability of cellulose on the mechanical properties of these composite materials. Thermal behavior has also been positively affected; TGA and DSC analyses from multiple studies indicate that NC can enhance the thermal stability and crystallinity of PCL composites, although this effect is strongly dependent on the type of NC and its dispersion quality (Mondal et al., 2021; Avella et al., 2022; Li and Wu, 2022; Chen et al., 2023). Moreover, NC acts as a nucleating agent, promoting faster crystallization kinetics, which is particularly advantageous for applications requiring rapid processing or dimensional stability (Chen et al., 2023). From a biodegradation point, incorporation of hydrophilic NC into PCL increases the hydrophilic character of PCL/NC composites, potentially enhancing water penetration, hydrolysis of ester bonds, and access for microbial/enzymatic attack. Factors such as dispersion of NC on the PCL matrix and the reduced crystal size of NC

contribute to increasing the degradation rate. Poor dispersion reduces water uptake, which hinders biodegradation. If the addition of NC significantly increases the crystallinity of the composite, the biodegradation rate decreases since the crystalline domains are less accessible to microbes and water compared to amorphous regions (Hong *et al.*, 2021; Jeon *et al.*, 2023). To summarize, the literature shows that NC is an effective, bio-based reinforcement for PCL. It offers multifunctional improvements that broaden the applicability of PCL in biomedical, packaging and environmental contexts, provided that interfacial compatibility and dispersion are properly managed.

Table 2.2. Summary of poly(ε-caprolactone)/nanocellulose bio-nanocomposites with source, structure, and application insights.

Composite	Source	Filler (wt.%)	Fabrication Method	Enhanced Properties	Application Area	References
PCL/CNCs	Sugarcane bagasse	2.5, 5.0, 7.5, 10.0, 12.5, and 15.0	Solution casting	Tensile modulus, storage modulus, biodegradability properties, and moisture barrier. Maximum increase in Young's modulus was about 77%, and it was achieved at 12.5 wt.% CNCs loading.	Food packaging	(Hassan *et al.*, 2012)
PCL/CNCs	Commercial	10	Melt blending and pressing	Rheological performance, crosslinking, and thermal stability.	Shape-memory applications	(Avella *et al.*, 2022)
PCL/CNCs	Marine algae biomass	0.5, 1.0, and 2.0	Solvent casting	Thermal stability, Young's modulus, and tensile strength.	Packaging	(Mondal *et al.*, 2021)
PCL/CNCs	Purchased	1.0, 3.0, 5.0, and 7.0	Solvent casting	Nucleation and crystallinity for all composites.	Energy storage	(Li and Wu, 2022)
PCL/CNCs	Sugarcane bagasse	2.0	Solution casting	Heterogeneous nucleation, crystallization rate, and improved tensile strength of PCL from 16.5 MPa to 17.8 MPa.	Packaging	(Chen et al., 2023)
PCL/CNCs	Orange peel	2.0	Solution casting	Heterogeneous nucleation, crystallization rate, and improved tensile strength of PCL.	Packaging	(Chen et al., 2023)
PCL/micro-cellulose	Wheat bran	2.0	Solution casting	Heterogeneous nucleation, crystallization rate, and improved tensile strength of PCL.	Packaging	(Chen et al., 2023)
PCL/CNCs	Starch	1.0, 3.0, and 5.0	Solution casting	Tearing strength increased by 68%, and oxygen transmission rate (from 1740 to 1250 cm^3/m^2 per day) and gas permeability were improved for the composite with 1.0 wt.% CNCs.	Packaging membrane	(Xu et al., 2018)

PCL-CaAlg/CNCs	Cotton	1.0 and 5.0	Solution casting	Degradation rate and hydrophilicity.	Wound dressing	(Rashtchian *et al.*, 2020)
PCL/CNFs	Rice straw	0.5, 1.0, 5.0, 10.0, and 15.0	Melt blending and pressing	Tensile strength and Young's modulus increment of 7.5% at 10 wt.% CNFs and 76% at 15 wt.% CNFs, respectively. Hydrophilicity at 15 wt.% CNFs. Nucleated crystallization.	Packaging and biomedical	(Qiao et al., 2022)
PCL/CNCs	Cotton waste fiber	0.5, 1.0, 1.5, 2.5, and 4.0	Electrospinning	Hydrophilicity and crystallization activation energy at 1.0 wt.% CNCs content.	Tissue engineering and wound dressing	(Hivechi *et al.*, 2021)
PCL/CNFs-*g*-PCL	Hardwood kraft pulp	10.0, 20.0, and 30.0	3D printing	Young's modulus and rigidity improved for all samples. Melting temperature increased. Tensile strength enhanced by 45.5% at CNFs-*g*-PCL 30.0 wt.% loading.	Sustainable products	(Ma *et al.*, 2024)
PCL/CNCs	Purchased	1.0, 2.0, and 3.0 wt.%	Wet spinning	Balanced tensile strength and flexibility (Young's modulus of 0.27 GPa). Biocompatibility.	Tissue engineering and anterior cruciate ligament	(Rocha *et al.*, 2025)

Note: PCL = polycaprolactone; CNCs = cellulose nanocrystals; CNFs = Cellulose nanofibrils; wt.% = weight percentage.

2.6 Poly(Lactic Acid)/nanocellulose Bio-Nanocomposites: Preparation and Property Enhancements

The integration of NC into PLA has been extensively studied as a strategy to overcome the inherent drawbacks of PLA, such as brittleness, low impact strength, and slow crystallization rate. The literature presents a variety of preparation methods for PLA/NC bio-nanocomposites, such as solvent casting, injection molding, melt blending, electro-spinning, and extrusion. Solvent casting, often used in early-stage studies, enables good initial dispersion of NC in PLA due to solvent-assisted mixing (Luzi et al., 2015; Miao and Hamad, 2016; Gan and Chow, 2019; Gond and Gupta, 2020; Khoo et al., 2023). However, industrial relevance has driven growing interest in melt processing techniques, which are environmentally favorable and scalable (Pracella et al, 2014; Wongthanaroj et al., 2022; Wu et al., 2022; Ahmad et al., 2023). Despite its advantages, melt processing poses challenges related to the incompatibility between hydrophobic PLA and hydrophilic NC, often leading to agglomeration. Relative to PLA, unmodified NC has a higher surface energy owing to its polar nature at ambient conditions. A direct consequence of the surface energy difference is poor compatibility and thus weak interfacial adhesion between the two components, leading to a non-uniform distribution of the nano-filler in the polyester matrix. Surface modification of NC has been shown to lower its sur-face energy, improving the polymer-filler interaction and thus achieving uniform dispersion (Khoshkava and Kamal, 2013). To address this, researchers have investigated surface modification techniques, such as grafting with glycidyl methacrylate, to enhance interfacial adhesion and dispersion of NC in PLA (Pracella et al., 2014). Grafting of PLA chains onto NC surfaces results in more homogeneous composites and superior mechanical behavior (Ye et al., 2025). For example, incorporation of poly(ethylene glycol) (PEG)-grafted CNCs into PLA through electrospinning enhanced mechanical properties such as tensile strength and elongation at break. Properties such as thermal stability, hydrophilicity, and enzymatic degradation rate were also enhanced by CNCs-g-PEG incorporation (Gong *et al.*, 2025). Incorporation of CNFs-g-PLA to PLA through 3D printing improved thermal stability and mechanical properties such as Young's modulus and tensile strength (Ma *et al.*, 2024). Significant mechanical property enhancements have been reported with the addition of NC to PLA (Table 2.3). As highlighted in the literature

(Pracella et al., 2014; Gond and Gupta, 2020; Gond et al., 2022; Wu et al., 2022; Ahmad et al., 2023; Khoo et al., 2023), tensile strength and Young's modulus of PLA composites increased notably with the incorporation of well-dispersed CNCs or CNFs, even at low filler contents (< 5 wt.%). These enhancements are largely due to the high stiffness and aspect ratio of NC, which enable efficient stress transfer across the matrix–filler interface. However, a trade-off in elongation at break is often observed, attributed to restricted polymer chain mobility, unless plasticizers or compatibilizers are introduced. Beyond mechanical improvements, thermal stability and crystallization behavior of PLA are positively influenced by NC (Islam *et al.*, 2025). Studies using DSC and TGA show that NC can act as a nucleating agent, accelerating PLA crystallization and enhancing its thermal resistance (Gan and Chow, 2019; Gond et al., 2022; Ahmad et al., 2023; Khoo et al., 2023). These effects are especially pronounced with CNCs due to their high surface area and crystalline nature.

From the biodegradation point, well-dispersed hydrophilic CNCs on the PLA matrix improve water uptake and increase the accessibility of ester bonds to microbes and hydrolysis, which speeds up the degradation rate (Trivedi and Gupta, 2024). Biodegradation is slowed by poor dispersion of CNCs on the PLA matrix or strong CNCs–PLA interfacial adhesion, which lowers water penetration and polymer chain mobility (Kelnar *et al.*, 2023). For example, Manzano et al. reported that the incorporation of CNCs alone into PLA decreases the degradation rate of the PLA/CNCs composite by 20%, but incorporating CNCs with micro-fibrillated cellulose into PLA increased the biodegradation of the composite by 60% under composting conditions. This might be due to the increased crystallinity of PLA by the high crystalline CNCs, which hinders microbial access and reduces water uptake. On the other hand, the inclusion of micro-fibrillated cellulose improved water uptake (Galera Manzano *et al.*, 2021). The literature confirms that NC is a highly effective, renewable nanofiller for PLA. It enables the development of biodegradable composites with tailored mechanical and thermal properties for use in biomedical, packaging, and environmental applications.

Table 2.3. Summary of poly(lactic acid)/nanocellulose bio-nanocomposites with source, structure, and application insights.

Composite	Source	Filler (wt.%)	Fabrication Method	Enhanced Properties	Application Area	References
PLA/CNCs	Sugarcane bagasse fiber	10.0	Solvent casting	Acid hydrolysis of cellulose was performed by sulfuric acid (S–CNCs) and phosphoric acid (P–CNCs). Both P–CNCs and S–CNCs improved thermal stability of PLA. TGA results had shown that PLA/P–CNCs exhibited higher thermal stability than PLA/S–CNCs nanocomposites.	Packaging	(Gan and Chow, 2019)
PLA/CNFs	Sugarcane bagasse	1.0, 2.0, 3.0, 4.0, and 5.0	Injection molding	Improvement in water resistance, thermal stability, and mechanical properties such as tensile and flexural strength, impact resistance, and fracture toughness was observed in nanocomposites with 2 wt.% CNFs loading.	Sustainable products	(Gond *et al.*, 2022)
PLA/CNCs	Sugarcane bagasse	5.0, 10.0, and 15.0	Solvent casting	Improved thermal stability and tensile strength at 10.0 wt.%	Packaging	(Khoo et al., 2023)
PLA/CNCs	Softwood pulp	1.0, 2.0, 3.0, and 5.0	Solution casting and co-extrusion	Improved storage moduli at 3.0 wt.%.	Packaging, Medical	(Miao and Hamad, 2016)
PLA/CNCs	Purchased	1.0, 3.0, and 5.0	Melt blending	Improved tensile properties at 3.0 wt.%.	Packaging	(Pracella et al., 2014)
PLA/CNCs	Neptune grass	1.0 and 3.0	Solvent casting	Accelerated degradation at 3.0 wt.%.	Food packaging	(Luzi *et al.*, 2015)
PLA/CNCs	Wood pulp	0.5	Melt blending and injection molding	Tensile strength increased from 57.9 to 79.6 MPa. Crystallinity increased from 35.9 to 42.5%.	Packaging	(Wu *et al.*, 2022)
PLA/CNCs	Purchased	0.75, 1.0, and 2.0	Single screw extrusion	Thermal stability increased at 2.0 wt.% CNCs, and tensile strength increased by 18.2% at 1.0 wt.% CNCs.	3D biomedical applications.	(Ahmad *et al.*, 2023)
PLA/CNCs	Purchased	2.0	Solvent-free cast extrusion	Reduced microbial growth, therefore, increased the shelf life of food that is oxygen sensitive.	Food packaging	(Wongthanaroj *et al.*, 2022)

PLA/CNCs-PEG	Cotton	0.5, 1.0, 2.0 and 4.0, and 8.0	Electrospinning	Tensile strength and elongation at break improved by factor of 2.8 and 1.9, respectively, at 4.0 wt.% CNCs-PEG loading, while thermal stability increased with increasing CNCs-PEG content. Hydrophilicity and enzyme degradation rate increased for all CNCs-PEG-containing samples compared to neat PLA.	Sustainable products	(Gong *et al.*, 2025)
PLA/CNFs-g-PLA	Hardwood kraft pulp	10.0, 20.0, and 30.0	3D printing	Young's modulus significantly increased at 20.0 wt.% CNFs-*g*-PLA loading. Tensile strength increased by 20.8% at 20.0 wt.% CNFs-*g*-PLA loading. Thermal stability is also enhanced by 20.0 wt.% CNFs-*g*-PLA loading.	Sustainable products	(Ma *et al.*, 2024)
PLA/MCNCs	Purchased	1.25	Solution casting	Enhanced crystallinity, biodegradation rate under soil burial, and mechanical properties (tensile strength by 34.6% and elongation at break by 84.3%).	Agriculture and packaging	(Wu *et al.*, 2025)
PLA/CNCs and PLA/CNCs-*g*-ECO	Purchased	1.0	Melt blending and (solvent casting followed by melt blending)	CNCs-*g*-ECO improved dispersion, acted as a nucleating agent, increased crystallinity, and thermal stability.	Sustainable products	(Wahbi *et al.*, 2025)

Note: PLA = poly(lactic acid); CNCs = cellulose nanocrystals; MCNCs = Mineralized cellulose nanocrystals; PEG = poly(ethylene) glycol; ECO = Epoxidized canola oil TGA = Thermogravimetric analysis; wt.% = weight percentage.

2.7 Poly(Lactic Acid)/poly(ε-caprolactone) Biopolymer Blends: Morphology, Compatibility and Properties

PLA and PCL blends have attracted considerable interest in the literature to synergistically combine the desirable properties of both polymers, thereby overcoming individual limitations. Table 2.4 summarizes the key findings from studies on PLA/PCL blends pre-pared mainly via melt blending, which remains the most widely used method due to its industrial relevance and scalability. PLA, characterized by high stiffness and brittleness, and PCL, known for its flexibility and toughness, are inherently immiscible due to differences in polarity and crystallinity, which results in phase-separated morphologies (Shin and Han, 2017; Botlhoko et al., 2018; Dadras et al., 2020; Zhu et al., 2020). Morphological studies using SEM and TEM consistently reveal a dispersed droplet-matrix or co-continuous phase morphology, depending on the blend composition and processing conditions (Shin and Han, 2017). The degree of miscibility dictates the extent of molecular-level interactions between the polyesters, which in turn strongly influences the development of the blend morphology, and thus the mechanical properties and thermal behavior of the blends (Gumede *et al.*, 2022; Vala *et al.*, 2025). In one study, incorporating 10 wt.% of PCL in the blends improved the crystallinity of PLA, and the highest crystallinity was achieved at 20 wt.%, owing to the nucleating effect of PCL, which promotes the crystal formation of PLA. Interestingly, the crystallinity was significantly decreased with the utilization of higher PCL content (i.e., > 20 wt.%). This was attributed to the disruption of the PLA crystal structure by excess PCL, which hinders the effective chain arrangement (Eryildiz *et al.*, 2025). In contrast, (Ivanov *et al.*, 2025) reported that an increase in PLA crystallinity was not observed until the PCL content in the blends reached ca. 40 wt.%. The relatively low crystallinity of PLA at lower PCL loadings was attributed to the characteristic sea–island morphology observed in these immiscible blend systems (Figure 2.4). The study further demonstrated that the optimum size of the PCL (i.e., dispersed phase) was strongly dependent on the crystallinity of the PLA (i.e., continuous phase). Indeed, the low PLA crystallinity resulted in the formation of larger PCL spheres (≈1 μm), whereas higher PCL crystallinity promoted finer phase dispersion, leading to smaller PLA droplets (≈0.5 μm) in the 30PLA/70PCL blend (Figure 2.4). In other studies, this PLA/PCL blend ratio (i.e., 80/20) was also used to fabricate the

blends, and it was found that both the mechanical and thermal properties of the resulting 3D printed scaffolds were significantly improved (Eryildiz et al., 2025; Kiani et al., 2025). (Vala *et al.*, 2025) reported the preparation of PLA/PCL blends using PCL derivatives, where PCL was chemically modified with either maleic anhydride or glycidyl methacrylate. It was shown that the functionalization of PCL enhanced interfacial adhesion and consequently led to improved thermal stability of the blends. In general, at low PCL content, PCL droplets are dispersed within the PLA matrix, which typically leads to improved impact resistance but limited enhancement in ductility. At higher PCL loadings (>30 wt.%), co-continuous morphologies can form (Figure 2.4), resulting in balanced stiffness and toughness (Botlhoko et al., 2018). The major challenge reported in the literature is the limited compatibility between PLA and PCL. This is evident in blends with 30/70 and 80/20 PLA/PCL ratios, which exhibit uneven dispersion of PLA phases (Shin and Han, 2017; Zhu *et al.*, 2020). This leads to weak interfacial adhesion and poor stress transfer, resulting in com-promised mechanical performance (Shin and Han, 2017; Zhu *et al.*, 2020). To address these compatibility challenges and further enhance the mechanical, thermal and functional properties of PLA/PCL blends, recent research has focused on reinforcing these systems with NC, ushering in a new generation of bio-nanocomposites with improved interfacial interactions and sustainability performance.

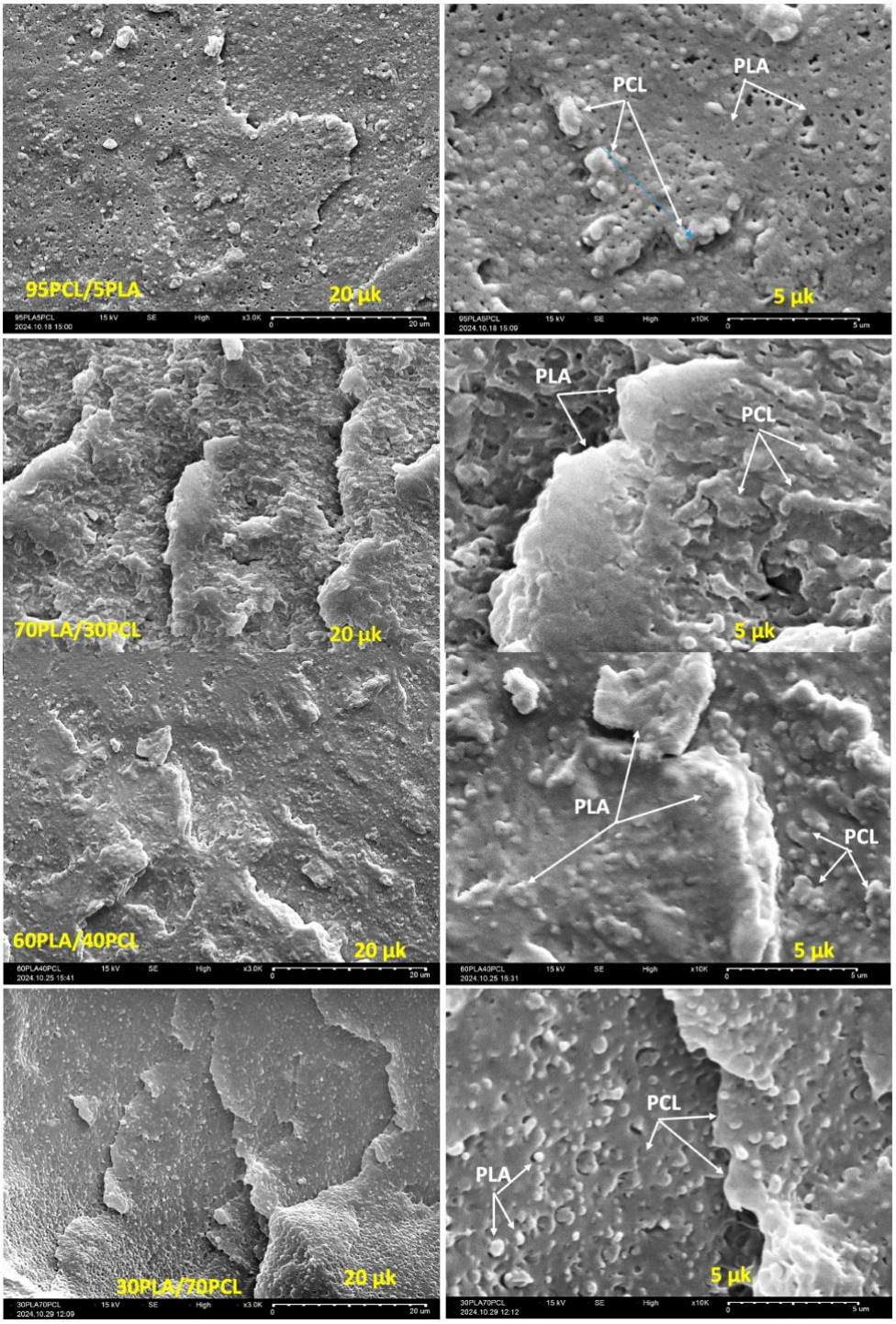

Figure 2.4. SEM micrographs of PLA/PCL blends at 95/5, 70/30, 60/40, and 30/70 *w/w* blend ratios at low (20 µm) and high (5 µm) magnifications. Arrows guide the reader to the PLA and the PCL phases. (Reproduced from (Ivanov *et al.*, 2025), Open Access).

Table 2.4. Processing methods and performance outcomes of poly(lactic acid)/poly(ε-caprolactone) blends.

Blend Composition (PLA/PCL wt.%)	Fabrication Technique	Key Processing Characteristics	Findings/Impact on Composite Performance	Applications	References
30/70	Melt blending	High temperature, direct mixing	Incompatible blends; poor interface adhesion; uneven PLA phase dispersion.	Not reported	(Zhu *et al.*, 2020)
100/0, 90/10, 80/20, 70/30, 60/40, 50/50, 40/60, 30/70, 20/80, 10/90, and 0/100	Melt blending	High temperature, direct mixing	Stiffness, strength, elongation at break, thermal stability, and activation energy balancing were enhanced for (60/40) PLA/PCL blend. However, other blends showed poor compatibility and mechanical properties.	Packaging, Biomedical	(Shin and Han, 2017)
80/20	Melt blending	High temperature, direct mixing	Large, dispersed particle sizes; poor mechanical properties.	Not reported	(Shin and Han, 2017)
100/0, 90/10, 80/20, 70/30, and 0/100	Melt blending	High temperature, direct mixing	All blends showed poor compatibility. Based on results, blend containing 30% PCL had superior thermal properties compared to other blend ratios.	Packaging, Biomedical	(Dadras et al., 2020)

Note: PLA = Poly(lactic acid); PCL = Poly(ε-caprolactone).

Property-wise, PLA/PCL blends exhibit a unique balance of mechanical, thermal, and barrier characteristics that can be tailored by adjusting the blend ratio and compatibilization approach. The literature reports that the addition of PCL generally improves the elongation at break and impact strength of PLA, mitigating its brittleness, while the stiffness and tensile strength tend to decrease proportionally with increasing PCL content (Botlhoko et al., 2018). Thermal analysis via DSC shows that blending can modify the crystallization behavior of both polymers, sometimes resulting in separate melting peaks indicative of phase immiscibility, although compatibilized blends can exhibit enhanced crystallinity due to improved phase interactions (Dadras et al., 2020). Furthermore, PLA/PCL blends maintain biodegradability and have been investigated for applications in packaging and biomedical devices (Botlhoko et al., 2018; Dadras et al., 2020).

2.8 Poly(Lactic Acid)/poly(ε-caprolactone)-Based Composites Hybrid Reinforcements: Processing and Performance

The development of PLA/PCL-based composites reinforced with fillers, such as NC and other bio- or inorganic reinforcements, has emerged as a promising approach to simultaneously enhance mechanical and thermal properties beyond what is achievable with single fillers. The literature shows that reinforcement strategies improve interfacial adhesion, dispersion, and composite functionality (Malinowski, 2016; Botlhoko et al., 2018; Dadras et al., 2020; Kalita et al., 2020; Slouf et al., 2020; Rytlewski et al., 2022; Chen et al., 2023). Processing methods for these nanocomposites typically involve melt blending, solvent casting, extrusion, injection molding, and 3D printing, with melt blending being the most industrially viable. However, achieving uniform dispersion and strong interfacial bonding remains a major challenge (Ilhan et al., 2025), often addressed through surface modification of fillers or compatibilizers tailored to interact with both the polymer matrix and the various fillers. Performance-wise, studies summarized in Table 2.5 report that composites of PLA/PCL exhibit improved tensile strength, modulus, and toughness compared to neat PLA/PCL blends (Malinowski, 2016; Rao et al., 2019; Rytlewski et al., 2022; Chen et al., 2023). For example, the PLA/PCL/TEMPO-oxidized bacterial cellulose (TOBC) composite, manufactured via 3D printing and using TEMPO oxidation surface modification, showed a 17.4% increase in tensile strength, alongside a 208% increase in elongation at break. This indicates improved ductility and strength, making it well-suited for biomedical applications where flexibility and resilience are important. The enhanced crystallinity (~60%), associated with TOBC, also supported better structural integrity (Chen et al., 2023). In contrast, the PLA/PCL/microcrystalline cellulose (MCC) composites demonstrated improved hydrophilicity and accelerated biodegradation, valuable attributes for a sustainable packaging solution. The melt extrusion and blending fabrication technique ensures effective dispersion of MCC at 1.0–3.0 wt.%, contributing to a moderate crystallinity (~45%) that balances mechanical performance and environmental degradability (Kalita *et al.*, 2020). Interestingly, MCC composites did not report additional surface modification, suggesting a natural compatibility between MCC and the PLA/PCL matrix. Incorporation of 1.0 wt.% CNCs, as well as CNCs-*g*-PCL and CNCs-*g*-PLLA nanofillers, into the PLA/PCL matrix via melt-

blending-accelerated biodegradation, improved compatibility, which enhanced mechanical properties such as elastic modulus and tensile strength (Sessini *et al.*, 2018). CNCs, PCL-PEG-PCL tri-block copolymer (BCP), and BCP-CNCs were incorporated into the PLA/PCL (60/40) matrix for phase compatibility improvement. BCP10-CNCs1.0 enhanced interfacial interaction, 10.0 wt.% BCP enhanced the crystallinity of PCL, and the porosity increased with CNCs content in the blend (Salmani *et al.*, 2024).

The “optimal” NC content largely depends on the polyester (i.e., PLA or PCL), blend ratio (for PLA/PCL blends), morphology, and chemical modification of NC, the presence or absence of a compatibilizer, processing method, as well as target properties. For example, in one study, 3 wt.% NC was found to be optimal for dispersion and overall properties in PLA (Sikhosana et al., 2023); however, another study reported an optimal NC content of 4 wt.% in PCL (Vidakis *et al.*, 2024). Although the optimal values are system specific, relatively low nanofiller contents (< 5 wt.%) lead to substantial enhancements in mechanical properties. Since NC has a high surface area, low concentrations permit even distribution within the matrix, promoting effective stress transfer. However, at high loadings, the filler particles aggregate, owing to strong intermolecular hydrogen bonding. These agglomerates no longer reinforce, but rather act as stress concentrators, initiating cracks and thus weakening the mechanical properties of the composites. Concerning the plastic deformation mechanism, PLA, being glassy at ambient conditions, is dominated by crazing and crack propagation. In contrast, PCL shows ductile behavior, allowing shear yielding and necking. However, in PLA/PCL blends, the deformation mechanism largely depends on interfacial adhesion, blend composition, and temperature (Batakliev *et al.*, 2025). Blending PLA with PCL, as well as the incorporation of CNCs into either matrix, can significantly influence the phase composition of these polyesters. For instance, CNCs have been shown to enhance the crystallinity of PCL (Hivechi et al., 2021; Li and Wu, 2022; Qiao et al., 2022; Chen et al., 2023). Similarly, it has been reported to accelerate the crystallization kinetics of PLA, thereby increasing its overall crystallinity (Wu *et al.*, 2022, 2025; Wahbi *et al.*, 2025). These observations clearly highlight the role of CNCs as an effective nucleating agent within these matrices,

promoting a more ordered and less amorphous polymer structure. Nevertheless, this nucleating effect is not exclusive to CNCs; as the dispersion of PCL in PLA (continuous phase) has also been found to facilitate faster crystallization kinetics, while the incorporation of PLA into PCL (continuous phase) similarly contributes to an increase in crystallinity (Ivanov *et al.*, 2025).

Concerning the mechanism of biodegradation, warm and moist conditions are essential, and hydrolysis is central to, and thus the initiating and rate-determining step in the process. Both PCL and PLA are aliphatic polyesters, comprising ester linkages along their backbones. It therefore logically follows that they are both susceptible to hydrolytic cleavage, albeit to varying degrees, depending on factors such as crystallinity, molecular weight, and hydrophobicity. Relative to NC, which is rich in hydroxyl groups, both PCL and PLA are hydrophobic; therefore, incorporation of cellulose nanofiller in either polyester's matrix reduces the lipophilic-to-hydrophilic ratio of the resulting composite material, enhancing the water uptake and thus promoting hydrolysis. In the case of blends, the PCL-PLA interface is typically a region of structural discontinuity, owing to the immiscibility between the two polyesters. In addition, NC has been shown to often localize in these regions and compatibilizes the two components. Therefore, given the fibrous and porous nature of cellulose, these weak interfacial areas increase water diffusion into the blend composites and accessibility for microbial attack.

Nanoclay fillers such as montmorillonite (MMT) and organo-modified MMT (O.MMT) enhance the mechanical performance of the composites primarily by improving the interface interaction between the PLA and PCL phases. Surface functionalization of MMT nanoclay promotes better polymer compatibility and increases tensile strength, essential for applications like printing plates (Rao et al., 2019). The O.MMT variant notably doubles the indentation modulus compared to neat PCL, indicating a significant increase in stiffness, which is desirable for rigid packaging materials (Slouf *et al.*, 2020). These composites were typically prepared via melt blending, a method that effectively distributes nanoclay particles within the polymer matrix. Synthetic additives such as Pluronic and triallyl isocyanurate (TAIC) serve as compatibilizers that enhance

mechanical properties by improving the miscibility of PLA and PCL. TAIC, added via melt blending, not only increases strength and modulus but also reduces phase separation in PLA/PCL blends, expanding its use in both packaging and biomedical fields (Malinowski, 2016). Pluronic, incorporated at 2.5 to 7.5 parts per hundred and processed through melt blending, improves tensile strength at optimal blend ratios, targeting packaging applications (Rytlewski *et al.*, 2022). Additionally, the inclusion of natural biopolymer reinforcements such as SFNPs improves the thermal stability and compatibility of PLA/PCL composites without the need for surface modifications. Melt blending these SFNPs at 1.0 wt.% offers benefits suitable for food packaging, where thermal resistance and safety are priorities (Dadras et al., 2020). Meanwhile, higher loading of natural fibers, such as flax fiber, at 20 wt.%, significantly enhances mechanical properties through extrusion and injection molding, demonstrating their potential for robust packaging materials (Rytlewski *et al.*, 2022). In general, this diverse range of fillers and fabrication methods highlights the adaptability of PLA/PCL composites. NC and natural fibers contribute to environmental sustainability and biodegradability, while nanoclays and synthetic compatibilizers address mechanical performance challenges related to phase incompatibility. The choice of surface modification, filler loading, and processing technique is crucial in tuning the final properties for targeted applications, whether in packaging, biomedical devices, food packaging, or printing technologies.

Table 2.5. Overview of poly(lactic acid)/poly(ε-caprolactone)-based composites with various fillers.

Composite Name	PLA/PCL Ratios	Filler Type and Source	Filler Content (wt.%)	Fabrication Method	Enhanced Properties	Application Area	References
PLA/PCL/TOBC	100/0, 95/5, 90/10, 85/15, and 80/20	TEMPO-oxidized bacterial cellulose	1.5	3D printing	10% PCL content increased tensile strength and elongation at break by 17.4% and 208% compared to that of neat PLA, respectively. Crystallinity increases with increasing PCL content.	Biomedical	(Chen et al., 2023)
PLA/PCL/MCC	90/10 and 80/20	Micro-crystalline cellulose (MCC) from cotton	1.0	Melt extrusion and blending	Enhanced hydrophilicity and accelerated biodegradation.	Packaging	(Kalita *et al.*, 2020)
PLA/PCL/CNCs	70/30	CNCs, CNCs-*g*-PCL and CNCs-*g*-PLLA	1.0	Melt blending	Enhanced shape-memory response, accelerated biodegradation, elastic modulus, and tensile strength.	Biomedicine and food packaging	(Sessini *et al.*, 2018)
PLA/PCL/CNCs, PLA/PCL/BCP, and PLA/PCL/BCP-CNCs	60/40	Cellulose nanocrystals (CNCs) from cotton and PCL-PEG-PCL (BCP) tri-block copolymer	CNCs (0.5, 1.0 and 2.0) BCP (5.0, 10.0 and 20.0)	Solvent casting	Enhanced water uptake for all samples. BCP10-CNCs1.0 enhanced interfacial interaction. 10.0 wt.% BCP enhanced crystallinity of PCL. Porosity increased with CNCs content in blend.	Biomedical	(Salmani *et al.*, 2024)
PLA/PCL/MMT nanoclay	80/20	Montmorillonite (MMT)	2.0, 4.0, and 6.0	Melt blending	Higher tensile strength and compatibility at 4.0 wt.% MMT.	Printing plates	(Rao et al., 2019)

PLA/PCL/Silk fibroin nanoparticles	100/0, 90/10, 80/20, and 70/30	Silk fibroin nanoparticles (SFNPs) from silkworm cocoons	1.0	Melt blending	Enhanced thermal stability and compatibility for 70/30 blend by 1.0 wt.% SFNPs.	Food packaging	(Dadras et al., 2020)
PLA/PCL/ Pluronic	100/0, 90/10, 85/15, 80/20, 75/25, and 70/30	Synthetic Pluronic	2.5, 5.0, and 7.5	Melt blending	Improved tensile strength for blends with 10, 15, and 20 wt.% PCL content at 2.5 parts per hundred.	Packaging	(Rytlewski *et al.*, 2022)
PLA/PCL/TAIC	80/20, 60/40, 40/60, and 20/80	Triallyl isocyanurate (TAIC)	3.0	Melt blending	Improved strength, modulus, and hindered phase separation for 20 PLA/80 PCL.	Packaging and Biomedical	(Malinowski, 2016)
PLA/PCL/MMT	70/30	Montmorillonite	1.0	Solvent casting, Melt blending	Improved PLA phase dispersion and better interface interaction.	Biomedical	(Zhu *et al.*, 2020)
PLA/PCL/ O.MMT	20/80	Organophilic Montmorillonite (O.MMT)	2.0	Melt blending	Improved indentation modulus by 50% compared to that of PCL.	Packaging	(Slouf *et al.*, 2020)
PLA/PCL/CNCs	70/30	CNCs (purchased)	1.0, 2.0, 3.0, and 5.0	Melt extrusion and blending	Improved compatibility and mechanical properties.	Various applications	(Motloung *et al.*, 2020)

Note: CNCs = cellulose nanocrystals; MCC = Microcrystalline cellulose; O.MMT = Organo-modified montmorillonite; PCL = Poly(ε-caprolactone); PLA = Poly(lactic acid); SFNPs = Silk fibroin nanoparticles; TAIC = Triallyl isocyanurate; TEMPO = 2,2,6,6-tetramethylpiperidine-1-oxyl; TOBC = (TEMPO)-oxidized bacterial cellulose.

2.9 Conclusions, Challenges, and Future Perspectives

The incorporation of nanocellulose (NC) into biodegradable polymers such as PLA and PCL has gained considerable attention in overcoming the inherent limitations of PLA and PCL. This includes the brittleness of PLA and the weak thermal and mechanical stability of PCL. This study focuses on the structure–property correlations and performance factors of PLA/NC, PCL/NC, PLA/PCL, and PLA/PCL/NC systems. The addition of NC functions as a reinforcing and nucleating agent, increasing stiffness, modulus, and, in some circumstances, biodegradation rate, depending on dispersion and surface functioning. Surface modification of NC (e.g., acetylation, silanization, or grafting with compatibilizers such as PLA or PCL chains) was found to be the most efficient in improving interfacial adhesion and dispersion inside hydrophobic matrices. For PLA/PCL composites, compatibilization with reactive agents and optimal blend ratios (usually 70/30 or 60/40 PLA/PCL) were discovered to be crucial for balancing stiffness, ductility, and biodegradability. The addition of NC to the PLA/PCL matrix increased mechanical reinforcement, crystallinity control, and interphase stability, provided that good dispersion was achieved. Key parameters influencing overall blend performance include NC surface chemistry, dispersion uniformity, blend content, degree of crystallinity, and processing technique and conditions. A synergistic balance between hydrophilic NC and the immiscible PLA/PCL phases can be achieved through appropriate compatibilization or surface functionalization, resulting in better structural integrity and adaptable degradation profiles. The cost of NC production, energy-intensive extraction and modification processes, and dispersion issues in polymer matrices continue to be barriers to large-scale implementation from an industrial and economic standpoint. However, the increasing demand for bio-based, compostable materials, as well as advancements in reactive extrusion and continuous NC manufacturing technologies, make these systems more and more viable for packaging, biomedical scaffolds, and agricultural films.

Overall, the integration of NC into PLA, PCL, and their blends provides a viable pathway toward high-performance, biodegradable composites.

Despite the promising potential of bio-nanocomposites, several challenges must be addressed to facilitate their widespread adoption and further advancement. These challenges include processing, interface compatibility, environmental assessments, and application enhancements. One significant challenge is based on optimizing the processing techniques for bio-nanocomposites to ensure consistent material properties and performance. Factors such as physical, chemical, and mechanical characteristics of the constituent materials must be carefully considered to prevent variations that could render the nanocomposite unsuitable for its intended use. Interface compatibility between polymer components, particularly in blends such as PLA and PCL, presents another hurdle. Immiscibility and weak interface interactions can limit the overall performance of the composite, necessitating the development of effective compatibilizers to enhance toughness and ensure homogeneity. Another challenge is industrial scalability, NCs' high cost and restricted availability, mostly due to energy-intensive extraction and purification, continue to be major challenges to commercialization. NC production costs typically vary from ZAR 173.16 to ZAR 346.32 per kg, whereas commodity fillers like $CaCO_3$ cost less than ZAR 34.63 per kg. Furthermore, establishing uniform dispersion of NCs inside hydrophobic polymer matrices necessitates surface modification or solvent-assisted compounding, which increases processing steps and costs. Regulatory aspects include adhering to food-contact requirements in packaging applications. PLA is already certified for food packaging, but NCs must adhere to purity and migration standards, particularly if made from plant sources containing residual lignin or hemicellulose. In biomedical applications, both PLA and PCL are approved by the Food and Drug Administration for specific implantable and drug-delivery applications; nevertheless, NCs must demonstrate biocompatibility and cytotoxicity before being integrated into medical devices. Comprehensive life cycle assessments (LCAs) are essential for evaluating the overall environmental impact of bio-nanocomposites. Assessments should cover the entire life cycle from component extraction to final disposal. This will ensure that bio-nanocomposites contribute positively to environmental sustainability and economic efficiency. Enhancing the properties and applications of bio-nanocomposites requires ongoing research and innovation.

Despite higher raw material costs, CNCs-reinforced PLA and PCL composites can reduce environmental impact through renewable sourcing and faster biodegradation, enabling compliance with extended producer responsibility and biodegradability certification frameworks. As NC production becomes more cost-effective, industrial adoption is expected to advance in specialized high-value industries such as biomedical scaffolds or biodegradable barrier films before spreading to commodity sectors. Future research should further explore the design, processing, and characterization of NC-reinforced PLA/PCL blend nanocomposites to improve breakage resistance, hydrophilicity, and water barrier properties in food packaging applications, as well as enhance cell attachment and drug release kinetics in biomedical applications. Key areas of focus should include optimizing dispersion methods, tailoring surface chemistry for interfacial compatibility, and understanding the synergistic effects of ternary systems on biodegradation, crystallinity, and functional performance. Exploring new applications in electronic devices, energy production, and environmental remediation will further expand the scope of bio-nanocomposites and contribute to sustainable technologies. Addressing the aforementioned challenges and advancing this line of investigation holds substantial promise for developing high-performance, scalable, and truly sustainable materials for packaging, agriculture, biomedical devices, and other environmentally critical sectors.

Author Contributions

Conceptualization, T.P.G., R.A.P.C., and B.M.; validation, M.N., T.P.G., R.A.P.C., and B.M.; investigation, M.N., T.P.G., R.A.P.C., and B.M.; data curation, M.N., T.P.G., R.A.P.C., and B.M.; writing—original draft preparation, M.N.; writing—review and editing, M.N., T.P.G., R.A.P.C., and B.M.; visualization, M.N., T.P.G., R.A.P.C., and B.M.; supervision, T.P.G., R.A.P.C., and B.M.; project ad-ministration, T.P.G. All authors have read and agreed to the published version of the manuscript.

Funding

This research was funded by the National Research Foundation (NRF) Thuthuka Programme (Grant No. TTK2204264865), the DSI-NRF postgraduate student fund (Grant No. PMDS22062125350), and the DSI-NRF Innovation Postdoctoral Fellowship (Grant No. PSTD2205057154). Additional financial support was provided by the postgraduate student fund of the Central University of Technology (Free State) and Future Coal Mining (Chelmsford Colliery).

Abbreviations

AgNPs	Silver nanoparticles
CNCs	Cellulose nanocrystals
CNFs	Cellulose nanofibers
DSC	Differential scanning calorimetry
FTIR	Fourier transform infrared spectroscopy
MCC	Microcrystalline cellulose
MMT	Montmorillonite
NC	Nanocellulose
O.MMT	Organically modified montmorillonite
PBAT	Poly(butylene adipate–*co*–terephthalate)
PCL	Poly(ε-caprolactone)
P–CNCs	Phosphoric acid cellulose nanocrystals
PEG	Poly(ethylene) glycol
PEO	Poly(ethylene oxide)
PVA	Poly(vinyl alcohol)
PLA	Poly(lactic acid)
ROP	Ring-opening polymerization
rROP	Radical ring-opening polymerization
S–CNCs	Sulfuric acid cellulose nanocrystals
SEM	Scanning electron microscopy
SFNPs	Silk fibroin nanoparticles

TAIC	Triallyl isocyanurate
TEM	Transmission electron microscopy
TEMPO	2,2,6,6-Tetramethylpiperidine-1-oxyl
TGA	Thermogravimetric analysis
TOBC	(TEMPO)-oxidized bacterial cellulose

References

Ahmad, N.D., Kusmono, Wildan, M.W. and Herianto (2023) “Preparation and properties of cellulose nanocrystals-reinforced Poly (lactic acid) composite filaments for 3D printing applications,” *Results in Engineering*, 17. Available at: https://doi.org/10.1016/j.rineng.2022.100842.

Avella, A., Idström, A., Mincheva, R., Nakayama, K., Evenäs, L., Raquez, J.M. and Lo Re, G. (2022) “Reactive melt crosslinking of cellulose nanocrystals/poly(ε-caprolactone) for heat-shrinkable network,” *Composites Part A: Applied Science and Manufacturing*, 163. Available at: https://doi.org/10.1016/j.compositesa.2022.107166.

Batakliev, T., Georgiev, V., Ivanov, E., Angelov, V. and Kotsilkova, R. (2025) “Tailored Polylactic Acid/Polycaprolactone Blends with Excellent Strength–Stiffness and Shape Memory Capacities,” *Processes*, 13(5). Available at: https://doi.org/10.3390/pr13051328.

Botlhoko, O.J., Sinha Ray, S. and Ramontja, J. (2018) *A new insight into morphological, thermal, and mechanical properties of melt-processed polylactide/poly(Ɛ-caprolactone) blends*. Available at: https://doi.org/https://doi.org/10.1016/j.polymdegradstab.2018.05.025.

Carotenuto, M.R., Cavallaro, G., Chinnici, I., Lazzara, G. and Milioto, S. (2025) “Thermomechanical properties of bionanocomposites based on polycaprolactone and halloysite clay nanotubes,” *Journal of Thermal Analysis and Calorimetry*, 150(10), pp. 7519–7528. Available at: https://doi.org/10.1007/s10973-025-14178-9.

Chaipakdee, N., Hemvichian, K., Lertsarawut, P., Rimdusit, S. and Tiptipakorn, S. (2025) “Effects of molecular weight of polycaprolactone on the thermal properties of V-fa/PCL blends added with cross-linking agent,” *IOP Conference Series: Materials Science and Engineering*, 1325(1), p. 012003. Available at: https://doi.org/10.1088/1757-899X/1325/1/012003.

Chanthavong, V., Cabo, M., Prabhakar, M.N., Woo, L.D. and Song, J. il (2025) “Fabrication of polycaprolactone/polyvinyl alcohol green composite film by reinforcing extracted micro cellulose fibers for food packaging applications,” *Polymer Engineering and Science*, 65(7), pp. 3673–3686. Available at: https://doi.org/10.1002/pen.27241.

Chen, J., Huang, Y., Deng, L., Jiang, H., Yang, Z., Yang, R. and Wu, D. (2023) “Preparation and research of PCL/cellulose composites: Cellulose derived from agricultural wastes,”

International Journal of Biological Macromolecules, 235, p. 123785. Available at: https://doi.org/10.1016/j.ijbiomac.2023.123785.

Chen, Y., Lu, T., Li, L., Zhang, H., Wang, H. and Ke, F. (2023) "Fully biodegradable PLA composite with improved mechanical properties via 3D printing," *Materials Letters*, 331. Available at: https://doi.org/10.1016/j.matlet.2022.133543.

Chitbanyong, K., Pisutpiched, S., Khantayanuwong, S., Theeragool, G. and Puangsin, B. (2020) "TEMPO-oxidized cellulose nanofibril film from nano-structured bacterial cellulose derived from the recently developed thermotolerant Komagataeibacter xylinus C30 and Komagataeibacter oboediens R37–9 strains," *International Journal of Biological Macromolecules*, 163, pp. 1908–1914. Available at: https://doi.org/10.1016/j.ijbiomac.2020.09.124.

Dadras Chomachayi, M., Jalali-Arani, A., Beltrán, F.R., De La Orden, U. and Urreaga, J.M. (2020) "Biodegradable Nanocomposite Developed from the PLA/PCL Blends and Silk Fibroin Nanoparticle: Study on the Microstructure, Thermal Behavior, Crystallinity, and Performance," *Journal of Polymers and the Environment*, 28, pp. 1252–1264. Available at: https://doi.org/10.1007/s10924.

D'Amario, J., Limsukon, W., Bher, A. and Auras, R. (2025) "Impact of hydrolysis pretreatment on the compostability of biodegradable poly(caprolactone) and poly(lactic acid) films," *RSC Applied Polymers*, 3(3), pp. 711–721. Available at: https://doi.org/10.1039/d5lp00041f.

Dias, J.R., Sousa, A., Augusto, A., Bártolo, P.J. and Granja, P.L. (2022) "Electrospun Polycaprolactone (PCL) Degradation: An In Vitro and In Vivo Study," *Polymers*, 14(16). Available at: https://doi.org/10.3390/polym14163397.

Eryildiz, M., Karakus, A. and Altan Eksi, M. (2025) "Development and Characterization of PLA/PCL Blend Filaments and 3D Printed Scaffolds," *Journal of Materials Engineering and Performance*, 34(14), pp. 14043–14054. Available at: https://doi.org/10.1007/s11665-024-10247-6.

Eryildiz, M., Karakus, A., Demirci, M., Altintas Kadirhan, O. and Eksi Altan, M. (2025) "Optimization of Thermal, Mechanical, Biodegradation, and Shape Memory Properties in 4D-Printed PLA/PCL Blends for Spinal Cages," *Polymers for Advanced Technologies*, 36(3). Available at: https://doi.org/10.1002/pat.70133.

Farah, S., Anderson, D.G. and Langer, R. (2016) "Physical and mechanical properties of PLA, and their functions in widespread applications — A comprehensive review," *Advanced Drug Delivery Reviews*. Elsevier B.V., pp. 367–392. Available at: https://doi.org/10.1016/j.addr.2016.06.012.

Fernández-Tena, A., Otaegi, I., Irusta, L., Sebastián, V., Guerrica-Echevarria, G., Müller, A.J. and Aranburu, N. (2023) "High-Impact PLA in Compatibilized PLA/PCL Blends: Optimization of Blend Composition and Type and Content of Compatibilizer," *Macromolecular Materials and Engineering*, 308(12). Available at: https://doi.org/10.1002/mame.202300213.

Fernández-Tena, A., Pérez-Camargo, R.A., Coulembier, O., Sangroniz, L., Aranburu, N., Guerrica-Echevarria, G., Liu, G., Wang, D., Cavallo, D. and Müller, A.J. (2023) "Effect of Molecular Weight on the Crystallization and Melt Memory of Poly(ϵ-caprolactone) (PCL),"

Macromolecules, 56(12), pp. 4602–4620. Available at: https://doi.org/10.1021/acs.macromol.3c00234.

Galera Manzano, L.M., Ruz Cruz, M.Á., Moo Tun, N.M., Valadez González, A. and Mina Hernandez, J.H. (2021) "Effect of cellulose and cellulose nanocrystal contents on the biodegradation, under composting conditions, of hierarchical pla biocomposites," *Polymers*, 13(11). Available at: https://doi.org/10.3390/polym13111855.

Gan, I. and Chow, W.S. (2019) "Synthesis of phosphoric acid-treated sugarcane bagasse cellulose nanocrystal and its thermal properties enhancement for poly(lactic acid) nanocomposites," *Journal of Thermoplastic Composite Materials*, 32(5), pp. 619–634. Available at: https://doi.org/10.1177/0892705718772866.

Ghanem, A.F., Yassin, M.A., Cosquer, R., Gouanvé, F., Espuche, E. and Abdel Rehim, M.H. (2024) "Polycaprolactone composite films infused with hyperbranched polyester/reduced graphene oxide: influence on biodegradability, gas/water transport and antimicrobial properties for sustainable packaging," *RSC Advances*, 14(9), pp. 5740–5753. Available at: https://doi.org/10.1039/d3ra08948g.

Gond, R.K. and Gupta, M.K. (2020) *CHEM-CONFLUX 20 Special Issue Development of PLA Based Nanocellulose Film for Packaging Applications*, *J. Indian Chem. Soc*.

Gond, R.K., Naik, T.P., Gupta, M.K. and Singh, I. (2022) "Development and characterisation of sugarcane bagasse nanocellulose/ PLA composites," *Materials Technology*, 37(14), pp. 2942–2954. Available at: https://doi.org/10.1080/10667857.2022.2088616.

Gong, C., Li, J., Yi, C. and Qu, S. (2021) "Catalytic Regulation of Oligomers in Polycaprolactone," *Molecular Catalysis*, 508. Available at: https://doi.org/10.1016/j.mcat.2021.111594.

Gong, W., Li, M., Sun, J., Zhang, F., Tian, T., Yin, Y. and Wang, C. (2025) "Enhancement of mechanical and thermal properties of PLA electrospun films based on PEG-grafted cellulose nanocrystals," *Composites Communications*, 58. Available at: https://doi.org/10.1016/j.coco.2025.102501.

Grace, D., Selikane, A., Gumede, P., Shingange, K., Malevu, T.D., Ngwenya, M. and Kumalo, F. (2024) *Characterization of Polycaprolactone/Eucomis autumnalis Cellulose Composite: Structural, Thermal, and Mechanical Analysis*. Available at: www.scientific.net.

Guarino, V., Gentile, G., Sorrentino, L. and Ambrosio, L. (2017) "Polycaprolactone: Synthesis, Properties, and Applications," in *Encyclopedia of Polymer Science and Technology*. Wiley, pp. 1–36. Available at: https://doi.org/10.1002/0471440264.pst658.

Gumede, T.P., Shingange, K., Mbule, P. and Motloung, B. (2022) "Miscibility effect of biodegradable aliphatic poly(butylene succinate)/aromatic polycarbonate blends," *Polymers from Renewable Resources*, 13(1–2), pp. 28–43. Available at: https://doi.org/10.1177/20412479221109912.

Haghgoo, G., Dadashi, P. and Babaei, A. (2025) "Effects of Cellulose Nanocrystals Localization on Compatibility Between Polylactic Acid and Polycaprolactone: Correlating the Microstructure and Mechanical Performance," *Polymers for Advanced Technologies*, 36(4). Available at: https://doi.org/10.1002/pat.70113.

Hassan, M.L., Bras, J., Hassan, E.A., Fadel, S.M. and Dufresne, A. (2012) "Polycaprolactone/modified bagasse whisker nanocomposites with improved moisture-barrier and biodegradability properties," *Journal of Applied Polymer Science*, 125(SUPPL. 2). Available at: https://doi.org/10.1002/app.36373.

Hivechi, A., Bahrami, S.H., Siegel, R.A., Siehr, A., Sahoo, A., Milan, P.B., Joghataei, M.T., Amoupour, M. and Simorgh, S. (2021) "Cellulose nanocrystal effect on crystallization kinetics and biological properties of electrospun polycaprolactone," *Materials Science and Engineering C*, 121. Available at: https://doi.org/10.1016/j.msec.2020.111855.

Hong, J.K., Cooke, S.L., Whittington, A.R. and Roman, M. (2021) "Bioactive Cellulose Nanocrystal-Poly(ε-Caprolactone) Nanocomposites for Bone Tissue Engineering Applications," *Frontiers in Bioengineering and Biotechnology*, 9. Available at: https://doi.org/10.3389/fbioe.2021.605924.

Hou, Y., Wang, W. and Bartolo, P. (2024) "In vitro investigations on the effects of graphene and graphene oxide on polycaprolactone bone tissue engineering scaffolds," *Bio-Design and Manufacturing*, 7(5), pp. 651–669. Available at: https://doi.org/10.1007/s42242-024-00280-8.

Ikhtiarini, N., Kamil, M.Z., Bukit, B.F., Juliadmi, D., Prasetiyo, K.W., Fransiska, D., Sedayu, B.B., Subiyanto, B., Sulastiningsih, I.M., Rochima, E., Arivendan, A. and Syamani, F.A. (2025) "Biocompatible composites based on alginate, polycaprolactone, and nanocellulose - A review," *International Journal of Biological Macromolecules*. Elsevier B.V. Available at: https://doi.org/10.1016/j.ijbiomac.2025.143423.

Ilhan, R., Gumus, O.Y. and Lekesiz, H. (2025) "Biodegradable Nanocomposite Filament Based on PLA/PCL/CNCs for FDM 3D Printing: Production, Characterization and Printability," *Polymer Composites* [Preprint]. Available at: https://doi.org/10.1002/pc.70459.

Islam, M.S., Elahee, G.M.F., Fang, Y., Yu, X. (Bill), Advincula, R.C. and Cao, C. (Chase) (2025) "Polylactic acid (PLA)-based multifunctional and biodegradable nanocomposites and their applications," *Composites Part B: Engineering*. Elsevier Ltd. Available at: https://doi.org/10.1016/j.compositesb.2025.112842.

Ivanov, E., Kotsilkova, R., Georgiev, V., Batakliev, T. and Angelov, V. (2025) "Advanced Rheological, Dynamic Mechanical and Thermal Characterization of Phase-Separation Behavior of PLA/PCL Blends," *Journal of Manufacturing and Materials Processing*, 9(2). Available at: https://doi.org/10.3390/jmmp9020035.

Jeon, H., Kim, M.S., Park, S.B., Kim, S., Lee, M., Park, S.A., Hwang, S.Y., Koo, J.M., Oh, D.X. and Park, J. (2023) "Improved mechanical properties of biodegradable polycaprolactone nanocomposites prepared using cellulose nanocrystals," *Cellulose*, 30(18), pp. 11561–11574. Available at: https://doi.org/10.1007/s10570-023-05615-9.

Kalita, N.K., Bhasney, S.M., Mudenur, C., Kalamdhad, A. and Katiyar, V. (2020) "End-of-life evaluation and biodegradation of Poly(lactic acid) (PLA)/Polycaprolactone (PCL)/Microcrystalline cellulose (MCC) polyblends under composting conditions," *Chemosphere*, 247. Available at: https://doi.org/10.1016/j.chemosphere.2020.125875.

Karpova, S.G., Olkhov, A.A., Varyan, I.A., Khan, O.I., Botin, A.A., Naletova, A. V., Popov, A.A. and Iordanskii, A.L. (2024) "Electrospun Polylactide—Poly(ε-Caprolactone) Fibers:

Structure Characterization and Segmental Dynamic Response," *Polymers*, 16(10). Available at: https://doi.org/10.3390/polym16101307.

Kelnar, I., Kaprálková, L., Krejčíková, S., Dybal, J., Vyroubalová, M. and Abdel-Mohsen, A.M. (2023) "Effect of Polydopamine Coating of Cellulose Nanocrystals on Performance of PCL/PLA Bio-Nanocomposites," *Materials*, 16(3), p. 1087. Available at: https://doi.org/10.3390/ma16031087.

Khoo, R.Z., Chow, W.S. and Ismail, H. (2023) "Tensile, thermal and ultra-violet shielding enhancement of poly(lactic acid) bionanocomposite film using cellulose nanocrystals extracted from sugarcane bagasse," *Journal of Thermoplastic Composite Materials*, 36(6), pp. 2543–2561. Available at: https://doi.org/10.1177/08927057221098972.

Khoshkava, V. and Kamal, M.R. (2013) "Effect of surface energy on dispersion and mechanical properties of polymer/nanocrystalline cellulose nanocomposites," *Biomacromolecules*, 14(9), pp. 3155–3163. Available at: https://doi.org/10.1021/bm400784j.

Kiani, P., Sedighi, M., Kasaeian-Naeini, M. and Jabbari, A.H. (2025) "Investigation of mechanical integrity and high-cycle fatigue behavior of 3D-printed PLA/PCL blend after exposure to a physiological environment," *Journal of Materials Research and Technology*, 36, pp. 3671–3683. Available at: https://doi.org/10.1016/j.jmrt.2025.04.082.

Kumalo, F.I., Malimabe, M.A., Mosoabisane, M.F.T. and Gumede, T.P. (2025) "Development and Characterization of PBS/EA Cellulose and PCL/EA Cellulose Biocomposites: Structural, Morphological, and Thermal Insights for Sustainable Applications." Available at: https://doi.org/10.20944/preprints202502.1813.v1.

Kurakula, M., Rao, G.S.N.K. and Yadav, K.S. (2020) "Fabrication and characterization of polycaprolactone-based green materials for drug delivery," in *Applications of Advanced Green Materials*. Elsevier, pp. 395–423. Available at: https://doi.org/10.1016/B978-0-12-820484-9.00016-7.

Kurniawan, T.W., Sulistyarti, H., Rumhayati, B. and Sabarudin, A. (2023) "Cellulose Nanocrystals (CNCs) and Cellulose Nanofibers (CNFs) as Adsorbents of Heavy Metal Ions," *Journal of Chemistry*. Hindawi Limited. Available at: https://doi.org/10.1155/2023/5037027.

Kusmono, Listyanda, R.F., Wildan, M.W. and Ilman, M.N. (2020) "Preparation and characterization of cellulose nanocrystal extracted from ramie fibers by sulfuric acid hydrolysis," *Heliyon*, 6(11). Available at: https://doi.org/10.1016/j.heliyon.2020.e05486.

Li, J. and Wu, D. (2022) "Nucleation roles of cellulose nanocrystals and chitin nanocrystals in poly(ε-caprolactone) nanocomposites," *International Journal of Biological Macromolecules*, 205, pp. 587–594. Available at: https://doi.org/10.1016/j.ijbiomac.2022.02.123.

Liu, Z.H., Li, Y., Zhang, C.J., Zhang, Y.Y., Cao, X.H. and Zhang, X.H. (2020) "Synthesis of high-molecular-weight poly(ε-caprolactone) via heterogeneous zinc-cobalt(III) double metal cyanide complex," *Giant*, 3. Available at: https://doi.org/10.1016/j.giant.2020.100030.

Luyt, A.S. and Malik, S.S. (2018) “Can biodegradable plastics solve plastic solid waste accumulation?,” in *Plastics to Energy: Fuel, Chemicals, and Sustainability Implications*. Elsevier, pp. 403–423. Available at: https://doi.org/10.1016/B978-0-12-813140-4.00016-9.

Luzi, F., Fortunati, E., Puglia, D., Petrucci, R., Kenny, J.M. and Torre, L. (2015) “Study of disintegrability in compost and enzymatic degradation of PLA and PLA nanocomposites reinforced with cellulose nanocrystals extracted from Posidonia Oceanica,” *Polymer Degradation and Stability*, 121, pp. 105–115. Available at: https://doi.org/10.1016/j.polymdegradstab.2015.08.016.

Ma, R., Zhang, Q., Wang, S., Li, B., Ma, L., Zhang, L., Yu, J., Fan, Y. and Wang, Z. (2024) “One-pot cellulose nanofibrillation, surface-modification and grafting by deep eutectic solvent towards high performance 3D printing nanocellulose-enriched bionanocomposites,” *Industrial Crops and Products*, 210. Available at: https://doi.org/10.1016/j.indcrop.2024.118134.

Malinowski, R. (2016) “Mechanical properties of PLA/PCL blends crosslinked by electron beam and TAIC additive,” *Chemical Physics Letters*, 662, pp. 91–96. Available at: https://doi.org/10.1016/j.cplett.2016.09.022.

Meneses, J., van de Kemp, T., Costa-Almeida, R., Pereira, R., Magalhães, F.D., Castilho, M. and Pinto, A.M. (2022) “Fabrication of Polymer/Graphene Biocomposites for Tissue Engineering,” *Polymers*. MDPI. Available at: https://doi.org/10.3390/polym14051038.

Miao, C. and Hamad, W.Y. (2016) “In-situ polymerized cellulose nanocrystals (CNC)—poly(L-lactide) (PLLA) nanomaterials and applications in nanocomposite processing,” *Carbohydrate Polymers*, 153, pp. 549–558. Available at: https://doi.org/10.1016/j.carbpol.2016.08.012.

Mohomane, S.M., Motloung, S. V, Koao, L.F. and Motaung, T.E. (2022) *effects of acid hydrolysis on the extraction of cellulose nanocrystals (cncs): a review*, *cellulose chemistry and technology Cellulose Chem. Technol*. Available at: https://doi.org/https://doi.org/10.35812/CelluloseChemTechnol.2022.56.61.

Mokhena, T.C. and John, M.J. (2020) “Esterified cellulose nanofibres from saw dust using vegetable oil,” *International Journal of Biological Macromolecules*, 148, pp. 1109–1117. Available at: https://doi.org/10.1016/j.ijbiomac.2020.01.278.

Mondal, K., Bhagabati, P., Goud, V. V., Sakurai, S. and Katiyar, V. (2021) “Utilization of microalgae residue and isolated cellulose nanocrystals: A study on crystallization kinetics of poly(ε-caprolactone) bio-composites,” *International Journal of Biological Macromolecules*, 191, pp. 521–530. Available at: https://doi.org/10.1016/j.ijbiomac.2021.09.114.

Motloung, B., Pfukwa, R. and Klumperman, B. (2024) “Ion-Mediated Gelation of Thermo-Responsive Cellulose Nanofibril/Poly(N-isopropylacrylamide) Hybrid Hydrogels with Tunable De-Swelling Kinetics,” *Macromolecular Materials and Engineering*, 309(8). Available at: https://doi.org/10.1002/mame.202300457.

Motloung, M.P., Ojijo, V., Bandyopadhyay, J. and Ray, S.S. (2020) “Morphological characteristics and thermal, rheological, and mechanical properties of cellulose nanocrystals-containing biodegradable poly(lactic acid)/poly(ε-caprolactone) blend

composites," *Journal of Applied Polymer Science*, 137(19). Available at: https://doi.org/10.1002/app.48665.

N'Gatta, K.M., Assanvo, E.F., El Hayek, J., Masquelez, N., Kamgang Syapnjeu, P., Deabate, S., Bonniol, V., Soussan, L., Zamora-Ledezma, C., Elango, J., Flaud, V., Boa, D. and Salameh, C. (2025) "3D-Printed Polycaprolactone Scaffolds Reinforced with Cellulose Nanocrystals and Silver Nanoparticles for Bone Tissue Engineering," *ACS Applied Materials and Interfaces* [Preprint]. Available at: https://doi.org/10.1021/acsami.5c06504.

Nourany, M., Makaremy, A., Bazrpash, S. and Hosseini, S. (2025) "Bimodal macroporous 3D scaffolds based on compatibilized PCL and PLA blend using PCL-PEG-PCL block copolymers and cellulose nanocrystals for osteogenic differentiation of hMSCs," *International Journal of Biological Macromolecules*, 299. Available at: https://doi.org/10.1016/j.ijbiomac.2025.140149.

Ntrivala, M.A., Pitsavas, A.C., Lazaridou, K., Baziakou, Z., Karavasili, D., Papadimitriou, M., Ntagkopoulou, C., Balla, E. and Bikiaris, D.N. (2025) "Polycaprolactone (PCL): the biodegradable polyester shaping the future of materials – a review on synthesis, properties, biodegradation, applications and future perspectives," *European Polymer Journal*. Elsevier Ltd. Available at: https://doi.org/10.1016/j.eurpolymj.2025.114033.

Phanthong, P., Reubroycharoen, P., Hao, X., Xu, G., Abudula, A. and Guan, G. (2018) "Nanocellulose: Extraction and application," *Carbon Resources Conversion*. KeAi Publishing Communications Ltd., pp. 32–43. Available at: https://doi.org/10.1016/j.crcon.2018.05.004.

Pracella, M., Haque, M.M.U. and Puglia, D. (2014) "Morphology and properties tuning of PLA/cellulose nanocrystals bio-nanocomposites by means of reactive functionalization and blending with PVAc," *Polymer*, 55(16), pp. 3720–3728. Available at: https://doi.org/10.1016/j.polymer.2014.06.071.

Qiao, X., Wang, Z. and Sun, K. (2022) "Renewable rice straw cellulose nanofibril reinforced poly(ε-caprolactone) composite films," *Materials Chemistry and Physics*, 292. Available at: https://doi.org/10.1016/j.matchemphys.2022.126879.

Rao R.Umamaheswara, Venkatanarayana, B. and Suman, KN.S. (2019) *ScienceDirect Enhancement of Mechanical Properties of PLA/PCL (80/20) Blend by Reinforcing with MMT Nanoclay*. Available at: https://doi.org/https://doi.org/10.1016/j.matpr.2019.06.280.

Rashtchian, M., Hivechi, A., Bahrami, S.H., Milan, P.B. and Simorgh, S. (2020) "Fabricating alginate/poly(caprolactone) nanofibers with enhanced bio-mechanical properties via cellulose nanocrystal incorporation," *Carbohydrate Polymers*, 233. Available at: https://doi.org/10.1016/j.carbpol.2020.115873.

Refinetti, D., Sonzogni, A., Manenti, F., Lima, N.M.N., Linan, L.Z. and Filho, R.M. (2014) "Modeling and simulation of poly(l-lactide) polymerization in batch reactor," *Chemical Engineering Transactions*, 37, pp. 691–696. Available at: https://doi.org/10.3303/CET1437116.

Rocha, J.M., Sousa, R.P.C.L., Sousa, D., Tohidi, S.D., Ribeiro, A., Fangueiro, R. and Ferreira, D.P. (2025) "Polycaprolactone-Based Fibrous Scaffolds Reinforced with

Cellulose Nanocrystals for Anterior Cruciate Ligament Repair," *Applied Sciences (Switzerland)*, 15(5). Available at: https://doi.org/10.3390/app15052301.

Ruz-Cruz, M.A., Herrera-Franco, P.J., Flores-Johnson, E.A., Moreno-Chulim, M. V., Galera-Manzano, L.M. and Valadez-González, A. (2022) "Thermal and mechanical properties of PLA-based multiscale cellulosic biocomposites," *Journal of Materials Research and Technology*, 18, pp. 485–495. Available at: https://doi.org/10.1016/j.jmrt.2022.02.072.

Rytlewski, P., Gohs, U., Stepczyńska, M., Malinowski, R., Karasiewicz, T. and Moraczewski, K. (2022) "Electron-induced structural changes in flax fiber reinforced PLA/PCL composites, analyzed using the rule of mixtures," *Industrial Crops and Products*, 188. Available at: https://doi.org/10.1016/j.indcrop.2022.115587.

Saeidlou, S., Huneault, M.A., Li, H. and Park, C.B. (2012) "Poly(lactic acid) crystallization," *Progress in Polymer Science*. Elsevier Ltd, pp. 1657–1677. Available at: https://doi.org/10.1016/j.progpolymsci.2012.07.005.

Salmani, M.R., Shirazi, F., Goodarzi, K., Noormohammadi, F. and Nourany, M. (2024) "Improving Phase Compatibility of PLA-PCL Matrix-Droplet Blend Using CNC/PCL-PEG-PCL Triblock Copolymer to Prepare Porous 3D Osteoinductive Scaffolds," *Journal of Polymers and the Environment* [Preprint]. Available at: https://doi.org/10.1007/s10924-024-03392-5.

Şen, İ. and Sever, K. (2025) "Production and characterization of agricultural waste natural fiber-filled polylactic acid composites," *Polymer Bulletin*, 82(9), pp. 4051–4074. Available at: https://doi.org/10.1007/s00289-025-05698-3.

Sessini, V., Navarro-Baena, I., Arrieta, M.P., Dominici, F., López, D., Torre, L., Kenny, J.M., Dubois, P., Raquez, J.M. and Peponi, L. (2018) "Effect of the addition of polyester-grafted-cellulose nanocrystals on the shape memory properties of biodegradable PLA/PCL nanocomposites," *Polymer Degradation and Stability*, 152, pp. 126–138. Available at: https://doi.org/10.1016/j.polymdegradstab.2018.04.012.

Shin, B.Y. and Han, D.H. (2017) "Viscoelastic properties of PLA/PCL blends compatibilized with different methods," *Korea Australia Rheology Journal*, 29(4), pp. 295–302. Available at: https://doi.org/10.1007/s13367-017-0029-8.

Sikhosana, S. T., Gumede, T.P., Malebo, N.J., Ogundeji, A.O. and Motloung, B. (2023) " The influence of cellulose content on the morphology, thermal, and mechanical properties of poly(lactic acid)/ Eucomis autumnalis cellulose biocomposites ," *Polymer Engineering & Science* [Preprint]. Available at: https://doi.org/10.1002/pen.26293.

Sikhosana, Sylvia T., Gumede, T.P., Malebo, N.J., Ogundeji, A.O. and Motloung, B. (2023) "Medicinal plants as a cellulose source for the fabrication of poly(lactic acid) composites: A mini-review," *Polymers from Renewable Resources*. SAGE Publications Ltd, pp. 44–57. Available at: https://doi.org/10.1177/20412479221146249.

Slouf, M., Ujcic, A., Nevoralova, M., Vackova, T., Fambri, L. and Kelnar, I. (2020) "Monitoring of Morphology and Properties During Preparation of PCL/PLA Microfibrillar Composites With Organophilic Montmorillonite," *Frontiers in Materials*, 7. Available at: https://doi.org/10.3389/fmats.2020.00188.

Soriano-Cuadrado, B., Fontecha-Cámara, M.Á., Mañas-Villar, M., Delgado-Blanca, I. and Ramírez-Rodríguez, M.D. (2024) “Mechanical, Thermal and Morphological Study of Bio-Based PLA Composites Reinforced with Lignin-Rich Agri-Food Wastes for Their Valorization in Industry,” *Polymers*, 16(17). Available at: https://doi.org/10.3390/polym16172462.

Trivedi, A.K. and Gupta, M.K. (2024) “PLA based biodegradable bionanocomposite filaments reinforced with nanocellulose: development and analysis of properties,” *Scientific reports*, 14(1), p. 23819. Available at: https://doi.org/10.1038/s41598-024-71619-5.

Vala, N.S., Bavaliya, K.J., Raj, M. and Raj, L. (2025) “Compatibilization Strategies for PLA/PCL Blends: Tuning Thermal, Mechanical, and Biodegradation Properties via Functionalized PCL Derivatives,” *Polymer-Plastics Technology and Materials* [Preprint]. Available at: https://doi.org/10.1080/25740881.2025.2560913.

Vidakis, N., Petousis, M., Michailidis, N., David, C., Mountakis, N., Papadakis, V., Sfakiotakis, E., Sagris, D. and Argyros, A. (2024) “Optimization of cellulose nanocrystal (CNC) concentration in polycaprolactone bio-composites for bio-plotting: a robust interpretation of the reinforcement mechanisms,” *Cellulose*, 31(6), pp. 3657–3680. Available at: https://doi.org/10.1007/s10570-024-05851-7.

Wahbi, M., Wen, Y., Kontopoulou, M. and De France, K.J. (2025) “Modification of cellulose nanocrystals with epoxidized canola oil for enhancing interfacial compatibility with poly(lactic acid),” *Carbohydrate Polymers*, 370. Available at: https://doi.org/10.1016/j.carbpol.2025.124471.

Wang, W., Niu, B., Liu, R., Chen, H., Fang, X., Wu, W., Wang, G., Gao, H. and Mu, H. (2023) “Development of bio-based PLA/cellulose antibacterial packaging and its application for the storage of shiitake mushroom,” *Food Chemistry*, 429. Available at: https://doi.org/10.1016/j.foodchem.2023.136905.

Wang, Z.P., Ruan, W.H., Rong, M.Z. and Zhang, M.Q. (2024) “Injection molding of highly filled microcrystalline cellulose/polycaprolactone composites with the aid of reversible Diels-Alder reaction,” *Journal of Materials Science and Technology*, 170, pp. 246–254. Available at: https://doi.org/10.1016/j.jmst.2023.07.017.

Widjaja, T., Hendrianie, N., Nurkhamidah, S., Altway, A., Yusuf, B., F, F., Alifatul, A. and Pahlevi, A. (2023) “Poly lactic acid production using the ring opening polymerization (ROP) method using Lewis acid surfactant combined iron (Fe) catalyst (Fe(DS)3),” *Heliyon*, 9(8). Available at: https://doi.org/10.1016/j.heliyon.2023.e17985.

Widjaja, T., Rohmah, A.A.Z., Nurkhamidah, S., Ni’mah, H., Wardhono, E.Y., Saputra, B.Y.E. and Sari, C.Y. (2025) “Effectiveness study of Cellulose Nanocrystal (CNC) filler usage on polylactic acid (PLA) properties through plasticizer addition optimization: Application in paper-coated tableware,” *Case Studies in Chemical and Environmental Engineering*, 11. Available at: https://doi.org/10.1016/j.cscee.2025.101186.

Wongthanaroj, D., Jessmore, L.A., Lin, Y., Bergholz, T.M., Stark, N.M., Sabo, R.C. and Matuana, L.M. (2022) “Sustainable and eco-friendly poly (Lactic acid)/cellulose nanocrystal nanocomposite films for the preservation of oxygen-sensitive food,” *Applied Food Research*, 2(2). Available at: https://doi.org/10.1016/j.afres.2022.100222.

Woodruff, M.A. and Hutmacher, D.W. (2010) “The return of a forgotten polymer - Polycaprolactone in the 21st century,” *Progress in Polymer Science (Oxford)*. Elsevier Ltd, pp. 1217–1256. Available at: https://doi.org/10.1016/j.progpolymsci.2010.04.002.

Wu, C., Wu, B., Abdalkarim, S.Y.H., Wang, M., Zou, Z., Jin, M. and Yu, H.Y. (2025) “Synergistic enhancement and spherulite growth mechanism of PLA composites by multi-dimensional mineralized cellulose nanocrystals,” *Carbohydrate Polymers*, 366. Available at: https://doi.org/10.1016/j.carbpol.2025.123926.

Wu, J. jun, Gao, N., Jiang, L., Zhong, G. ji, Deng, C. and Gao, X. (2022) “The coupling effect of cellulose nanocrystal and strong shear field achieved the strength and toughness balance of Polylactide,” *International Journal of Biological Macromolecules*, 207, pp. 927–940. Available at: https://doi.org/10.1016/j.ijbiomac.2022.03.172.

Xiao, Y., Ding, Y., Qiu, J., Zhang, X., Zheng, Y., Huang, C., Zhao, L., Tang, Z., Chen, Y., Liu, Y., Zhao, K., Guo, K., Jing, L., Ding, M., Zong, C., He, J. and Tian, L. (2024) “Treatment effects of 3D-printed PCL/Fe3O4@ ZIF-8 magnetic nanocomposite on infected bone defect,” *International Journal of Bioprinting*, 10(4), pp. 297–318. Available at: https://doi.org/10.36922/ijb.2271.

Xu, C., Chen, C. and Wu, D. (2018) “The starch nanocrystal filled biodegradable poly(ε-caprolactone) composite membrane with highly improved properties,” *Carbohydrate Polymers*, 182, pp. 115–122. Available at: https://doi.org/10.1016/j.carbpol.2017.11.001.

Yamane, H. and Sasai, K. (2003) “Effect of the addition of poly(D-lactic acid) on the thermal property of poly(L-lactic acid),” *Polymer*, 44(8), pp. 2569–2575. Available at: https://doi.org/10.1016/S0032-3861(03)00092-2.

Ye, G., Yong, Q., Hu, L., Rosqvist, E., Peltonen, J., Hu, Y., Xu, W. and Xu, C. (2025) “Molecular engineering of nanocellulose-poly(lactic acid) bio-nanocomposite interface by reactive surface grafting from copolymerization,” *International Journal of Biological Macromolecules*, 306. Available at: https://doi.org/10.1016/j.ijbiomac.2025.141371.

Ye, G., Yu, Y., Wu, C., Zhang, H., Zhao, Y., Bi, H. and Xu, C. (2025) “Molecular engineering of nanocellulose copolymer by grafting from homopolymerization of caprolactone: A revisit to temperature condition,” *Industrial Crops and Products*, 235. Available at: https://doi.org/10.1016/j.indcrop.2025.121699.

Zhu, B., Wang, Y., Liu, H., Ying, J., Liu, C. and Shen, C. (2020) “Effects of interface interaction and microphase dispersion on the mechanical properties of PCL/PLA/MMT nanocomposites visualized by nanomechanical mapping,” *Composites Science and Technology*, 190. Available at: https://doi.org/10.1016/j.compscitech.2020.108048.

Chapter 3

EXPERIMENTAL PAPER

This chapter will be submitted to a peer-reviewed journal under the title:

Effect of sugarcane bagasse-derived cellulose nanocrystals on the thermal, structural, morphological and biodegradation properties of poly(ε-caprolactone) and poly(lactic acid)

Mbongeni Ngwenya[1], Thandi P. Gumede[1], Ricardo Arpad Pérez Camargo[2] and Bennie Motloung[3*]*

[1]Department of Life Sciences, Faculty of Health and Environmental Sciences, Central University of Technology, Free State, Bloemfontein 9301, South Africa

[2]POLYMAT and Department of Polymers and Advanced Materials: Physics, Chemistry, and Technology, Faculty of Chemistry, University of the Basque Country UPV/EHU, Paseo Manuel de Lardizábal, 3, Donostia-San Sebastián 20018, Spain

[3]Department of Chemistry and Polymer Science, Faculty of Science, Stellenbosch University, Matieland 7602, South Africa

*Corresponding authors:

Thandi P. Gumede, tgumede@cut.ac.za and Bennie Motloung, motloung@sun.ac.za

Abstract

Biodegradable materials have gained significant attention as alternatives for petroleum-based non-biodegradable polymers. This study investigates biodegradable nanocomposites based on poly(ε-caprolactone) (PCL) and poly(lactic acid) (PLA), reinforced with 1, 3 and 5 wt.% cellulose nanocrystals (CNCs) extracted from sugarcane bagasse, *via* melt blending, i.e., PCL/CNC and PLA/CNC. DSC, SEM, WAXS/SAXS, FTIR, TGA and biodegradation tests were used to evaluate the influence of CNCs on the thermal, morphological, structural and biodegradation properties of the polymers. The results showed that CNCs enhanced the crystallinity of PLA only at 1 wt.% CNCs loading, while PCL crystallinity increased at 3 and 5 wt.% CNCs loading. The incorporation of CNCs did not improve the thermal stability of either polymer. The biodegradation rate of PCL/CNCs nanocomposites increased with the increasing CNCs loading, with weight losses of 6.3%, 12.1% and 36.4% for 1, 3 and 5 wt.% CNCs, respectively, compared to 5.4% for neat PCL over 112 days. For PLA, only 3 and 5 wt.% CNCs loading significantly accelerated biodegradation, resulting in weight losses of 8 and 82.2%, respectively, over the same period. The novelty of this study lies in the systematic comparative evaluation of sugarcane-derived CNCs on both PLA and PCL nanocomposites under identical processing and characterization conditions, providing new insights into how a single renewable nanofiller influences two major biodegradable polymers. These findings demonstrate that CNCs derived from agricultural waste can accelerate the biodegradation of PCL and PLA, offering a promising route for developing sustainable, environmentally friendly polymeric materials.

Keywords: poly(ε-caprolactone); poly(lactic acid); cellulose nanocrystals; biodegradable; sugarcane bagasse

3.1 Introduction and Background

The global demand for sustainable and biodegradable materials has driven significant interest in biopolymers such as poly(lactic acid) (PLA) and poly(ε-caprolactone) (PCL). PLA is derived from renewable resources such as corn starch, providing degradation under specific conditions. PLA is known for its high tensile strength and biodegradability yet suffers from brittleness and low thermal stability (Wang *et al.*, 2023). PCL, despite being a synthetic polymer, also offers biodegradable characteristics while promising alternatives to conventional petroleum-based plastics (Fernández-Tena *et al.*, 2023) PCL exhibits excellent flexibility and thermal stability but degrades more slowly and has lower mechanical strength (Kurakula, Rao and Yadav, 2020).

A growing body of research has shown that the incorporation of nanoscale reinforcements, such as cellulose nanocrystals (CNCs), can further enhance the performance of biopolymer matrices without affecting their biodegradable features (Ngwenya *et al.*, 2025). CNCs are rod-like crystalline domains derived from native cellulose, characterized by their high surface area, mechanical strength and biodegradability. Among the various lignocellulosic biomass sources (Selikane *et al.*, 2022; Sylvia T. Sikhosana *et al.*, 2023), sugarcane bagasse, an abundant agricultural byproduct, offers a cost-effective and sustainable source for the production of CNCs. CNCs extracted from sugarcane bagasse not only contribute to value-added waste utilization but also serve as excellent nanofillers due to their relative compatibility with biopolymer matrices (Mahmud and Anannya, 2021; Gond et al., 2022; Chen et al., 2023; Khoo et al, 2023; Sriwong et al, 2023).

Incorporating CNCs into PLA and PCL matrices has been shown to influence key material properties, including thermal behavior, crystallinity, morphology, mechanical performance and biodegradability (Ngwenya *et al.*, 2025). The degree of these effects depends on factors such as CNCs dispersion, interfacial interaction and polymer blend composition. Numerous studies have investigated PCL/CNCs composites, detailing different nanocellulose sources, compositions, fabrication techniques and improved properties across various target applications. It is clear that the incorporation of CNCs has a profound effect on enhancing the properties of PCL such as tensile modulus, thermal stability and barrier properties. For example, PCL/CNCs prepared by solution

casting demonstrate promising enhancements in several key properties, including tensile modulus, biodegradability and moisture barrier behavior (Hassan *et al.*, 2012). Similarly, PLA/CNCs composites exhibit improvements in mechanical, thermal and barrier properties, tailored for applications such as packaging, medical engineering and automotive industries (Zhao et al., 2018; Gond et al., 2022; Khoo et al, 2023).

Despite these prior studies, few investigations have systematically evaluated the effect of sugarcane bagasse-derived CNCs on both PLA and PCL with respect to their thermal, structural, morphological and biodegradation behaviour under identical processing and characterization conditions.

The novelty of this study lies in providing a comprehensive comparative analysis of the influence of sugarcane bagasse-derived CNCs on both PLA and PCL matrices, elucidating their synergistic impact on multiple performance parameters (thermal, structural, morphological, and biodegradation properties) in a single, systematic framework. Through detailed characterization, the work seeks to elucidate how the addition of a renewable nanofiller influences the performance of these biopolymers, providing insights into the development of advanced, eco-friendly materials for sustainable applications.

3.2 Materials and methods

3.2.1 Materials

Cellulose nanocrystals

Saccharum officinarum, commonly known as sugarcane (Figure 3.1a), is a grass species that belongs to the family Poaceae, class Liliopsida, and order Poales. It is a globally cultivated cash crop and the primary feedstock for sugar production (Zhao *et al.*, 2018; Gan and Chow, 2019; Wani *et al.*, 2023). After sugar extraction through milling, the remaining fibrous residues are known as bagasse (Figure 3.1b). In this study, bagasse was collected from a farm in KwaZulu-Natal, South Africa. It typically comprises approximately 40–50% cellulose, 25–35% hemicellulose and 5–10% lignin (Alokika *et al.*,

2021; Melesse, Hone and Mekonnen, 2022). The focus of this study was on cellulose because of its high tensile strength, biodegradability, biocompatibility and chemical modifiability characteristics in line with those of the PCL and PLA, making it a key interest in green composite development (Chaka, 2022; Fitch-Vargas *et al.*, 2023; S. T. Sikhosana *et al.*, 2023).

Cellulose extraction:

Figure 3.1 illustrates the process of extracting CNCs from sugarcane bagasse. Ground sugarcane bagasse (40 g) (Figure 3.1b) was screened to 30-mesh particle size, and de-waxed using a 2:1 (v/v) toluene:ethanol mixture for six hours to remove surface waxes and extractive. The de-waxed bagasse (Figure 3.1c) was then treated with 800 mL distilled water at 80 °C for two hours to remove soluble impurities. Delignification was achieved using a 1.3% sodium chlorite solution, maintaining pH between 3.5 and 4.0 with 6 M acetic acid, repeated until a cream white product was obtained (Figure 3.1d). The delignified fibers were further treated with 2% NaOH for two hours, followed by 5% NaOH at 90 °C for two hours. The residue was filtered, washed to a neutral pH, and oven-dried at 105 °C for six hours (Figure 3.1e) (Alokika *et al.*, 2021; Zhu *et al.*, 2022).

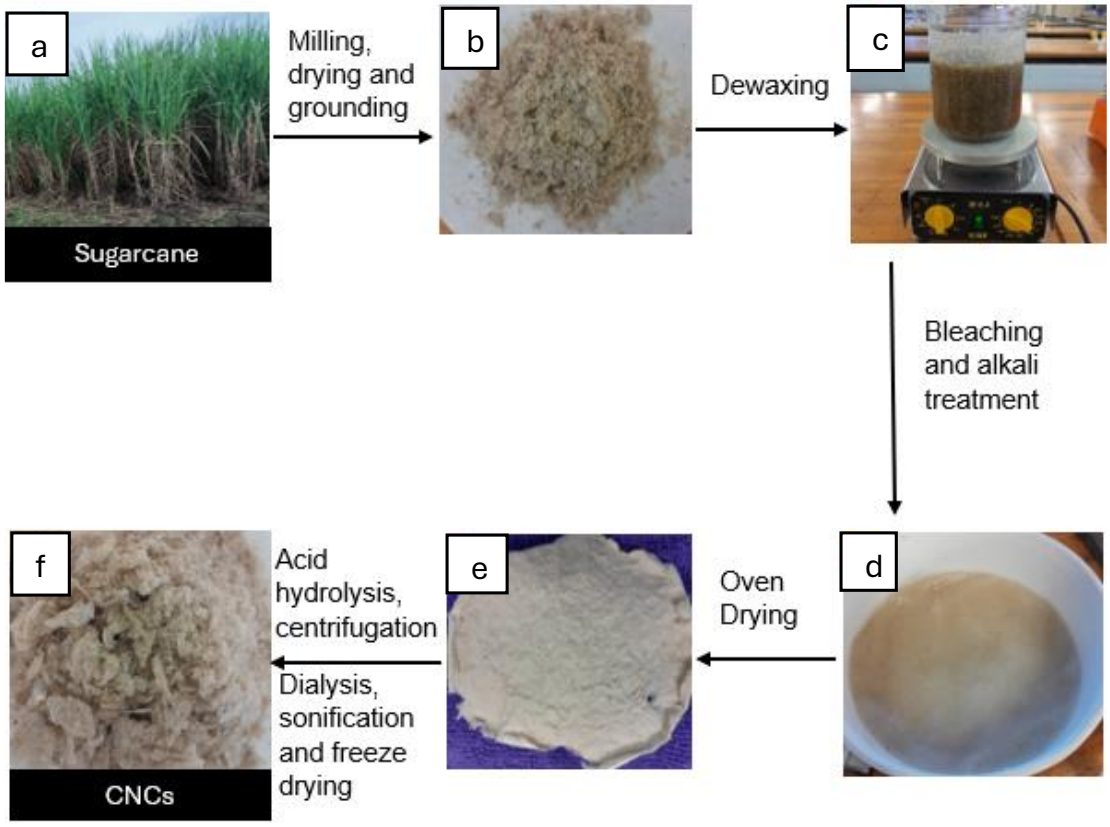

Figure 3.1. Extraction of CNCs from sugarcane bagasse.

Cellulose nanocrystals extraction:

The dried cellulose (Figure 3.1e) was subjected to acid hydrolysis using 50% H_2SO_4 at a cellulose-to-acid ratio of 1:10 g/mL at 45°C for one hour, with constant stirring using a homogenizer. To terminate the reaction, 10-fold ice-cold distilled water was added, followed by centrifugation at 10 000 rpm for 15 minutes (three cycles, at 10°C). The collected sediment was dialyzed against distilled water for ~48 hours until a neutral pH was achieved. The resulting suspension (5 mg/mL) was sonicated for 10 minutes in an ice bath to prevent overheating. The resulting CNCs (Figure 3.1f) were obtained by freeze-drying the suspension (0.2 wt.% in distilled water) at reduced pressure and low temperature, producing a light brownish fine powder while preserving particle integrity and porosity (Padhi, Singh and Routray, 2023; Asadnia and Sadat-Shojai, 2025; Dabhi *et al.*, 2025). Table 3.1 presents the percentage yield of cellulose and CNCs. From 40 g of sugarcane bagasse, 10.5 g of cellulose was obtained (26.3% yield), which was further converted into 7.7 g of CNCs (19.25% yield). These values indicate an efficient extraction

process, consistent with literature ranges (18–25%). Furthermore, the yield provides sufficient CNCs for subsequent incorporation into the selected polymer matrices, namely PCL and PLA.

Table 3.1 Extraction yield of cellulose and cellulose nanocrystals from sugarcane bagasse

Sample	Mass of the ground powder (g)	Mass of cellulose (g)	% yield of cellulose	Mass of CNCs (g)	% yield of CNCs
Sugarcane bagasse	40	10.5	26.3	7.7	19.25

Note: CNCs = cellulose nanocrystals

Poly(lactic acid)

PLA granules were purchased from 2M BIOTEC LLP 180 Annal Gandhiadigal Salai, Ramanathapuram 623501, TN in India. It has a glass transition temperature (T_g) of 55–60°C, a melting temperature (T_m) of 145–155°C, and a density of 1,23 g/cm^3.

Poly(ε-caprolactone)

PCL granules were purchased from 2M BIOTEC LLP 180 Annal Gandhiadigal Salai, Ramanathapuram 623501, TN in India. It has a glass transition temperature (T_g) of −60°C, a melting temperature (T_m) of 40–60°C, and a density of 1,10 g/cm^3.

3.3 Sample preparation

Conditioning

Table 3.2 summarizes the drying conditions used to remove residual moisture from PLA, PCL and CNCs before melt-blending. PLA and CNCs were dried at 50°C, while PCL was dried at 40°C, all under vacuum overnight. Proper drying at these controlled temperatures is important for preventing hydrolytic degradation during processing, as both PLA and PCL are moisture sensitive at elevated temperatures, while CNCs readily retain bound water due to their hydroxyl-rich surfaces. Ensuring consistent drying

therefore improved process reproducibility and minimized variations in the resulting thermal and morphological properties.

Table 3.2 Drying conditions for poly(lactic acid), poly(ε-caprolactone) and cellulose nanocrystals

Material	Drying conditions
Poly(lactic acid)	50°C, in vacuum oven, overnight
Poly(ε-caprolactone)	40°C, in vacuum oven, overnight
Cellulose nanocrystals	50°C, in vacuum oven, overnight

Melt blending

Table 3.3 shows the compositions of PCL, PLA and CNCs in the nanocomposites prepared in this study. CNCs were incorporated into each polymer at 1, 3, and 5 wt.% to investigate the effects of filler concentration, with 1 wt.% representing a low content, 3 wt.% an intermediate level and 5 wt.% a high loading where agglomeration might occur. A total of 40 g of the combined materials (PCL, PLA and CNCs) were weighed and processed. Melt blending was carried out using a Brabender Plastograph at 180 °C and 50 rpm for 12 minutes. The blended samples were allowed to cool at room temperature overnight for recrystallization, and the solidified materials were then compression-molded using a hydraulic press at 180 °C for five minutes under 50 kPa pressure. This systematic variation in CNCs concentration allowed for the correlation of filler content with the thermal, structural and biodegradation performance of the resulting nanocomposites.

Table 3.3 Compositions of PCL, PLA and CNCs in the prepared nanocomposites.

Sample name	PLA (wt.%)	PCL (wt.%)	CNCs (wt.%)
Neat PLA	100	0	0
Neat PCL	0	100	0

Neat CNCs	0	0	100
PCL/CNCs (99/1)	0	99	1
PCL/CNCs (97/3)	0	97	3
PCL/CNCs (95/5)	0	95	5
PLA/CNCs (99/1)	99	0	1
PLA/CNCs (97/3)	97	0	3
PLA/CNCs (95/5)	95	0	5

Note: PCL = poly(ε-caprolactone); PLA = poly(lactic acid) and CNCs = cellulose nanocrystals

3.4 Sample characterization

Differential scanning calorimetry

DSC was performed using PerkinElmer DSC 6000. Prior to sample analysis, the DSC instrument was calibrated using the onset melting temperatures of 419.5 °C for zinc, 156.6 °C for indium, and also the melting enthalpy of 28 J/g for indium, and 108 J/g for zinc. Samples (~6.0 mg) were heated from 0 to 180 °C (first heating scan), held at this temperature for three minutes to erase the thermal history, next cooled from 180 to 0 °C (cooling scan), held for one minute at 0 °C for conditioning, and finally subsequently heated from 0 to 180 °C (second heating scan). The scanning rate in all steps was 10 °C per minute, and the experiments were conducted using a 20 mL per minute nitrogen flow. Cooling and second heating scans were used to determine thermal transitions.

Scanning electron microscopy

Samples were cryo-fractured, mounted on aluminium pin stubs using epoxy glue, and sputter-coated with Iridium using a Leica EM ACE600 Imaging was performed on a JEOL JSM-7800F Extreme-resolution analytical field emission SEM, at 5 kV, 10 mm working distance.

X-ray diffraction analysis

Simultaneous SAXS/WAXS was performed at beamline BL11-NCD, ALBA Synchrotron, Barcelona, Spain. Samples were placed in DSC pans on a Linkam THMS600 hot stage, cooled/heated via a liquid nitrogen system. The thermal protocol involved: Heat 20 °C per minute from 25 to 180 °C, held for three minutes at 180 °C, cool 20 °C per minute from 180 °C to 0 °C, held for one minute at 0 °C, heat 20 °C per minute from 0 to 180 °C, mimicking the employed conditions in the DSC, and taken SAXS/WAXS patterns during the heating and cooling ramps. The X-ray energy was 12,4 keV (ʎ = 1,0 Å). The X-ray energy was 12,4 keV (ʎ = 1,0 Å). Two detectors. Calibrated with silver behenate (SAXS) and Cr_2O_3 (WAXS) standards, were employed: ADSC Q315r detector, 3 070 × 3 070 pixels, pixel size 102 μm^2, distance 6 495 mm, tilt angle 0° for SAXS. Rayonix LX255-HS detector, 1 920 × 5 760 pixels, pixel size 44 μm^2, distance 132.6 mm, tilt angle 21.2° for WAXS. The scattering intensity versus scattering vector ($q = 4\pi\sin\theta/\lambda$) was analyzed.

Fourier transformed infrared spectroscopy

Fourier transformed infrared spectroscopy (FTIR) spectra were obtained using a PerkinElmer Spectrum 100 FTIR spectrometer equipped with a PIKE MiracleTM attenuated total reflectance, with a diamond crystal. Background scans were collected before each measurement. Scans were recorded over a range of 4 000 and 650 cm^{-1}, at 8 cm^{-1} resolution, with eight scans per sample.

Thermogravimetric analysis

Thermogravimetric analysis (TGA) was carried out using PerkinElmer STA 6000 under 20 mL per minute nitrogen. Samples (~23 mg) were heated from 30 to 600 °C at a rate of 10 °C per minute. Data analysis was done using Pyris software.

Tensile testing

Tensile testing was carried out using AGS-X machine. Tensile specimens with dimensions of 75 mm length, 5 mm width, 2 mm thickness, and a gauge length of 20 mm were analyzed. The tensile testing analysis was carried out at 10 mm per minute test rate.

Biodegradation analysis

Aerobic biodegradability was determined by cutting small specimens of each sample and burying them in soil (4 cm deep, 39% moisture) at room temperature for 112 days following ASTM D5988. At 14-day intervals, samples were retrieved, washed with water, dried at 30°C for one hour, and weighed. Photographs were taken at each point to visually monitor degradation.

3.5 Results and discussion

3.5.1 Thermal properties

Differential scanning calorimetry

Thermal properties were analyzed using DSC, focusing on parameters such as crystallization temperature (T_c), glass transition temperature (T_g), cold crystallization temperature (T_{cc}), melting temperature (T_m), enthalpies (ΔH) and degree of crystallinity (X_c), which was calculated using Equation 3.1. These parameters provided insights into how CNCs influence the thermal transitions of PCL and PLA,as shown in Figures 3.2 to 3.4 and Tables 3.4 and 3.5.

$$X_c = \left(\frac{\Delta H_m - \Delta H_{cc}}{w\Delta H_{m^o}}\right) \times 100\% \qquad 3.1$$

In Equation 3.1, X_c is the degree of crystallinity, ΔH_m is the melting enthalpy of the measured sample, ΔH_{cc} is the cold crystallization enthalpy of the measured sample, $\Delta H_m{}^o$ is the melting enthalpy of 100% crystalline polymer, and w is the weight fraction of a polymer in the blend or composite. The values of $\Delta H_m{}^o$ used for PCL and PLA are 139 J/g and 93.7 J/g, respectively (Naseem *et al.*, 2022; Fernández-Tena *et al.*, 2023). DSC results for neat PLA and neat PCL, and their nanocomposites with 1, 3, and 5 wt.% CNCs are presented in Figures 3.2 and 3.3 and Tables 3.4 and 3.5.

Figures 3.2a and 3.2b present the cooling and second heating scans for neat PCL and PCL/CNCs nanocomposites with 1, 3 and 5 wt.% CNCs loading. Figure 3.2a shows that PCL has a T_c of 18.4 °C, which increases with increasing CNCs content, reaching a

maximum at 3 wt.%. This shift reflects a nucleating effect of CNCs on the PCL matrix. In contrast, for CNCs content of 5 wt.%, the T_c is lower than that of the neat PCL, thus acting as an anti-nucleating agent, a behavior, in this case, attributed to CNCs agglomeration, in line with other works in the literature.

Figure 3.2b show the melting behavior, in which two endothermic peaks in both neat PCL and nanocomposites is present, and attributed to a melting/recrystallization process. At CNC contents ≤ 3 wt.%, where CNCs act as nucleating agent, the T_m positions is slightly higher than neat PCL, indicating that CNCs improve the thermal stability of the crystals, but for CNCs content > 3 wt.%, the T_m decreases due to agglomeration, in which CNCs limit or interrupt the crystallization of PCL. The melting temperatures as a function of CNCs content are presented in the appendix as Figure A1.

The competition between nucleation effect and anti-nucleating effect (cause by agglomeration) is also reflected in the X_c, which displayed higher values as CNCs content increase, and next a decrease at the highest CNCs content. Li and Wu reported that CNCs enhance crystallinity of PCL at low concentrations but decrease it at higher loadings due to agglomeration (Li and Wu, 2022).

Neat PCL shows two distinct melting peaks at 45.6°C and 52.2°C, suggesting the coexistence of crystals with different levels of perfection, which might be due to the crystallization process (Lattimer *et al.*, 1992; Xu, Chen and Wu, 2018). The measured ΔH_m of 56 J/g closely matches the ΔH_c of 54 J/g, with a T_c of 18.4°C and the degree of crystallinity of 40.3%. For PCL/CNCs, at 1 wt.% CNCs, there is minimal impact on the transitions, but at 3 wt.%, CNCs act as nucleating agents, increasing T_c and ordering PCL crystals into a single melting peak (Bi *et al.*, 2023; Chen *et al.*, 2023). At 5 wt.% CNCs, the melting peaks shift to lower temperatures, suggesting CNCs saturation, possibly due to agglomeration effects.

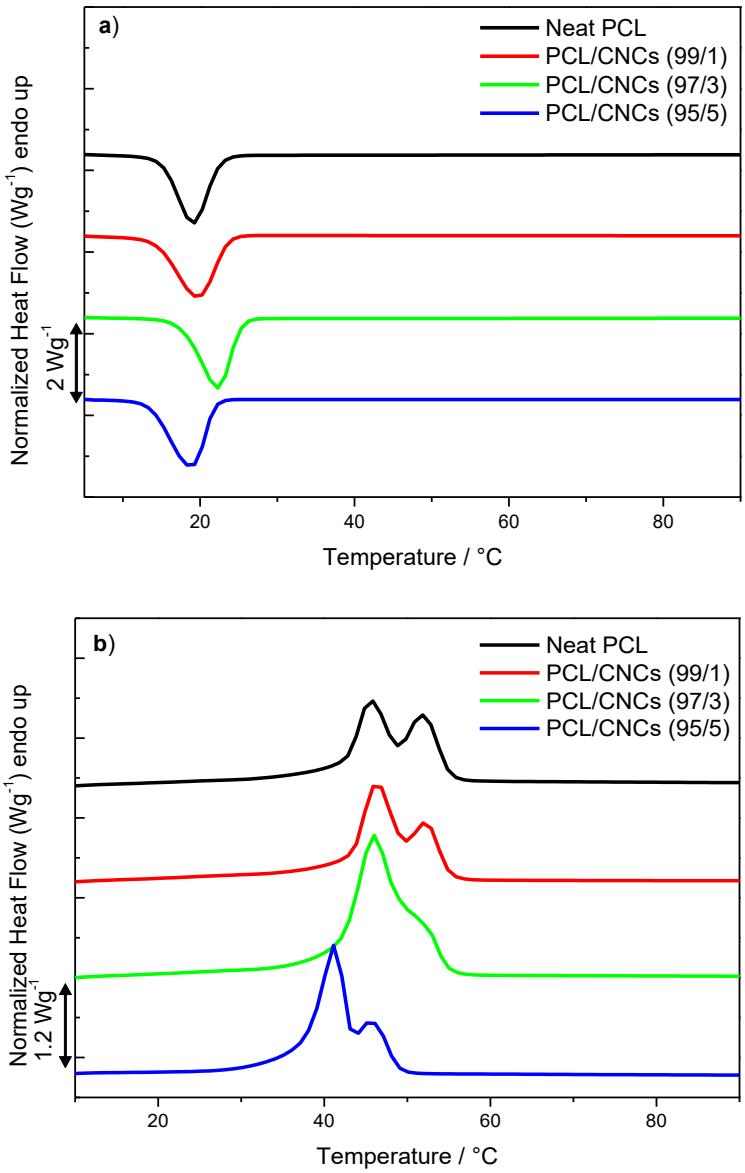

Figure 3.2 Differential scanning calorimetry curves: (a) cooling curves for neat PCL and PCL/CNCs nanocomposites, and (b) second heating curves for neat PCL and PCL/CNCs nanocomposites containing 1, 3 and 5 wt.% CNCs.

Figure 3.3a and b present the cooling and the second heating scans of neat PLA and PLA/CNCs nanocomposites with 1, 3 and 5 wt.% CNCs loading. Neat PLA exhibits a T_g at 59.6°C, a T_{cc} at 113.3°C, and a T_m at 149.1 °C, with a degree of crystallinity of 7.5%. The presence of a cold crystallization peak indicates that PLA cannot crystallize completely during cooling. PLA/CNCs (Figure 3.3b) show reduced T_g, indicating certain flexibility of PLA chains in the presence of CNCs, due to poor interaction between hydrophilic CNCs and hydrophobic PLA. However, only 5 wt.% of CNCs can shift T_{cc} to lower values, as a

nucleating agent. At all filler loadings, a T_{cc} is detected for PLA, indicating that even in the presence of CNCs, it cannot crystallize during cooling. The presence of CNCs provokes a decrease in the T_m values with increasing CNCs content (presented in the supporting information as Figure 1Ab), which can be attributed to agglomeration problems or interactions that affect the mobility of the chains. Double melting peaks are observed at 3 and 5 wt.% CNCs loading, indicating the formation of α'- and α-form crystals due to disrupted chain alignment during blending (Goffin *et al.*, 2011; Ruz-Cruz *et al.*, 2022). The reduced crystallinity of PLA at higher CNCs loadings may be attributed to CNCs agglomeration, which can disrupt polymer chain ordering. This phenomenon also helps explain the shift in melting behavior observed in the DSC curves (Figure 3.3b). The presence and extent of CNCs agglomeration will be further examined in the SEM analysis presented in the following section.

Figure 3.4 presents the effect of incorporating 1, 3 and 5 wt.% CNCs on the degree of crystallinity of PCL and PLA. On one hand, the results show that incorporating CNCs into PCL increased crystallinity at 3 and 5 wt.% CNCs loadings. In particular, 3 wt.% CNCs acted as nucleating agent, increasing the crystallinity of PCL by 14.6%. On the other hand, the degree of crystallinity of PLA slightly increased by 2.2% only at 1 wt.% CNCs loading. Increasing CNCs loading (3 and 5 wt.%) decreases the X_c of neat PLA.

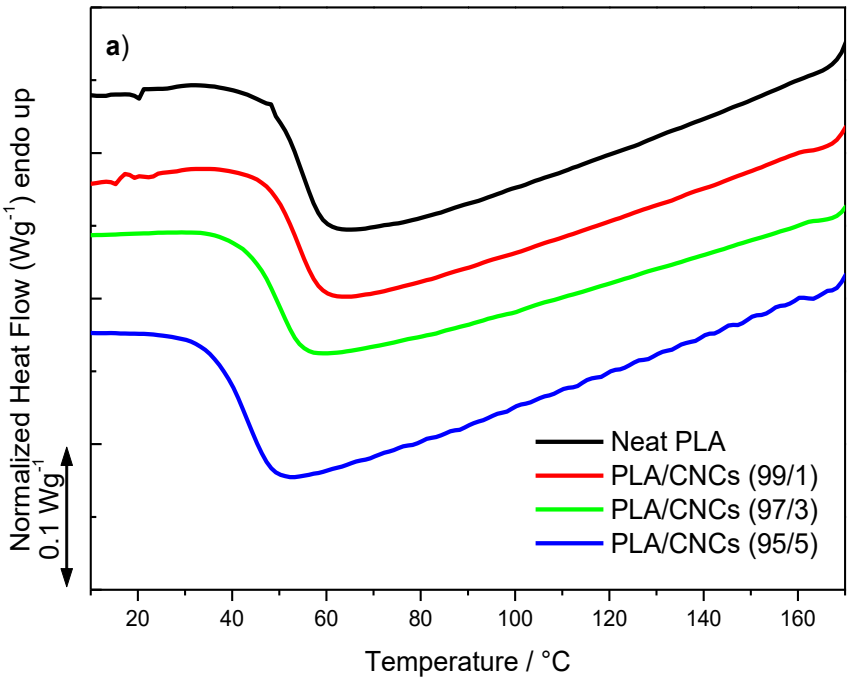

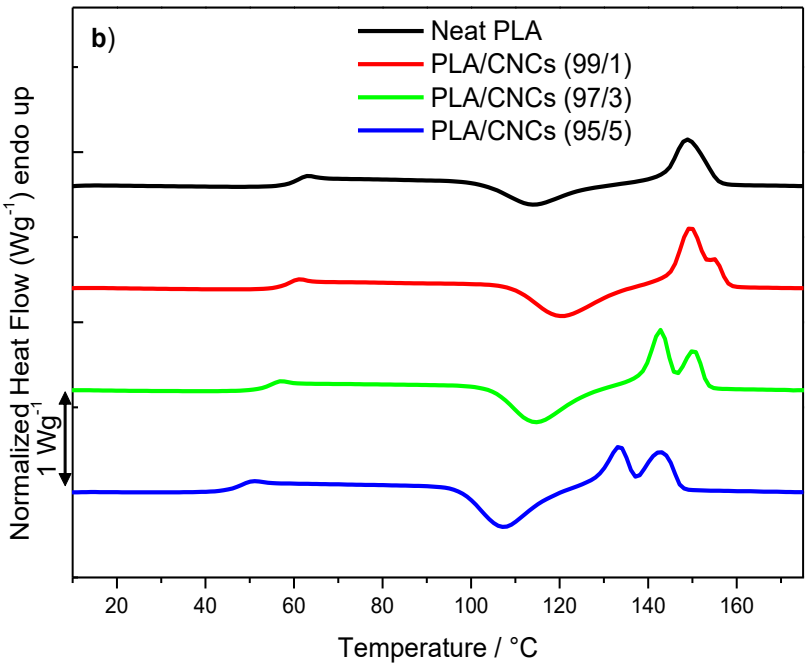

Figure 3.3 **Differential scanning calorimetry curves: (a) cooling curves for neat PLA and PLA/CNCs nanocomposites, and (b) second heating curves for neat PLA and PLA/CNCs nanocomposites containing 1, 3 and 5 wt.% CNCs.**

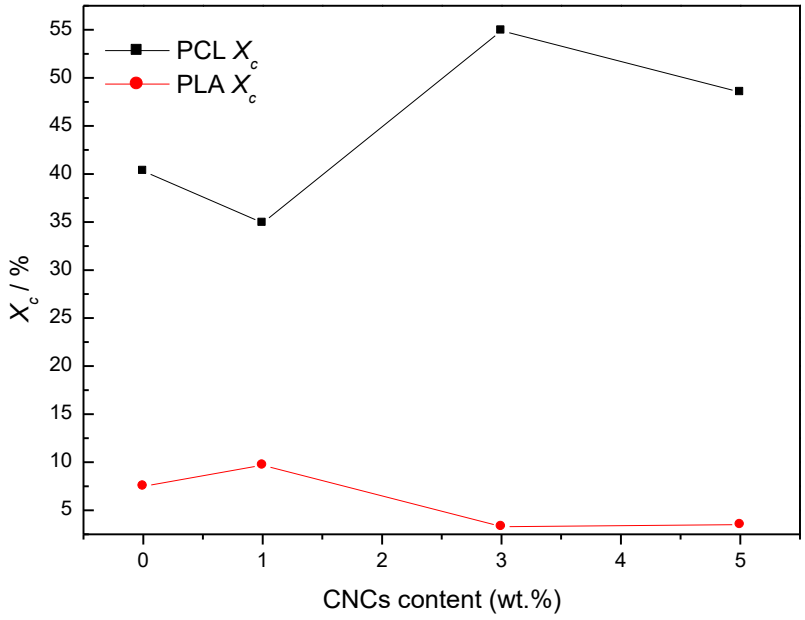

Figure 3.4 **Degree of crystallinity of PCL and PLA in nanocomposites containing 1, 3 and 5 wt.% CNCs.**

Table 3.4 DSC results for PCL and PCL/CNCs nanocomposites containing 1, 3 and 5 wt.% CNCs.

Sample	PCL T_c / °C & ΔH_c / J/g		PCL T_m / °C & ΔH_m / J/g			PCL X_c / %
	T_c	ΔH_c	T_{m1}	T_{m2}	ΔH_m	
Neat PCL	18.4±0.0	54±0.1	45.6±0.2	52.2±0.1	56±0.4	40.3
PCL/CNCs (99/1)	21.5±0.0	57±0.1	46.3±0.2	52.5±0.2	48±0.4	34.9
PCL/CNCs (97/3)	22.2±0.0	80±0.7	46.1±0.0	–	74±0.4	54.9
PCL/CNCs (95/5)	19.0±0.0	56±0.3	41.1±0.0	45.2±0.3	64±0.2	48.5

Note: PCL = Poly(ε-caprolactone); CNCs = Cellulose nanocrystals; ΔH_m = melting enthalpy; ΔH_c = crystallization enthalpy; ΔH_{cc} = cold crystallization enthalpy; T_c = crystallization temperature; T_{cc} = cold crystallization temperature; T_g = glass transition temperature; T_m = melting peak temperature; and X_c = degree of crystallinity.

Table 3.5 DSC results for PLA and PLA/CNCs nanocomposites containing 1, 3, and 5 wt.% CNCs.

Sample	PLA T_g / °C	PLA T_{cc} / °C & ΔH_{cc} / J/g		PLA T_m / °C & ΔH_m / J/g			PLA X_c / %
		T_{cc}	ΔH_{cc}	T_{m1}	T_{m2}	ΔH_m	
Neat PLA	59.6±0.1	113.3±0.5	14±1.5	149.1±0.1	–	21±0.2	7.5
PLA/CNCs (99/1)	57.6±0.2	120.1±0.1	21±1.0	149.0±1.1	155.3±0.1	30±0.3	9.7
PLA/CNCs (97/3)	53.6±0.0	115.7±0.0	21±0.8	142.8±0.0	150.4±0.2	24±0.0	3.3
PLA/CNCs (95/5)	46.6±0.1	108.6±0.0	20±1.8	133.6±0.0	142.4±0.3	23±0.4	3.5

Note: PLA = Poly(lactic acid); CNCs = Cellulose nanocrystals; ΔH_m = melting enthalpy; ΔH_c = crystallization enthalpy; ΔH_{cc} = cold crystallization enthalpy; T_c = crystallization temperature; T_{cc} = cold crystallization temperature; T_g = glass transition temperature; T_m = melting peak temperature; and X_c = degree of crystallinity.

3.5.2 Morphological analysis

Scanning electron microscopy

Figure 3.5 presents SEM micrographs illustrating the morphological characteristics of neat CNCs, neat polymers (PCL and PLA), and their nanocomposites with 1, 3 and 5 wt.%

CNCs. SEM analysis provides insights into phase compatibility, dispersion and interfacial interactions of the components. Neat CNCs (Figure 3.5a) appear as rod-like structures with a length range from 230 nm to 850 nm, consistent with their nanoscale dimensions (Nang Vu *et al.*, 2024). Neat PCL (Figure 3.5b), in contrast, exhibits a smooth and homogeneous surface, characteristic of its ductile and semicrystalline nature. Neat PLA (Figure 3.5c) displays a rough fractured surface, indicative of its brittle nature and amorphous morphology. These morphological features align with WAXS and SAXS results, where PLA showed minimal crystalline order, while PCL exhibited broader but distinct crystalline reflections.

For PCL/CNCs nanocomposites (Figure 3.5d to 3.5f), the fractured surface remains smooth at low CNCs content, for example, PCL/CNCs (99/1) (Figure 3.5d), with a slight increase in roughness due to CNCs inclusion. For PCL/CNCs (97/3), the nanocomposite morphology (Figures 3.5e) suggests an interaction between PCL and CNCs, as CNCs are embedded in the PCL matrix. DSC results also suggest that 3 wt.% CNCs ordered the crystals of PCL to be of the same size and increased the crystallinity of the nanocomposite. At higher CNCs loadings, for example, PCL/CNCs (95/5) (Figure 3.5f), surface roughness increases significantly, and CNCs aggregates are visible, reflecting reduced dispersion, which might be due to saturation.

In PLA/CNCs nanocomposites (Figures 3.5g to 3.5i), poor interfacial adhesion is evident, with edge formation and cracking observed on the fractured surfaces. These defects increase with CNCs content, highlighting compatibility issues between the hydrophilic CNCs and the hydrophobic PLA matrix. At 5 wt.% CNCs (Figure 3.5i), large CNCs agglomerates form (see the arrow). The observed CNCs agglomeration at higher loadings changes surface roughness as well as reduces dispersion uniformity. Gond *et al.,* also reported in similar observations (Gond and Gupta, 2020; Gond *et al.*, 2022). These authors evaluated the properties of PLA/CNCs nanocomposites (with CNCs loadings of 1, 2, 3, 4 and 5 wt.%). They discovered that higher CNCs loadings (>2 wt.%) in the PLA matrix result in agglomeration. SEM analysis revealed that at higher CNCs loadings (5 wt.%), nanoparticles tended to agglomerate, disrupting the uniformity of the polymer matrix. This agglomeration correlates with the DSC results, where a decrease in crystallinity and a shift in the melting temperature was observed. The reduced

crystallinity can thus be attributed to the presence of CNCs clusters, which hinder polymer chain ordering and act as less effective nucleation sites compared to well-dispersed nanoparticles.

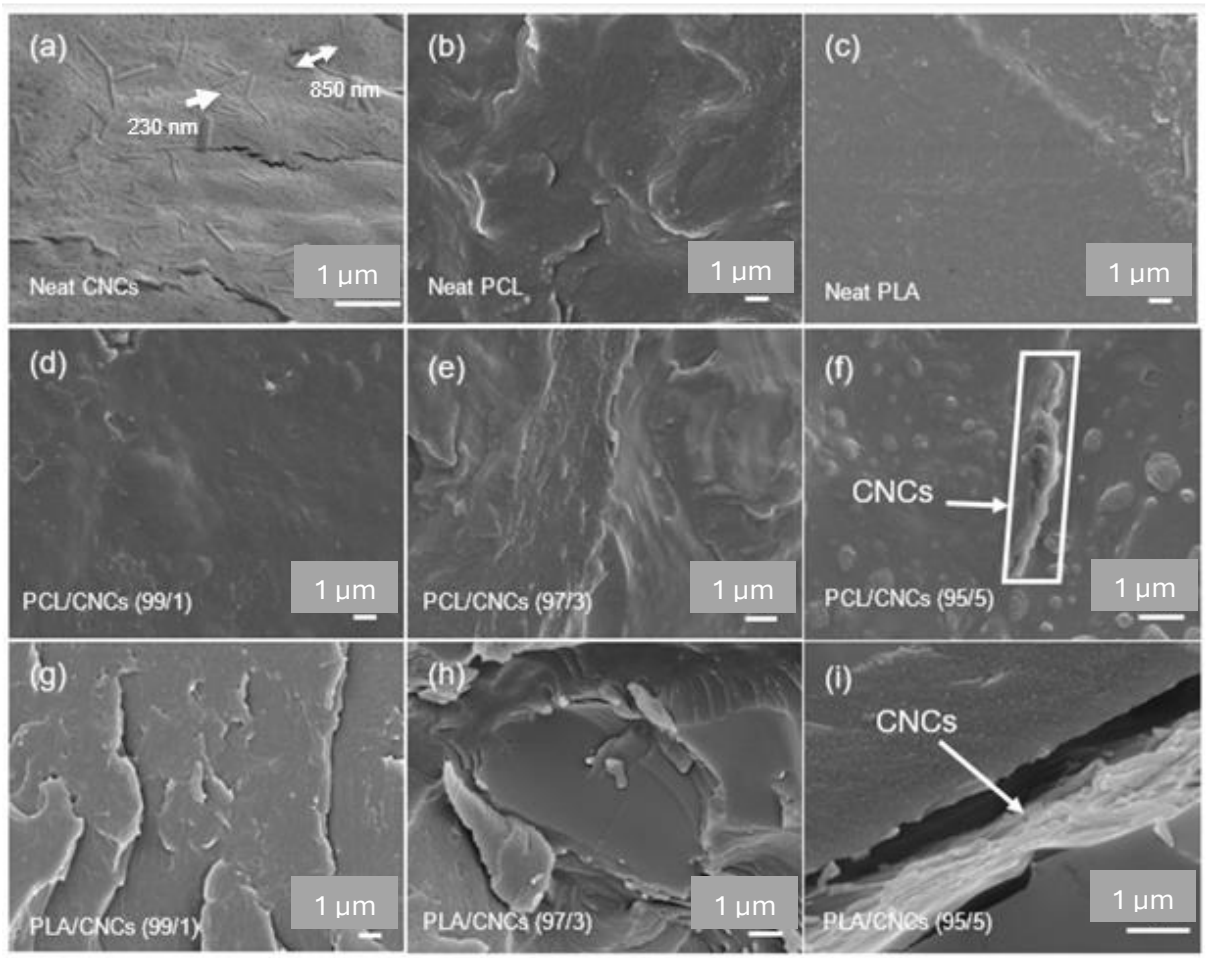

Figure 3.5 Morphological features of neat CNCs, neat PCL and PCL/CNCs nanocomposites, and neat PLA and PLA/CNCs nanocomposites with CNCs loadings of 1, 3, and 5 wt.%.

3.5.3 Structural analysis

Wide angle X-ray scattering

The WAXS patterns, intensity (*I*) vs scattering vector (*q*) (Figure 3.6), provide insight into the crystalline structures of neat polymers (PCL and PLA), neat CNCs, and their

nanocomposites with 1, 3 and 5 wt.% CNCs loading. Table 6 presents their crystallinity (X_{cx}) which was calculated by Equation 2:

$$X_{cx} = \frac{I_c}{I_c + I_a} \qquad 3.2$$

where I_c and I_a are respectively the integrated intensities of the crystalline and amorphous phases. Illustrative example for crystallinity calculation is presented in appendix Figure A1.

Figure 3.6a presents the WAXS spectra of neat PCL and its nanocomposites with 1, 3 and 5 wt.% CNCs. Neat PCL presents broader peaks at q = 15.0 and 17.0 nm^{-1}, with crystallinity of 17.9% assigned to its 110 and 200 planes (Sun *et al.*, 2014; Gumede *et al.*, 2017). Minor peaks around 27.0 and 31.0 nm^{-1} indicate a long-range crystalline order (Motloung *et al.*, 2020). Neat CNCs reveal sharp, intense peaks at q = 26.8, 31.0, 44.1, 51.2 and 53.8 nm^{-1}, indicating high crystallinity (75.9%). The CNCs peaks are deviated to higher q values compared to the q values reported in literature which might be due to the source and processing of CNCs (Motloung *et al.*, 2020; Salmani *et al.*, 2024; Islam *et al.*, 2025). For example, Motloung *et al.*, presented WAXS results for spray dried CNCs with q = 10.6, 14.6, 15.8 and 24.1 nm^{-1}. The shift is due to the decreased inter-planar spacing (d) in the CNCs. The decrease in d-spacing may be caused by thicker packing of crystals or a modification process such as drying methods (Kádár, Spirk and Nypelö, 2021). PCL/CNCs nanocomposite scans show characteristics of PCL peaks with a slight shift to higher q values, which confirms the interaction of PCL and CNCs. At 1 wt.% CNCs loading, PCL crystallinity decreased, while it increased at 3 and 5 wt.%. Three weight percentage CNCs are the optimum loading for better crystallinity. These results are in agreement with DSC results, where 3 wt.% CNCs acted as a nucleating agent and also arranged PCL crystals of the same order.

Figure 3.6b presents WAXS patterns for neat PLA, neat CNCs, and their nanocomposites with 1, 3 and 5 wt.% CNCs. Neat PLA exhibits two sharp crystalline peaks at q values of 11.6 and 13.3 nm^{-1}, with crystallinity of 8.9%, corresponding to the 110/200 and 203 planes of the α-form crystal structure (Sun *et al.*, 2014; Díez-Rodríguez *et al.*, 2025). The PLA/CNCs nanocomposites spectra do not show any crystal peaks either for PLA or

CNCs. Only a halo band from 5 to 17 $nm^{-1,}$ which corresponds to the amorphous phase of PLA. This suggests that CNCs were unable to effectively induce crystallization during the cooling of PLA, probably due to agglomeration observed in SEM, which indicated that PLA and CNCs were not homogeneously dispersed (Figure 3.5i).

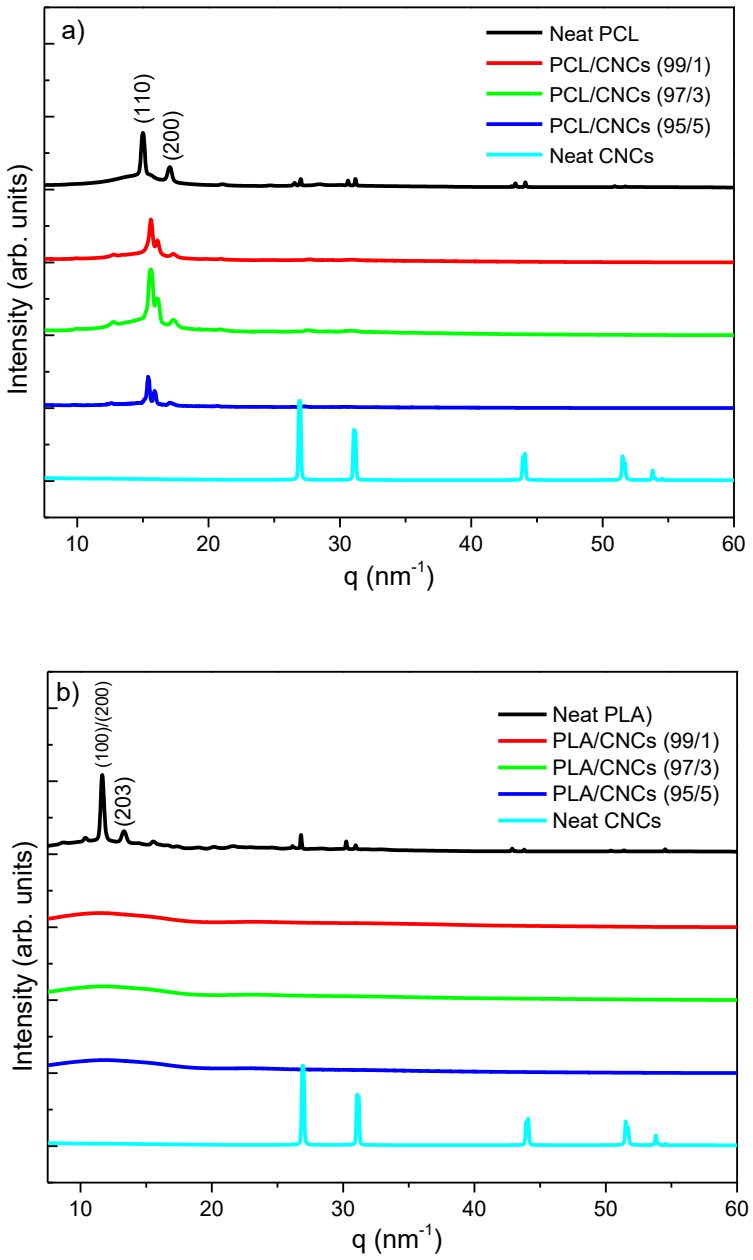

Figure 3.6 WAXS patterns of (a) neat PCL, neat CNCs and PCL/CNCs nanocomposites with 1, 3 and 5 wt.% CNCs, and (b) neat PLA, neat CNCs and PLA/CNCs nanocomposites with 1, 3 and 5 wt.% CNCs (data obtained from the second heating at 25 °C). (Results taken from second heating at 25 °C)

Table 3.6 Crystallinity of neat polymers (PCL and PLA), neat CNCs, and their nanocomposites.

Sample	I_c / %	(I_c+I_a) / %	X_{cx} / %
Neat PLA	0.00349	0.0392	8.9
Neat PCL	0.00756	0.0422	17.9
Neat CNCs	0.01265	0.02357	(75.9)
PCL/CNCs (99/1)	0.00651	0.03871	16.8
PCL/CNCs (97/3)	0.0140	0.06556	21.4
PCL/CNCs (95/5)	0.00399	0.0237	16.8
PLA/CNCs (99/1)	–	0.06553	–
PLA/CNCs (97/3)	–	0.06575	–
PLA/CNCs (95/5)	–	0.05862	–

Note: PLA = Poly(lactic acid); PCL = poly(ε-caprolactone); CNCs = cellulose nanocrystals

Small angle X-ray scattering

Figure 3.7 presents SAXS profiles for neat PCL, neat PLA, neat CNCs and their nanocomposites with 1, 3 and 5 wt.% CNCs loadings. SAXS provides insights into nanoscale morphology by analyzing periodicities of crystalline and amorphous layers. Table 3.7 presents the long period (L), representing the average spacing of lamellar structures, which was calculated using Equation 3.3, and lamellar thickness (l_c) calculated using Equation 3.4:

$$L = \frac{2\pi}{q_{max}} \qquad 3.3$$

where q_{max} is the position of the peak maximum in nm^{-1}.

$$l_c = L.X_{cx} \quad 3.4$$

where L is long period in nm and X_{cx} is the crystallinity.

Figure 3.7a presents SAXS patterns for neat PCL, neat CNCs and their nanocomposites with 1, 3 and 5 wt.% CNCs. Neat PCL exhibits a broader and more intense SAXS peak, with an *L* value of approximately 16.5 nm, suggesting the presence of semicrystalline lamellae with limited order (Gumede *et al.*, 2017). Neat CNCs do not show any peak in the SAXS range due to the lack of lamellar or long-range periodicity, CNCs are single crystallites, not lamellar systems. The addition of 1 and 5 wt.% CNCs to PCL resulted in very weak SAXS peaks, while the incorporation of 3 wt.% CNCs resulted in a broad intense SAXS peak, with an *L* value of approximately 13,7 nm, which is below that of neat PCL. This means that the spacing between crystalline lamellae (crystal + amorphous thickness) is smaller, suggesting that at 3 wt.% CNCs facilitate lamellar organization. These results are in agreement with WAXS and DSC results where it is observed that 3 wt.% CNCs improved the crystallinity of PCL. Figure 3.7b presents the scans of neat PLA, neat CNCs and their nanocomposites. Neat PLA and its nanocomposites show very weak or absent SAXS peaks, indicating a mostly amorphous structure, supported by the broad, less intense peaks in WAXS. SAXS profiles of intensity (*I*) as a function of scattering vector (*q*) are presented in the appendix (Figure A5), and they provide information like that presented in Figure 3.7.

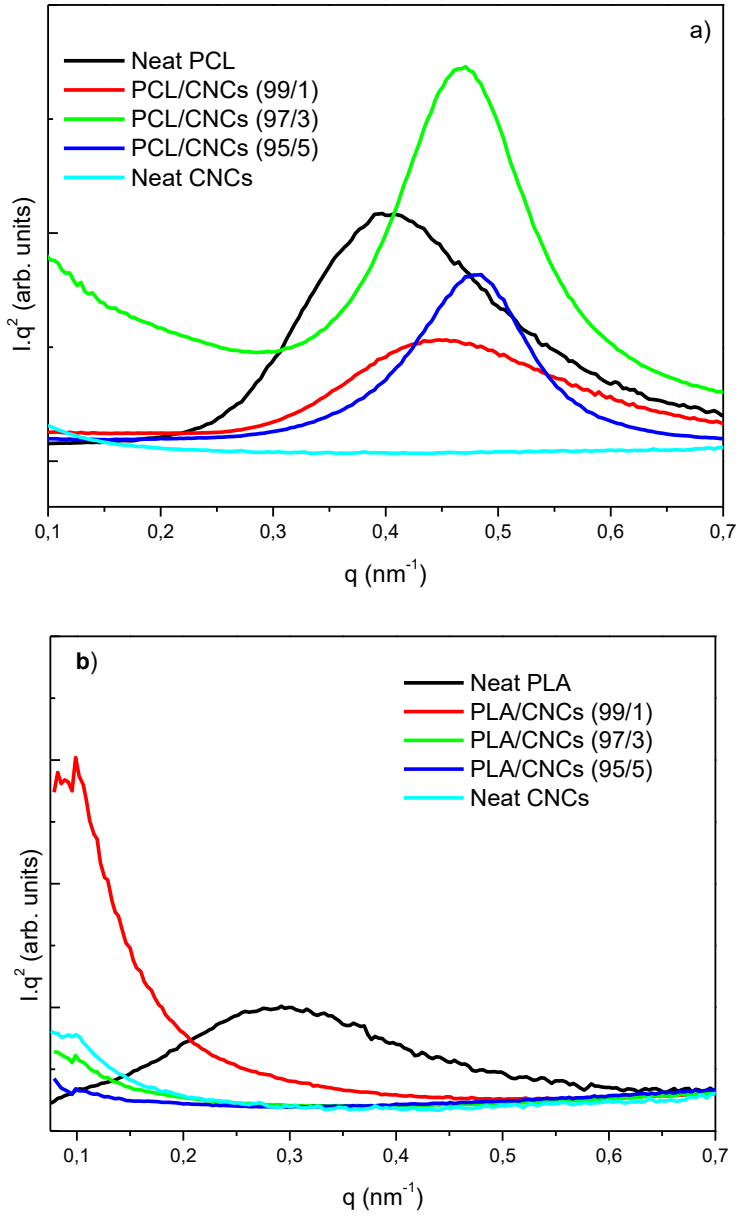

Figure 3.7 **SAXS patterns of (a) neat PCL, neat CNCs and PCL/CNCs nanocomposites with 1, 3 and 5 wt.% CNCs, and (b) neat PLA, neat CNCs and PLA/CNCs nanocomposites with 1, 3, and 5 wt.% CNCs (data obtained from the second heating at 25 °C.** (Results taken from second heating at 25 °C)

Table 3.7 **Small angle X-ray scattering parameters obtained from neat polymers, blends, and nanocomposites**

Sample	q_{max} / nm^{-1}	L / nm	l_c / nm.%
Neat PLA	0.29	21.7	193.1

Neat PCL	0.40	15.1	270.3
Neat CNCs	–	–	–
PCL/CNCs (99/1)	0.44	14.3	240.2
PCL/CNCs (97/3)	0.46	13.7	293.2
PCL/CNCs (95/5)	0.48	13.1	220.1
PLA/CNCs (99/1)	–	–	–
PLA/CNCs (97/3)	–	–	–
PLA/CNCs (95/5)	–	–	–

Note: PLA = Poly(lactic acid); PCL = poly(ε-caprolactone); CNCs = cellulose nanocrystals

Fourier transform infrared spectroscopy

The FTIR scans shown in Figure 3.8 present the characteristic functional groups of neat PCL, neat PLA, neat CNCs and nanocomposites with varying CNCs compositions. According to Figure 3.8a, neat PCL exhibits characteristic features, including a strong C=O stretching band at 1 730 cm^{-1}, and prominent C–O–C peaks at 1 263 cm^{-1} (asymmetric) and 1 173 cm^{-1} (symmetric). Additionally, C–H stretching vibrations are observed at 2 960 and 2 882 cm^{-1}. The FTIR spectrum of neat CNCs (Figure 3.8a and 3.8b) is characterized by a broad O–H stretching band at 3 330 cm^{-1}, reflecting intra- and intermolecular hydrogen bonding between hydroxyl groups. C–H stretching occurs at 2 977–2 892 cm^{-1}, while CH_2 symmetric bending bands appear at 1 437 cm^{-1} and 1 326 cm^{-1}, associated with aromatic ring vibrations in polysaccharides. The peak at 1 050 cm^{-1} is attributed to C–O–C stretching and C–H rocking vibrations of the pyranose ring (Kargarzadeh et al., 2012; Sirviö et al., 2016; Kostryukov et al., 2023; S. T. Sikhosana et al., 2023; Motloung et al, 2024).

The FTIR spectra of PCL/CNCs nanocomposites are in Figure 3.8a. The spectra are dominated by the characteristic peaks of PCL, likely due to the relatively low CNCs

content in the nanocomposites. No peak shifts or new bands were observed, indicating the absence of chemical interaction between PCL and CNCs. Similar findings have been reported by Grace *et al.*, Kumalo *et al.*, and Qiao *et al.* (Qiao et al, 2022; Grace et al., 2024; Kumalo et al., 2025).

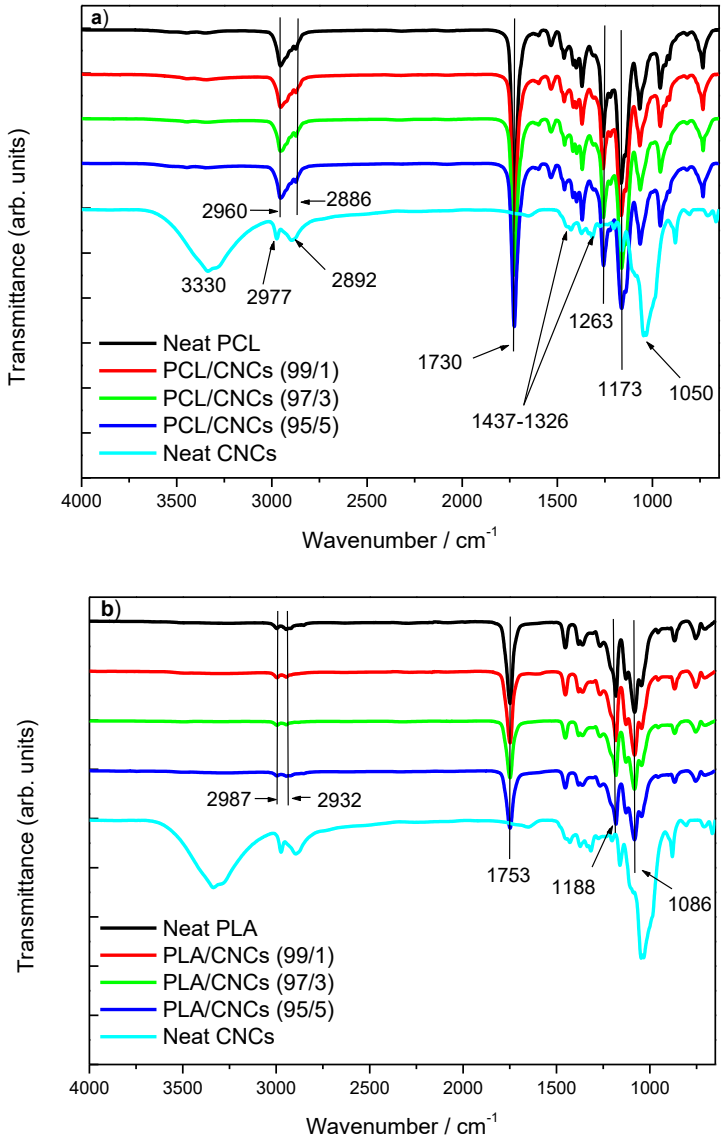

Figure 3.8 FTIR spectra for (a) neat PCL, neat CNCs and PCL/CNCs nanocomposites with 1, 3, and 5 wt.% CNCs; (b) neat PLA, neat CNCs and PLA/CNCs nanocomposites with 1, 3 and 5 wt.% CNCs.

Figure 3.8b presents the FTIR spectra of neat PLA, neat CNCs and PLA/CNCs nanocomposites with 1, 3 and 5 wt.% CNCs loadings. Neat PLA exhibits a medium-intensity C=O stretching peak at 1 753 cm^{-1}, corresponding to ester carbonyl groups. C–H stretching vibrations are observed at 2 987 and 2932 cm^{-1}, and C–O–C asymmetric

and symmetric stretching peaks appear at approximately 1 188 cm^{-1} and 1 086 cm^{-1}, respectively. In the PLA/CNCs nanocomposites, the spectra are dominated by PLA peaks, with only slight intensity changes as CNCs content increases. The minor reduction in intensity at higher CNCs loadings (e.g. PLA/CNCs (95/5)) might be attributed to hydrogen bonding between CNCs hydroxyl and PLA ester carbonyls, which can reduce the number of free hydroxyl groups and decrease the O–H stretching intensity. Sample thickness and CNCs concentration can also influence band intensities. Overall, no peak shifts or new bands were observed, indicating the absence of chemical interactions between PLA and CNCs (Dadras Chomachayi *et al.*, 2020; Gond and Gupta, 2020; Kalita *et al.*, 2020; Gond *et al.*, 2022; S. T. Sikhosana *et al.*, 2023).

3.5.4 Thermal stability

Thermogravimetric analysis

Thermal stability was assessed using TGA, as shown in Figures 3.9 and 3.10. The onset degradation temperature (T_{onset}), maximum degradation temperature (T_{max}), and residual weight ($W_{residue}$) for neat CNCs, neat polymers, and their nanocomposites are summarized in Tables 3.8 and 3.9. Figures 3.9a and 3.9b present the TGA and DTG curves, respectively, for neat PCL, neat CNCs and PCL/CNCs nanocomposites with varying CNCs loadings. Figures 10a and 10b show the TGA and DTG curves, respectively, for neat PLA, neat CNCs, and PLA/CNCs nanocomposites. The TGA curve of neat CNCs shows an initial weight loss around 100°C, attributed to moisture evaporation. Neat CNCs exhibit a two-step degradation process: the first step corresponds to the degradation of sulphated cellulose (sulphate-containing CNCs), while the second step is associated with the breakdown of the interior of non-sulphated crystalline cellulose (Xing *et al.*, 2018; Wang *et al.*, 2019). The T_{onset}, T_{max}, and $W_{residue}$ values for CNCs are reported in Table 8.

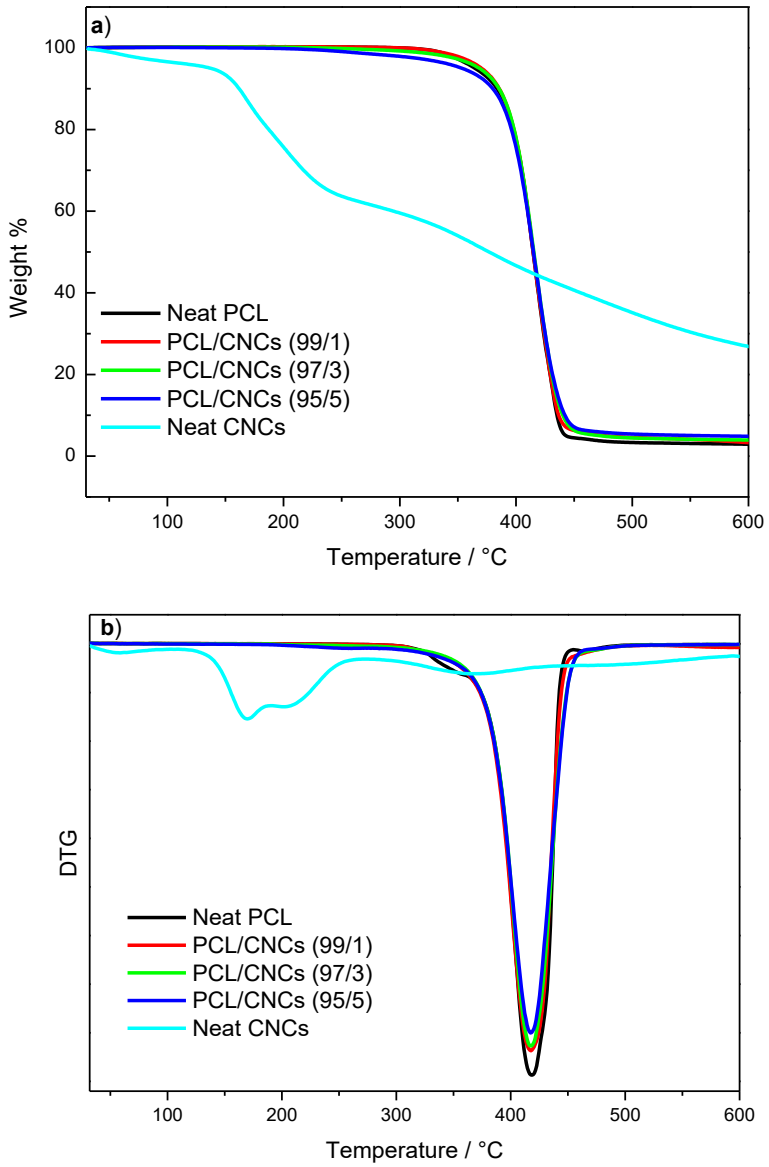

Figure 3.9 (a) TGA and (b) DTG curves for neat PCL, neat CNCs and PCL/CNCs nanocomposites with 1, 3 and 5 wt.% CNCs.

The addition of CNCs affects the thermal stability of PCL and PLA nanocomposites differently. For PCL/CNCs nanocomposites (Figures 3.9a and 3.9b), a low CNCs content (1 wt.%) slightly improves thermal stability, as indicated by an increased T_{onset} compared to neat PCL. However, at higher CNCs loadings (3 and 5 wt.%), thermal stability decreases, likely due to chain disruptions induced by CNCs agglomeration, as reported in Table 3.9. These results align with previous reports by (Hassan *et al.*, 2012; Motloung *et al.*, 2020).

In PLA/CNCs nanocomposites (Figures 3.10a and 3.10b), both T_{onset} and T_{max} decrease with increasing CNCs content (Table 3.9), reflecting the incorporation of thermally unstable CNCs. Despite this reduction in thermal stability, the presence of CNCs suppresses the escape of volatile degradation products, resulting in an increased char yield of the nanocomposites. These observations are in agreement with the DSC results, which show reduced PLA crystallinity at higher CNCs loadings.

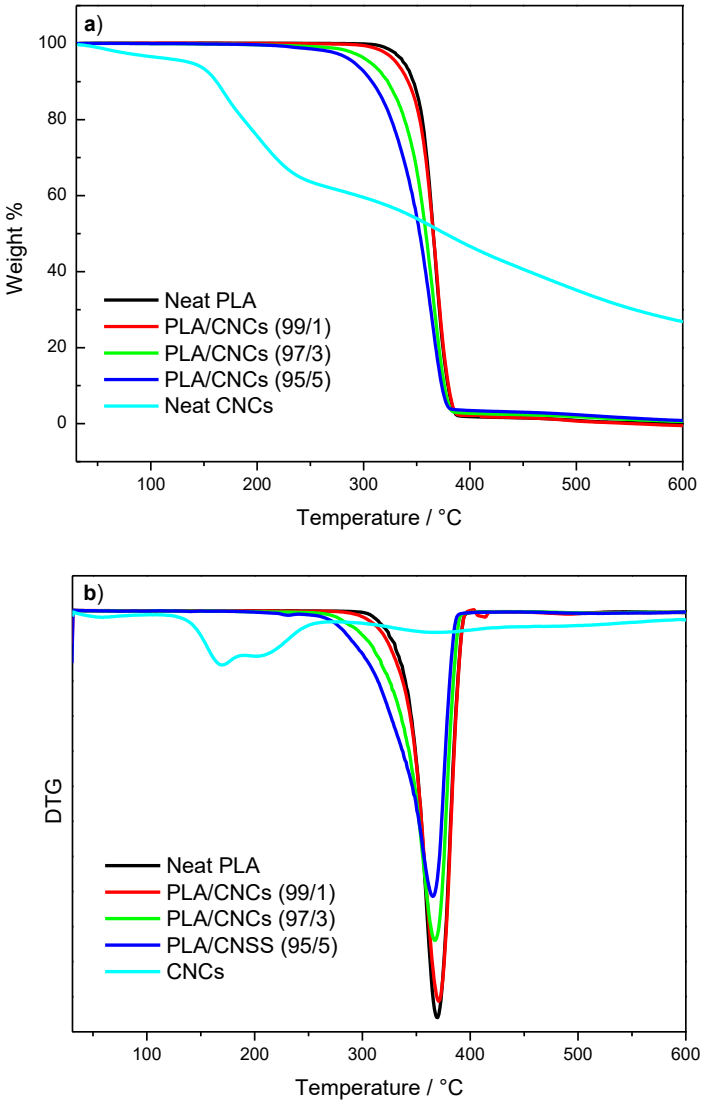

Figure 3.10 (a) TGA and (b) DTG curves for neat PLA, neat CNCs and PLA/CNCs nanocomposites with 1, 3 and 5 wt.% CNCs.

Table 3.8 Thermal characteristics of CNCs, including onset temperature, peak temperature and residual weight.

Sample	T_{1onset} / °C	T_{1max} / °C	T_{2onset} / °C	T_{2max} / °C	$W_{residue}$ / %
CNCs	128.4	168.8	299,4	368.8	26,9

Note: CNCs = Cellulose nanocrystals; T_{onset} = Onset temperatures; T_{max} = Peak temperatures; $W_{residue}$ = Residual weight

Table 3.9 Thermal characteristics of CNCs, including onset temperature, peak temperature and residual weight.

Sample	PLA T_{onset} / °C	PLA T_{max} / °C	PCL T_{onset} / °C	PCL T_{max} / °C	$W_{residue}$ / %
Neat PCL	–	–	298.9	418.0	3.1
PCL/CNCs (99/1)	–	–	310.3	417.9	3.3
PCL/CNCs (97/3)	–	–	289.6	417.9	3.9
PCL/CNCs (95/5)	–	–	243.1	417.9	4.8
Neat PLA	305.8	369.0	–	–	0.0
PLA/CNCs (99/1)	282.8	371.0	–	–	0.0
PLA/CNCs (97/3)	259.0	366.8	–	–	0.4
PLA/CNCs (95/5)	218.6	364.7	–	–	1.0

Note: PCL = poly(ε-caprolactone); PLA = poly(lactic acid) and CNCs = cellulose nanocrystals; T_{onset} = Onset temperatures; T_{max} = Peak temperatures; $W_{residue}$ = Residual weight

3.5.5 Biodegradation response and functional integration

Soil burial

The biodegradation of neat polymers and their nanocomposites was evaluated using a soil burial test, with results presented in Figure 3.11 and Tables 3.10 and 3.11. Degradation patterns for neat PCL and PCL/CNCs nanocomposites are shown in Figure

3.11a, while those for neat PLA and PLA/CNCs nanocomposites are presented in Figure 3.11b.

Comparing the neat polymers, PLA degraded by 0.3% over 112 days, whereas PCL exhibited a weight loss of 5.4% during the same period. Degradation rates are influenced by factors such as temperature, moisture, pH, and microbial activity. PLA typically requires higher temperature and humidity, as found in industrial composting conditions (Muniyasamy *et al.*, 2016; Kalita *et al.*, 2020), while PCL degrades faster in soil because of its flexibility, enzyme-accessible structure, low T_g, more permeable crystallinity, and direct susceptibility to microbial attack (Al Hosni, Pittman and Robson, 2019). Consequently, the soil conditions in this study favored faster degradation of PCL.

The incorporation of CNCs accelerated the degradation of PCL, with higher CNCs loadings resulting in greater weight loss (Figure 3.11a). Similarly, PLA/CNCs nanocomposites showed minimal effect at 1 wt.% CNCs, a slight increase in degradation at 3 wt.% CNCs (8%weight loss at day 112), and a pronounced increase at 5 wt.% CNCs, reaching 82.2% weight loss over the same period (Figure 3.11b). These results indicate that CNCs enhance the biodegradability of both PCL and PLA, with the effect being more pronounced at higher filler loadings. Table 3.11 provides digital images of the neat polymers and the nanocomposites samples with varying CNCs content at days 0, 42, 84 and 112, which visually correspond to the quantitative degradation data shown in Figure 3.11 and Table 3.10.

To summarize, biodegradation was accelerated significantly at both 3 and 5 wt.% CNCs loadings, for both polyesters, but it was only more pronounced at 5 wt.% CNCs.

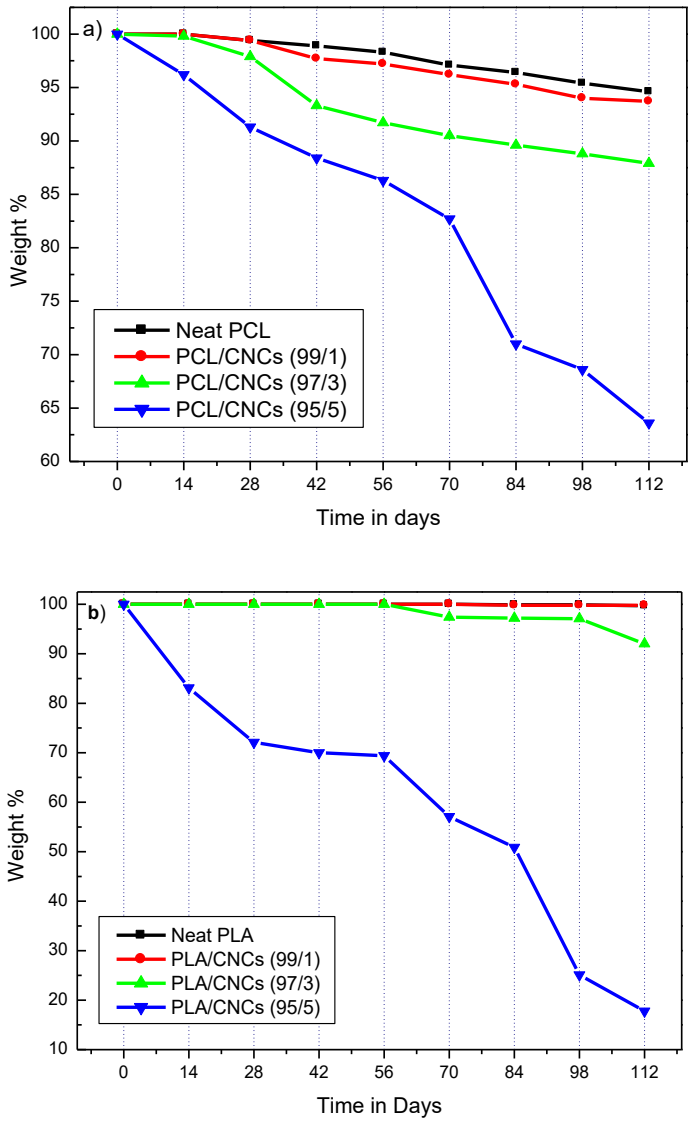

Figure 3.11 Mass loss (%) as a function of time (days) for (a) neat PCL and PCL/CNCs nanocomposite with 1, 3 and 5 wt.% CNCs and (b) neat PLA and PLA/CNCs nanocomposites with 1, 3 and 5 wt.% CNCs.

Table 3.10 Thermal characteristics of CNCs, including onset temperature, peak temperature and residual weight.

Sample	Day 0	Day 14	Day 28	Day 42	Day 56	Day 70	Day 84	Day 98	Day 112
Neat PCL	100	100	99.4	98.9	98.3	97.1	96.4	95.4	94.6
PCL/CNCs (99/1)	100	100	99.4	97.7	97.2	96.2	95.3	94.0	93.7
PCL/CNCs (97/3)	100	99.8	97.9	93.3	91.7	90.5	89.6	88.8	87.9
PCL/CNCs (95/5)	100	96.2	91.3	88.4	86.3	82.7	71.0	68.6	63.6

Neat PLA	100	100	100	100	100	100	99.9	99.9	99.7
PLA/CNCs (99/1)	100	100	100	100	100	100	99.8	99.8	99.8
PLA/CNCs (97/3)	100	100	100	100	100	97.4	97.2	97.1	92.0
PLA/CNCs (95/5)	100	83.1	72.1	70.0	69.4	57.1	50.9	25.1	17.8

Note: PCL = poly(ε-caprolactone); PLA = poly(lactic acid) and CNCs = cellulose nanocrystals

Table 3.11. Biodegradation of neat polymers, and their nanocomposites containing 1, 3 and 5 wt.% CNCs, with images captured at days 0, 42, 84 and 112.

Day 0		Day 42		Day 84		Day 112	
 Neat PLA	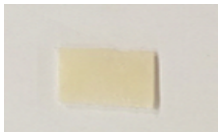 Neat PCL	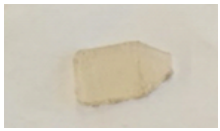 Neat PLA	 Neat PCL	 Neat PLA	 Neat PCL	 Neat PLA	 Neat PCL
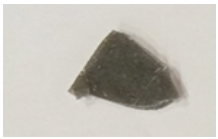 PLA/CNCs 99/1	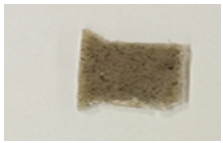 PCL/CNCs 99/1	 PLA/CNCs 99/1	 PCL/CNCs 99/1	 PLA/CNCs 99/1	 PCL/CNCs 99/1	 PLA/CNCs 99/1	 PCL/CNCs 99/1
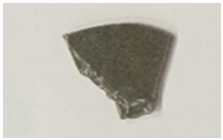 PLA/CNCs 97/3	 PCL/CNCs 97/3	 PLA/CNCs 97/3	 PCL/CNCs 97/3	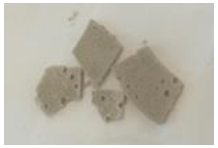 PLA/CNCs 97/3	 PCL/CNCs 97/3	 PLA/CNCs 97/3	 PCL/CNCs 97/3
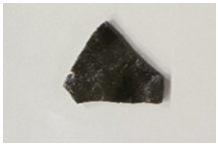 PLA/CNCs 95/5	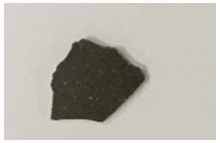 PCL/CNCs 95/5	 PLA/CNCs 95/5	 PCL/CNCs 95/5	 PLA/CNCs 95/5	 PCL/CNCs 95/5	 PLA/CNCs 95/5	 PCL/CNCs 95/5

3.6 Conclusions

This study investigated the fabrication and characterization of PCL/CNCs and PLA/CNCs biodegradable nanocomposites reinforced with cellulose nanocrystals (CNCs) extracted from sugarcane bagasse. The addition of CNCs influenced the thermal, morphological and structural behavior of both polymers in a composition-dependent manner. The incorporation of CNCs enhanced the biodegradation rate of PCL progressively with increasing CNCs loading. For PLA, 1 wt.% CNCs showed minimal effect, a slight increase in degradation at 3 wt.% CNCs (8%weight loss at day 112), and a pronounced increase at 5 wt.% CNCs, reaching 82.2% weight loss over the same period. CNCs had minimal effect on the thermal stability of PCL but reduced the thermal stability of PLA at higher loadings due to the intrinsic thermal instability of CNCs. Incorporation of 3 and 5 wt.% CNCs disrupted PLA crystal size and order, leading to reduced crystallinity and the appearance of double melting peaks. The prepared nanocomposites maintained properties similar to those of the neat polymers but degrade substantially faster. These observations were supported by DSC, SEM, WAXS, SAXS, FTIR, TGA, and soil burial biodegradation analysis.

The study confirms the feasibility of using sugarcane bagasse-derived CNCs to enhance the performance and biodegradation of PCL and PLA. Furthermore, the results suggest that agro-waste-derived CNCs hold strong potential as sustainable nanofiller for reinforcing PCL/PLA blends in packaging and biomedical applications, contributing to the development of environmentally friendly, high-performance materials. Future work will include dynamic mechanical analysis (DMA) to further evaluate the performance of the developed nanocomposites.

Author Contributions: Conceptualization, T.P.G., R.A.P.C. and B.M.; validation, M.N., T.P.G., R.A.P.C. and B.M.; investigation, M.N., T.P.G., R.A.P.C. and B.M.; data curation, M.N., T.P.G., R.A.P.C. and B.M.; writing - original draft preparation, M.N.; writing—review and editing, M.N., T.P.G., R.A.P.C. and B.M; visualization, M.N., T.P.G., R.A.P.C. and B.M.; supervision, T.P.G., R.A.P.C. and B.M.; project administration, T.P.G.

Funding: This research was funded by the National Research Foundation (NRF) of South Africa through the Thuthuka Programme (Grant No. TTK2204264865), the DSI-NRF postgraduate student fund (Grant No. PMDS22062125350) and the DSI-NRF Innovation Postdoctoral Fellowship (Grant No. PSTD2205057154). Additional financial support was provided by the postgraduate student fund of the Central University of Technology (Free State) and Future Coal Mining (Chelmsford Colliery).

Acknowledgements: ALBA synchrotron facility for SAXS/WAXS analysis.

Institutional Review Board Statement: Not applicable

Conflicts of Interest: The authors declare no conflicts of interest.

Abbreviations

CNCs	Cellulose nanocrystals
DSC	Differential scanning calorimetry
FTIR	Fourier transform infrared spectroscopy
H_2SO_4	Sulphuric acid
NaOH	Sodium hydroxide
PCL	Poly(ε-caprolactone)
PLA	Poly(lactic acid)
SAXS	Small angle x-ray scattering
SEM	Scanning electron microscopy
TGA	Thermogravimetric analysis
WAXS	Wide angle x-ray scattering

References

Alokika, Anu, Kumar, A., Kumar, V. and Singh, B. (2021) “Cellulosic and hemicellulosic fractions of sugarcane bagasse: Potential, challenges and future perspective,”

International Journal of Biological Macromolecules. Elsevier B.V., pp. 564–582. Available at: https://doi.org/10.1016/j.ijbiomac.2020.12.175.

Asadnia, M. and Sadat-Shojai, M. (2025) "Recent perspective of synthesis and modification strategies of cellulose nanocrystals and cellulose nanofibrils and their beneficial impact in scaffold-based tissue engineering: A review," *International Journal of Biological Macromolecules*. Elsevier B.V. Available at: https://doi.org/10.1016/j.ijbiomac.2024.139409.

Bi, S., Zhang, Z., Yang, Z., Shen, Z., Cai, J., Hu, J., Jin, H., Qiu, T., Yu, P. and Tan, B. (2023) "Protein modified cellulose nanocrystals on reinforcement and self-driven biodegradation of aliphatic polyester," *Carbohydrate Polymers*, 322. Available at: https://doi.org/10.1016/j.carbpol.2023.121312.

Chaka, K.T. (2022) "Extraction of cellulose nanocrystals from agricultural by-products: a review," *Green Chemistry Letters and Reviews*. Taylor and Francis Ltd., pp. 582–597. Available at: https://doi.org/10.1080/17518253.2022.2121183.

Chen, J., Huang, Y., Deng, L., Jiang, H., Yang, Z., Yang, R. and Wu, D. (2023) "Preparation and research of PCL/cellulose composites: Cellulose derived from agricultural wastes," *International Journal of Biological Macromolecules*, 235, p. 123785. Available at: https://doi.org/10.1016/j.ijbiomac.2023.123785.

Dabhi, M., Dange, H., Bonde, C. and Bonde, S. (2025) "A comprehensive review on sustainable production of nano crystalline cellulose from sugarcane bagasse and its applications," *Chemical Engineering Communications* [Preprint]. Taylor and Francis Ltd. Available at: https://doi.org/10.1080/00986445.2025.2469588.

Dadras Chomachayi, M., Jalali-Arani, A., Beltrán, F.R., De La Orden, U. and Urreaga, J.M. (2020) "Biodegradable Nanocomposite Developed from the PLA/PCL Blends and Silk Fibroin Nanoparticle: Study on the Microstructure, Thermal Behavior, Crystallinity, and Performance," *Journal of Polymers and the Environment*, 28, pp. 1252–1264. Available at: https://doi.org/10.1007/s10924.

Díez-Rodríguez, T.M., Blázquez-Blázquez, E., Lourenço, J.P., Martínez, J.C., Cerrada, M.L. and Pérez, E. (2025) "Preparation and characterization of Santa Barbara Amorphous-15 particles functionalized with mercaptopropyl groups and of their composites with poly(lactic acid)," *Microporous and Mesoporous Materials*, 382. Available at: https://doi.org/10.1016/j.micromeso.2024.113391.

Fernández-Tena, A., Otaegi, I., Irusta, L., Sebastián, V., Guerrica-Echevarria, G., Müller, A.J. and Aranburu, N. (2023) "High-Impact PLA in Compatibilized PLA/PCL Blends: Optimization of Blend Composition and Type and Content of Compatibilizer," *Macromolecular Materials and Engineering*, 308(12). Available at: https://doi.org/10.1002/mame.202300213.

Fitch-Vargas, P.R., Camacho-Hernández, I.L., Rodríguez-González, F.J., Martínez-Bustos, F., Calderón-Castro, A., Zazueta-Morales, J. de J. and Aguilar-Palazuelos, E. (2023) "Effect of compounding and plastic processing methods on the development of bioplastics based on acetylated starch reinforced with sugarcane bagasse cellulose fibers," *Industrial Crops and Products*, 192. Available at: https://doi.org/10.1016/j.indcrop.2022.116084.

Gan, I. and Chow, W.S. (2019) “Synthesis of phosphoric acid-treated sugarcane bagasse cellulose nanocrystal and its thermal properties enhancement for poly(lactic acid) nanocomposites,” *Journal of Thermoplastic Composite Materials*, 32(5), pp. 619–634. Available at: https://doi.org/10.1177/0892705718772866.

Goffin, A.L., Raquez, J.M., Duquesne, E., Siqueira, G., Habibi, Y., Dufresne, A. and Dubois, P. (2011) “From interfacial ring-opening polymerization to melt processing of cellulose nanowhisker-filled polylactide-based nanocomposites,” *Biomacromolecules*, 12(7), pp. 2456–2465. Available at: https://doi.org/10.1021/bm200581h.

Gond, R.K. and Gupta, M.K. (2020) *CHEM-CONFLUX 20 Special Issue Development of PLA Based Nanocellulose Film for Packaging Applications*, *J. Indian Chem. Soc*.

Gond, R.K., Naik, T.P., Gupta, M.K. and Singh, I. (2022) “Development and characterisation of sugarcane bagasse nanocellulose/ PLA composites,” *Materials Technology*, 37(14), pp. 2942–2954. Available at: https://doi.org/10.1080/10667857.2022.2088616.

Grace, D., Selikane, A., Gumede, P., Shingange, K., Malevu, T.D., Ngwenya, M. and Kumalo, F. (2024) *Characterization of Polycaprolactone/Eucomis autumnalis Cellulose Composite: Structural, Thermal, and Mechanical Analysis*. Available at: www.scientific.net.

Gumede, T.P., Luyt, A.S., Pérez-Camargo, R.A., Tercjak, A. and Müller, A.J. (2017) “Morphology, nucleation, and isothermal crystallization kinetics of poly(ε-caprolactone) mixed with a polycarbonate/MWCNTs masterbatch,” *Polymers*, 9, p. 709. Available at: https://doi.org/10.3390/polym912070.

Hassan, M.L., Bras, J., Hassan, E.A., Fadel, S.M. and Dufresne, A. (2012) “Polycaprolactone/modified bagasse whisker nanocomposites with improved moisture-barrier and biodegradability properties,” *Journal of Applied Polymer Science*, 125(SUPPL. 2). Available at: https://doi.org/10.1002/app.36373.

Al Hosni, A.S., Pittman, J.K. and Robson, G.D. (2019) “Microbial degradation of four biodegradable polymers in soil and compost demonstrating polycaprolactone as an ideal compostable plastic,” *Waste Management*, 97, pp. 105–114. Available at: https://doi.org/10.1016/j.wasman.2019.07.042.

Islam, M.M., Islam, M.A., Rahman, A.N.M.M., Xuepeng, Z., Li, J. and Liu, L. (2025) “Development of hybrid nanocellulose-reinforced PLA biocomposites from waste jute bags and ramie fabric with enhanced mechanical and thermal properties,” *Biomass Conversion and Biorefinery* [Preprint]. Available at: https://doi.org/10.1007/s13399-025-06577-7.

Kádár, R., Spirk, S. and Nypelö, T. (2021) “Cellulose Nanocrystal Liquid Crystal Phases: Progress and Challenges in Characterization Using Rheology Coupled to Optics, Scattering, and Spectroscopy,” *ACS Nano*. American Chemical Society, pp. 7931–7945. Available at: https://doi.org/10.1021/acsnano.0c09829.

Kalita, N.K., Bhasney, S.M., Mudenur, C., Kalamdhad, A. and Katiyar, V. (2020) “End-of-life evaluation and biodegradation of Poly(lactic acid) (PLA)/Polycaprolactone (PCL)/Microcrystalline cellulose (MCC) polyblends under composting conditions,” *Chemosphere*, 247. Available at: https://doi.org/10.1016/j.chemosphere.2020.125875.

Kargarzadeh, H., Ahmad, I., Abdullah, I., Dufresne, A., Zainudin, S.Y. and Sheltami, R.M. (2012) “Effects of hydrolysis conditions on the morphology, crystallinity, and thermal stability of cellulose nanocrystals extracted from kenaf bast fibers,” *Cellulose*, 19(3), pp. 855–866. Available at: https://doi.org/10.1007/s10570-012-9684-6.

Khoo, R.Z., Chow, W.S. and Ismail, H. (2023) “Tensile, thermal and ultra-violet shielding enhancement of poly(lactic acid) bionanocomposite film using cellulose nanocrystals extracted from sugarcane bagasse,” *Journal of Thermoplastic Composite Materials*, 36(6), pp. 2543–2561. Available at: https://doi.org/10.1177/08927057221098972.

Kostryukov, S.G., Matyakubov, H.B., Masterova, Y.Y., Kozlov, A.S., Pryanichnikova, M.K., Pynenkov, A.A. and Khluchina, N.A. (2023) “Determination of Lignin, Cellulose, and Hemicellulose in Plant Materials by FTIR Spectroscopy,” *Journal of Analytical Chemistry*, 78(6), pp. 718–727. Available at: https://doi.org/10.1134/S1061934823040093.

Kumalo, F.I., Malimabe, M.A., Mosoabisane, M.F.T. and Gumede, T.P. (2025) “Development and Characterization of PBS/EA Cellulose and PCL/EA Cellulose Biocomposites: Structural, Morphological, and Thermal Insights for Sustainable Applications.” Available at: https://doi.org/10.20944/preprints202502.1813.v1.

Kurakula, M., Rao, G.S.N.K. and Yadav, K.S. (2020) “Fabrication and characterization of polycaprolactone-based green materials for drug delivery,” in *Applications of Advanced Green Materials*. Elsevier, pp. 395–423. Available at: https://doi.org/10.1016/B978-0-12-820484-9.00016-7.

Lattimer, M.P., Hobbs, J.K., Hill, M.J. and Barham, P.J. (1992) *On the origin of the multiple endotherms in PEEK*.

Li, J. and Wu, D. (2022) “Nucleation roles of cellulose nanocrystals and chitin nanocrystals in poly(ε-caprolactone) nanocomposites,” *International Journal of Biological Macromolecules*, 205, pp. 587–594. Available at: https://doi.org/10.1016/j.ijbiomac.2022.02.123.

Mahmud, M.A. and Anannya, F.R. (2021) “Sugarcane bagasse - A source of cellulosic fiber for diverse applications,” *Heliyon*. Elsevier Ltd. Available at: https://doi.org/10.1016/j.heliyon.2021.e07771.

Melesse, G.T., Hone, F.G. and Mekonnen, M.A. (2022) “Extraction of Cellulose from Sugarcane Bagasse Optimization and Characterization,” *Advances in Materials Science and Engineering*, 2022. Available at: https://doi.org/10.1155/2022/1712207.

Motloung, B., Pfukwa, R. and Klumperman, B. (2024) “Ion-Mediated Gelation of Thermo-Responsive Cellulose Nanofibril/Poly(N-isopropylacrylamide) Hybrid Hydrogels with Tunable De-Swelling Kinetics,” *Macromolecular Materials and Engineering*, 309(8). Available at: https://doi.org/10.1002/mame.202300457.

Motloung, M.P., Ojijo, V., Bandyopadhyay, J. and Ray, S.S. (2020) “Morphological characteristics and thermal, rheological, and mechanical properties of cellulose nanocrystals-containing biodegradable poly(lactic acid)/poly(ε-caprolactone) blend composites,” *Journal of Applied Polymer Science*, 137(19). Available at: https://doi.org/10.1002/app.48665.

Muniyasamy, S., Ofosu, O., John, M.J. and Anandjiwala, R.D. (2016) “Mineralization of poly(lactic acid) (PLA), Poly(3-hydroxybutyrate-co-valerate) (PHBV) and PLA/PHBV blend

in compost and soil environments," *Journal of Renewable Materials*, 4(2), pp. 133–145. Available at: https://doi.org/10.7569/JRM.2016.634104.

Nang Vu, A., Hoang Nguyen, L., Yoshimura, K., Duy Tran, T. and Van Le, H. (2024) "Cellulose nanocrystals isolated from sugarcane bagasse using the formic/peroxyformic acid process: Structural, chemical, and thermal properties," *Arabian Journal of Chemistry*, 17(8). Available at: https://doi.org/10.1016/j.arabjc.2024.105841.

Naseem, R., Montalbano, G., German, M.J., Ferreira, A.M., Gentile, P. and Dalgarno, K. (2022) "Influence of PCL and PHBV on PLLA Thermal and Mechanical Properties in Binary and Ternary Polymer Blends," *Molecules*, 27(21). Available at: https://doi.org/10.3390/molecules27217633.

Ngwenya, M., Gumede, T.P., Pérez Camargo, R.A. and Motloung, B. (2025) "Nanocellulose-Reinforced Poly(Lactic Acid) and Poly(ε-caprolactone) Bio-Nanocomposites: A Review and Future Outlook for Poly(Lactic Acid)/Poly(ε-caprolactone) Blend Systems," *Materials*, 18(22), p. 5172. Available at: https://doi.org/10.3390/ma18225172.

Padhi, S., Singh, A. and Routray, W. (2023) "Nanocellulose from agro-waste: a comprehensive review of extraction methods and applications," *Reviews in Environmental Science and Biotechnology*. Springer Science and Business Media B.V., pp. 1–27. Available at: https://doi.org/10.1007/s11157-023-09643-6.

Qiao, X., Wang, Z. and Sun, K. (2022) "Renewable rice straw cellulose nanofibril reinforced poly(ε-caprolactone) composite films," *Materials Chemistry and Physics*, 292. Available at: https://doi.org/10.1016/j.matchemphys.2022.126879.

Ruz-Cruz, M.A., Herrera-Franco, P.J., Flores-Johnson, E.A., Moreno-Chulim, M. V., Galera-Manzano, L.M. and Valadez-González, A. (2022) "Thermal and mechanical properties of PLA-based multiscale cellulosic biocomposites," *Journal of Materials Research and Technology*, 18, pp. 485–495. Available at: https://doi.org/10.1016/j.jmrt.2022.02.072.

Salmani, M.R., Shirazi, F., Goodarzi, K., Noormohammadi, F. and Nourany, M. (2024) "Improving Phase Compatibility of PLA-PCL Matrix-Droplet Blend Using CNC/PCL-PEG-PCL Triblock Copolymer to Prepare Porous 3D Osteoinductive Scaffolds," *Journal of Polymers and the Environment* [Preprint]. Available at: https://doi.org/10.1007/s10924-024-03392-5.

Selikane, D.G.A., Gumede, T.P., Shingange, K. and Malevu, T.D. (2022) "A Brief Overview on the Extraction of Cellulose from Medicinal Plants for Advanced Applications," *Materials Science Forum*, 1059 MSF, pp. 81–85. Available at: https://doi.org/10.4028/p-9hut2u.

Sikhosana, S. T., Gumede, T.P., Malebo, N.J., Ogundeji, A.O. and Motloung, B. (2023) " The influence of cellulose content on the morphology, thermal, and mechanical properties of poly(lactic acid)/ Eucomis autumnalis cellulose biocomposites ," *Polymer Engineering & Science* [Preprint]. Available at: https://doi.org/10.1002/pen.26293.

Sikhosana, Sylvia T., Gumede, T.P., Malebo, N.J., Ogundeji, A.O. and Motloung, B. (2023) "Medicinal plants as a cellulose source for the fabrication of poly(lactic acid)

composites: A mini-review," *Polymers from Renewable Resources*. SAGE Publications Ltd, pp. 44–57. Available at: https://doi.org/10.1177/20412479221146249.

Sirviö, J.A., Visanko, M., Heiskanen, J.P. and Liimatainen, H. (2016) "UV-absorbing cellulose nanocrystals as functional reinforcing fillers in polymer nanocomposite films," *Journal of Materials Chemistry A*, 4(17), pp. 6368–6375. Available at: https://doi.org/10.1039/c6ta00900j.

Sriwong, C., Boonrungsiman, S. and Sukyai, P. (2023) "Sugarcane bagasse cellulose-based scaffolds incorporated hydroxyapatite for promoting proliferation, adhesion and differentiation of osteoblasts," *Industrial Crops and Products*, 192. Available at: https://doi.org/10.1016/j.indcrop.2022.115979.

Sun, H., Yu, B., Han, J., Kong, J., Meng, L. and Zhu, F. (2014) "Microstructure, thermal properties and rheological behavior of PLA/PCL blends for melt-blown nonwovens," *Polymer (Korea)*, 38(4), pp. 477–483. Available at: https://doi.org/10.7317/pk.2014.38.4.477.

Wang, W., Niu, B., Liu, R., Chen, H., Fang, X., Wu, W., Wang, G., Gao, H. and Mu, H. (2023) "Development of bio-based PLA/cellulose antibacterial packaging and its application for the storage of shiitake mushroom," *Food Chemistry*, 429. Available at: https://doi.org/10.1016/j.foodchem.2023.136905.

Wang, Z., Yao, Z., Zhou, J., He, M., Jiang, Q., Li, S., Ma, Y., Liu, M. and Luo, S. (2019) "Isolation and characterization of cellulose nanocrystals from pueraria root residue," *International Journal of Biological Macromolecules*, 129, pp. 1081–1089. Available at: https://doi.org/10.1016/j.ijbiomac.2018.07.055.

Wani, A.K., Rahayu, F., Fauziah, L. and Suhara, C. (2023) "Advances in safe processing of sugarcane and bagasse for the generation of biofuels and bioactive compounds," *Journal of Agriculture and Food Research*, 12. Available at: https://doi.org/10.1016/j.jafr.2023.100549.

Xing, L., Gu, J., Zhang, W., Tu, D. and Hu, C. (2018) "Cellulose I and II nanocrystals produced by sulfuric acid hydrolysis of Tetra pak cellulose I," *Carbohydrate Polymers*, 192, pp. 184–192. Available at: https://doi.org/10.1016/j.carbpol.2018.03.042.

Xu, C., Chen, C. and Wu, D. (2018) "The starch nanocrystal filled biodegradable poly(ε-caprolactone) composite membrane with highly improved properties," *Carbohydrate Polymers*, 182, pp. 115–122. Available at: https://doi.org/10.1016/j.carbpol.2017.11.001.

Zhao, Z., Yan, H., Zheng, R., Khan, M.S., Fu, X., Tao, Z. and Zhang, Z. (2018) "Anthocyanins characterization and antioxidant activities of sugarcane (Saccharum officinarum L.) rind extracts," *Industrial Crops and Products*, 113, pp. 38–45. Available at: https://doi.org/10.1016/j.indcrop.2018.01.015.

Zhu, H., Han, Z., Cheng, J.H. and Sun, D.W. (2022) "Modification of cellulose from sugarcane (Saccharum officinarum) bagasse pulp by cold plasma: Dissolution, structure and surface chemistry analysis," *Food Chemistry*, 374. Available at: https://doi.org/10.1016/j.foodchem.2021.131675.

Chapter 4

EXPERIMENTAL PAPER

This chapter will be submitted to a peer-reviewed journal under the title:

Thermal, structural, morphological, and biodegradation properties of poly(ε-caprolactone) and poly(lactic acid) nanocomposites reinforced with sugarcane bagasse-derived cellulose nanocrystals

Mbongeni Ngwenya[1], Thandi P. Gumede[1], Ricardo Arpad Pérez Camargo[2] and Bennie Motloung[3*]*

[1]Department of Life Sciences, Faculty of Health and Environmental Sciences, Central University of Technology, Free State, Bloemfontein 9301, South Africa

[2]POLYMAT and Department of Polymers and Advanced Materials: Physics, Chemistry, and Technology, Faculty of Chemistry, University of the Basque Country UPV/EHU, Paseo Manuel de Lardizábal, 3, Donostia-San Sebastián 20018, Spain

[3]Department of Chemistry and Polymer Science, Faculty of Science, Stellenbosch University, Matieland 7602, South Africa

*Corresponding authors:

Thandi P. Gumede, tgumede@cut.ac.za and Bennie Motloung, motloung@sun.ac.za

Abstract

Biopolymers such poly(lactic acid) (PLA) and poly(ε-caprolactone) (PCL) have gained considerable attention as alternative for petroleum-based and non-biodegradable polymers, in a field of packaging and biomedical. PLA lacks flexibility and thermal stability, while PCL lacks mechanical strength. PLA/PCL blends are incompatible and immiscible. To address these drawbacks, 1, 3 and 5 wt.% cellulose nanocrystals (CNCs) extracted from sugarcane bagasse, were incorporated to 70/30 and 30/70 PLA/PCL. The influence of CNCs on the thermal, morphological, structural, and biodegradation properties of the nanocomposites was evaluated. Tensile testing was performed only on neat PLA, neat PCL, and PLA/PCL blends, as CNCs-reinforced nanocomposite samples were prone to premature failure. The results showed that CNCs increased the biodegradation rate and enhanced crystallinity. Thermal stability slightly increased only at 1 wt.% CNCs loading, while higher loadings (3 and 5 wt.%) led to thermally unstable nanocomposites. Scanning electron microscopy confirmed improved interfacial adhesion and reduced phase separation at 1 wt.% CNCs content. For instance, PLA T_{cc} decreased from 113 °C (neat PLA) to 91 °C at 5 wt.% CNCs, indicating strong nucleating activity. Similarly, 5 wt.% CNCs accelerated biodegradation of 70/30 PLA/PCL to complete mass loss within 112 days, unlike neat PLA, which lost only 0.3%. These findings suggest that CNCs derived from agro-waste can effectively enhance the thermal, structural, and biodegradation performance of PLA/PCL blends, offering a promising route for developing sustainable and high-performance biodegradable materials.

Keywords: poly(lactic acid), poly(ε-caprolactone), cellulose nanocrystals, blends, nanocomposites, compatibility, crystallinity, interfacial adhesion, biodegradation.

4.1 Introduction

The increasing accumulation of plastic waste and its detrimental impact on the environment have driven global interest towards the development of biodegradable and renewable alternatives. Among the biopolymers currently being explored, poly(lactic acid) (PLA) and poly(ε-caprolactone) (PCL) have gained considerable attention due to their biodegradability, biocompatibility, and potential applications in packaging, biomedical, and environmental sectors. However, both polymers have individual limitations: PLA is brittle with low thermal stability (Wang et al., 2023), while PCL is ductile but degrades slowly (Kurakula et al., 2020). Blending PLA with PCL can complement these drawbacks by combining the stiffness of PLA with the flexibility of PCL, although immiscibility between the two often leads to phase-separated morphologies and poor mechanical performance (Fernández-Tena et al., 2023).

Challenges such as phase separation, limited compatibility, and mechanical property mismatches have been identified in the PCL/PLA blends, which hinder their widespread application (Luyt and Malik, 2018; Sessini et al., 2016; Wachirahuttapong et al., 2016). However, integrating a third component, such as a compatibilizer or filler, into PCL/PLA blends presents a promising solution to overcome these challenges. By incorporating cellulose, the resulting PCL/PLA/nanocellulose-based composites can exhibit enhanced mechanical strength, improved compatibility between components, and potentially accelerated degradation (Chen et al., 2023; Kalita et al., 2020a; Sessini et al., 2018)., thus, making them suitable for a broader range of sustainable applications in the fields such as packaging, biomedical engineering, and beyond. The impact of incorporating a third component such as triallyl isocyanurate, montmorillonite, flax fiber, and silk fibroin nanoparticles on the properties of PLA/PCL blends demonstrate improvements in flexural modulus, compatibility, and mechanical strength. These findings show the importance of exploring novel composite formulations to overcome inherent limitations and unlock the full potential of PLA/PCL blends across diverse applications.

A comprehensive study by Sessini et al., 2018, conducted an investigation on 70/30 PLA/PCL (M70 PLA) blend and its composites, incorporating 1 wt.% CNCs, CNC–*g*–PLA,

and CNCs–*g*–PCL. M70 PLA/CNCs composite exhibited a notable increase in thermal stability compared to neat M70 PLA. The M70 PLA/CNCs composite showed to be 11 °C more thermally stable than neat M70 PLA at $T_{5\%}$. This observation shows the potential of cellulose-based reinforcements in improving the thermal properties of biocomposites (Sessini et al., 2018). Chen et al. (2023) evaluated the thermal transitions of PLA, PCL, and PLA/PCL composites reinforced with 2,2,6,6–tetramethylpiperidine–1–oxyl (TEMPO)–oxidized bacterial cellulose (TOBC). Differential scanning calorimetry (DSC) results revealed that the addition of TOBC promoted the crystallization of PLA, leading to increased crystallinity compared to neat PLA. Moreover, the cold crystallization temperature was found to be influenced by the PCL content in the composite, indicating the synergistic effects of polymer blending and cellulose reinforcement on thermal behavior. Research by Kalita et al. (2020a) explored the biodegradation rate of neat PLA, neat PCL, their blends, and PLA/PCL/microcrystalline composites under composting conditions. The results revealed that PCL exhibited a higher biodegradation rate compared to PLA. The addition of microcrystalline composites to the PLA/PCL blend proved to enhance the biodegradability of the composites.

A study by Motloung et al. (2020a) investigated the effect of cellulose nanocrystal (CNCs) loading (1, 2, 3, 4 and 5 wt.%) on the properties of a PLA/PCL (70/30) blend processed in a twin-screw extruder. These authors discovered that 2 wt.% CNCs improved compatibility, increased mechanical properties such as impact strength, and further nucleated the crystallization of PCL. The incorporation of CNCs did not affect the thermal stability of the blend. Salmani et al. (2024) investigated the compatibility of a PLA/PCL (60/40) blend with 0.5, 1.0 and 2.0 wt.% CNCs (from cotton) prepared through solvent casting. These authors reported that 2,0 wt.% CNCs reduced the size of PCL droplets which is the dispersed phase.

This study aimed to enhance compatibility and improve overall composite performance using CNCs. CNCs derived from agricultural waste have been identified as effective nanoscale reinforcements. CNCs are renewable, biodegradable, and possess excellent mechanical properties and high aspect ratios, making them ideal candidates for polymer reinforcement. However, the impact of CNCs on polymer blends depends significantly on their dispersion, interfacial interactions, and concentrations. Previous studies have

shown that excessive CNCs can lead to agglomeration, reducing the performance benefits expected from nanofiller incorporation (Kalita et al., 2020b; Sessini et al., 2018b; Ye et al., 2025).

This study focused on the fabrication and comprehensive characterization of PLA/PCL/CNCs nanocomposites using CNCs extracted from sugarcane bagasse – an abundant agricultural byproduct. Most previous studies have used CNCs obtained from cotton, bacterial cellulose, or commercial sources. Very few have reported PLA/PCL composites reinforced with CNCs derived from sugarcane bagasse, an abundant agro-waste. Thus, our study addressed this gap by systematically comparing two blend ratios (70/30 and 30/70 PLA/PCL) with varying CNCs loadings (1–5 wt.%) extracted from sugarcane bagasse. The main objective of this study was to investigate the thermal, morphological, structural, and biodegradation effects of CNCs at varying loadings on PLA/PCL blends with different composition ratios. The manuscript is organized as follows: It starts with a description of the materials and methods used for nanocomposite preparation and characterization followed by the results and discussion on thermal, morphological, structural, and biodegradation behavior and finally, the main conclusions of the work.

4.2 Materials and methods

4.2.1 Materials

Cellulose nanocrystals

Saccharum officinarum, commonly known as sugarcane (Figure 4.1a), is a grass species that belongs to the family Poaceae, class Liliopsida, and order Poales. It is a globally cultivated cash crop and the primary feedstock for sugar production (Zhao *et al.*, 2018; Gan and Chow, 2019; Wani *et al.*, 2023). After sugar extraction through milling, the remaining fibrous residues are known as bagasse (Figure 4.1b). In this study, bagasse was collected from a farm in KwaZulu-Natal, South Africa. It typically comprises approximately 40–50% cellulose, 25–35% hemicellulose and 5–10% lignin (Alokika *et al.*, 2021; Melesse *et al*, 2022). The focus of this study was on cellulose because of its high tensile strength, biodegradability, biocompatibility and chemical modifiability

characteristics in line with those of the PCL and PLA, making it a key interest in green composite development (Chaka, 2022; Fitch-Vargas *et al.*, 2023; Sikhosana *et al.*, 2023).

Cellulose extraction:

Figure 4.1 illustrates the process of extracting CNCs from sugarcane bagasse. Ground sugarcane bagasse (40 g) (Figure 4.1b) was screened to 30-mesh particle size, and de-waxed using a 2:1 (v/v) toluene:ethanol mixture for six hours to remove surface waxes and extractive. The de-waxed bagasse (Figure 1c) was then treated with 800 mL distilled water at 80°C for two hours to remove soluble impurities. Delignification was achieved using a 1.3% sodium chlorite solution, maintaining pH between 3.5 and 4.0 with 6 M acetic acid, repeated until a cream white product was obtained (Figure 4.1d). The delignified fibers were further treated with 2% NaOH for two hours, followed by 5% NaOH at 90°C for two hours. The residue was filtered, washed to a neutral pH, and oven-dried at 105°C for six hours (Figure 4.1e) (Alokika *et al.*, 2021; Zhu *et al.*, 2022).

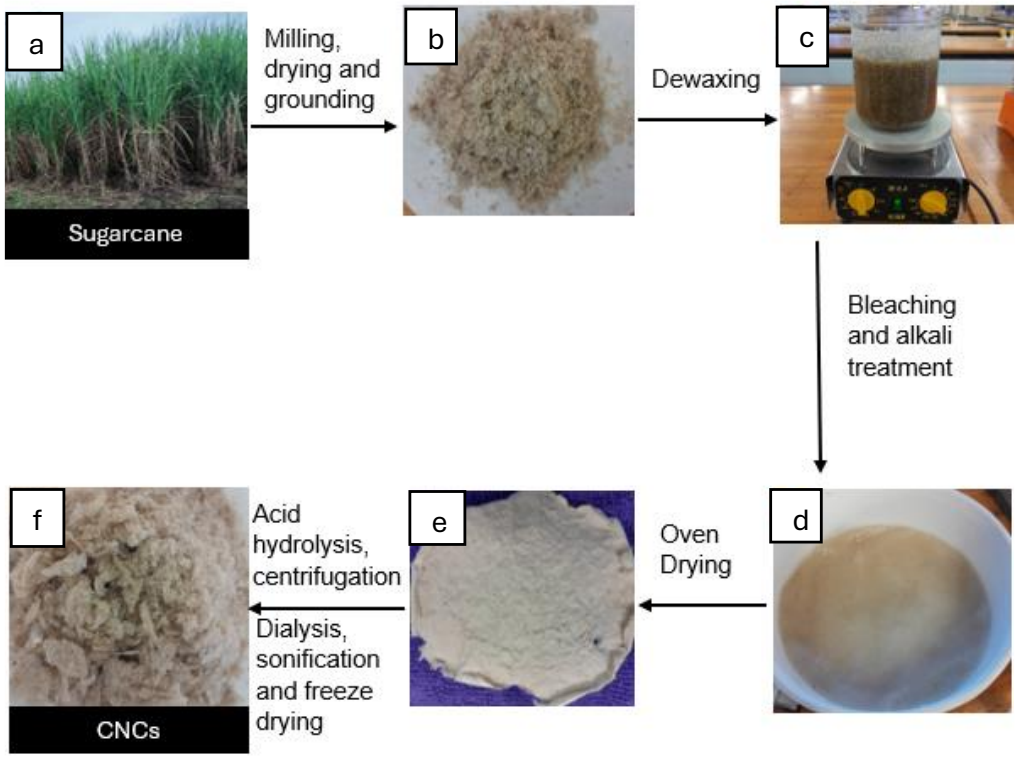

Figure 4.1 Cellulose nanocrystals extraction from sugarcane bagasse.

Cellulose nanocrystals extraction:

The dried cellulose (Figure 4.1e) was subjected to acid hydrolysis using 50% H_2SO_4 at a cellulose-to-acid ratio of 1:10 g/mL at 45 °C for one hour, with constant stirring using a homogenizer. To terminate the reaction, 10-fold ice-cold distilled water was added, followed by centrifugation at 10 000 rpm for 15 minutes (three cycles, at 10 °C). The collected sediment was dialyzed against distilled water for ~48 hours until a neutral pH was achieved. The resulting suspension (5 mg/mL) was sonicated for 10 minutes in an ice bath to prevent overheating. The resulting CNCs (Figure 4.1f) were obtained by freeze-drying the suspension (0.2 wt.% in distilled water) at reduced pressure and low temperature, producing a light brownish fine powder while preserving particle integrity and porosity (Padhi, Singh and Routray, 2023; Asadnia and Sadat-Shojai, 2025; Dabhi *et al.*, 2025). Table 4.1 presents the percentage yield of cellulose and CNCs. From 40 g of sugarcane bagasse, 10.5 g of cellulose was obtained (26.3% yield), which was further converted into 7.7 g of CNCs (19.25% yield). These values indicate an efficient extraction process, consistent with literature ranges (18–25%). Furthermore, the yield provides sufficient CNCs for subsequent incorporation into the selected polymer matrices, namely PCL and PLA.

Table 4.1 Extraction yield of cellulose and cellulose nanocrystals from sugarcane bagasse

Sample	Mass of the ground powder (g)	Mass of cellulose (g)	% yield of cellulose	Mass of CNCs (g)	% yield of CNCs
Sugarcane bagasse	40	10.5	26.3	7.7	19.25

Note: CNCs = cellulose nanocrystals

Poly(lactic acid)

PLA granules were purchased from 2M BIOTEC LLP 180 Annal Gandhiadigal Salai, Ramanathapuram 623501, TN in India. It has a glass transition temperature (T_g) of 55–60 °C, a melting temperature (T_m) of 145–155 °C, and a density of 1,23 g/cm^3.

Poly(ε-caprolactone)

PCL granules were purchased from 2M BIOTEC LLP 180 Annal Gandhiadigal Salai, Ramanathapuram 623501, TN in India. It has a glass transition temperature (T_g) of −60 °C, a melting temperature (T_m) of 40–60 °C, and a density of 1,10 g/cm^3.

4.3 Sample preparation

Conditioning

Table 4.2 summarizes the drying conditions used to remove residual moisture from PLA, PCL and CNCs before melt-blending. PLA and CNCs were dried at 50 °C, while PCL was dried at 40 °C, all under vacuum overnight. Proper drying at these controlled temperatures is important for preventing hydrolytic degradation during processing, as both PLA and PCL are moisture sensitive at elevated temperatures, while CNCs readily retain bound water due to their hydroxyl-rich surfaces. Ensuring consistent drying therefore improved process reproducibility and minimized variations in the resulting thermal and morphological properties.

Table 4.2 Drying conditions for poly(lactic acid), poly(ε-caprolactone) and cellulose nanocrystals

Material	Drying conditions
Poly(lactic acid)	50 °C, in vacuum oven, overnight
Poly(ε-caprolactone)	40 °C, in vacuum oven, overnight
Cellulose nanocrystals	50 °C, in vacuum oven, overnight

Melt blending

A total of 40 g of each material (neat, blend, and composite) was weighed and processed. Melt blending was carried out using a Brabender Plastograph at 180 °C, 50 rpm for 12 minutes. Blended samples were allowed to cool overnight at room temperature for recrystallization. The solidified materials were then compression-molded using a hydraulic press at 180 °C for 5 minutes under 50 kPa pressure. Table 4.3 shows the

compositions of the neat polymers, blends, and nanocomposites prepared in this study. Two blend ratios were selected (PLA/PCL = 70/30 and 30/70) to represent PLA-rich and PCL-rich systems, thereby allowing evaluation of how CNCs influence each matrix. CNCs were incorporated at 1, 3, and 5 wt.% to investigate concentration effects, with 1 wt.% representing low filler content, 3 wt.% an intermediate level, and 5 wt.% a high loading, where agglomeration effects might appear. This systematic variation makes it possible to correlate CNCs concentration with structural, thermal, and biodegradation performance.

Table 4.3 Weight percentage composition of poly(lactic acid), poly(ε-caprolactone) and cellulose nanocrystal samples

Sample name	PLA (wt.%)	PCL (wt.%)	CNCs (wt.%)
Neat PLA	100	0	0
Neat PCL	0	100	0
Neat CNCs	0	0	100
PLA/PCL (70/30)	70	30	0
PLA/PCL (30/70)	30	70	0
PLA/PCL/CNCs (29.7/69.3/1)	29.7	69.3	1
PLA/PCL/CNCs (29.1/67.9/3)	29.1	67.9	3
PLA/PCL/CNCs (28.5/66.5/5)	28.5	66.5	5
PLA/PCL/CNCs (69.3/29.7/1)	69.3	29.7	1
PLA/PCL/CNCs (67.9/29.1/3)	67.9	29.1	3
PLA/PCL/CNCs (66.5/28.5/5)	66.5	28.5	5

Note: PCL = poly(ε-caprolactone); PLA = poly(lactic acid) and CNCs = cellulose nanocrystals.

4.4 Sample characterization

Differential scanning calorimetry

DSC was performed using PerkinElmer DSC 6000. Prior to sample analysis, the DSC instrument was calibrated using the onset melting temperatures of 419.5 °C for zinc, 156.6 °C for indium, and also the melting enthalpy of 28 J/g for indium, and 108 J/g for zinc. Samples (~6.0 mg) were heated from 0 to 180 °C (first heating scan), held at this temperature for three minutes to erase the thermal history, next cooled from 180 to 0 °C (cooling scan), held for one minute at 0 °C for conditioning, and finally subsequently

heated from 0 to 180°C (second heating scan). The scanning rate in all steps was 10°C per minute, and the experiments were conducted using a 20 mL per minute nitrogen flow. Cooling and second heating scans were used to determine thermal transitions.

Scanning electron microscopy

Samples were cryo-fractured, mounted on aluminium pin stubs using epoxy glue, and sputter-coated with Iridium using a Leica EM ACE600 Imaging was performed on a JEOL JSM-7800F Extreme-resolution analytical field emission SEM, at 5 kV, 10 mm working distance.

X-ray diffraction analysis

Simultaneous SAXS/WAXS was performed at beamline BL11-NCD, ALBA Synchrotron, Barcelona, Spain. Samples were placed in DSC pans on a Linkam THMS600 hot stage, cooled/heated via a liquid nitrogen system. The thermal protocol involved: Heat 20°C per minute from 25 to 180°C, held for three minutes at 180°C, cool 20°C per minute from 180°C to 0°C, held for one minute at 0°C, heat 20°C per minute from 0 to 180°C, mimicking the employed conditions in the DSC, and taken SAXS/WAXS patterns during the heating and cooling ramps. The X-ray energy was 12,4 keV (ʎ = 1,0 Å). The X-ray energy was 12,4 keV (ʎ = 1,0 Å). Two detectors. Calibrated with silver behenate (SAXS) and Cr_2O_3 (WAXS) standards, were employed: ADSC Q315r detector, 3 070 × 3 070 pixels, pixel size 102 μm^2, distance 6 495 mm, tilt angle 0° for SAXS. Rayonix LX255-HS detector, 1 920 × 5 760 pixels, pixel size 44 μm^2, distance 132.6 mm, tilt angle 21.2° for WAXS. The scattering intensity versus scattering vector ($q = 4\pi\sin\theta/\lambda$) was analyzed.

Fourier transformed infrared spectroscopy

Fourier transformed infrared spectroscopy (FTIR) spectra were obtained using a PerkinElmer Spectrum 100 FTIR spectrometer equipped with a PIKE MiracleTM attenuated total reflectance, with a diamond crystal. Background scans were collected before each measurement. Scans were recorded over a range of 4 000 and 650 cm^{-1}, at 8 cm^{-1} resolution, with eight scans per sample.

Thermogravimetric analysis

Thermogravimetric analysis (TGA) was carried out using PerkinElmer STA 6000 under 20 mL per minute nitrogen. Samples (~23 mg) were heated from 30 to 600°C at a rate of 10°C per minute. Data analysis was done using Pyris software.

Tensile testing

Tensile testing was carried out using AGS-X machine. Tensile specimens with dimensions of 75 mm length, 5 mm width, 2 mm thickness, and a gauge length of 20 mm were analyzed. The tensile testing analysis was carried out at 10 mm per minute test rate.

Biodegradation analysis

Aerobic biodegradability was determined by cutting small specimens of each sample and burying them in soil (4 cm deep, 39% moisture) at room temperature for 112 days following ASTM D5988. At 14-day intervals, samples were retrieved, washed with water, dried at 30°C for one hour, and weighed. Photographs were taken at each point to visually monitor degradation.

4.5 Results and discussion

4.5.1 Thermal properties

Differential scanning calorimetry

Thermal transitions and their enthalpies were analyzed using DSC, focusing on parameters such as crystallization temperature (T_c), glass transition temperature (T_g), cold crystallization temperature (T_{cc}), melting temperature (T_m), enthalpies (ΔH) and degree of crystallinity (X_c) calculated using Equation 4.1. These parameters provide insights into the interactions between PLA, PCL, and CNCs, as shown in Figures 4.2 and 4.3, and Table 4.4.

$$X_c = \left(\frac{\Delta H_m - \Delta H_{cc}}{w\Delta H_{m^o}}\right) \times 100 \qquad 4.1$$

X_c is the degree of crystallinity; ΔH_m is the melting enthalpy of the measured sample; ΔH_{cc} is the cold crystallization of the measured sample; ΔH_m^o is the melting enthalpy of a 100% crystalline polymer; and w is the weight fraction of the polymer in the blend or composite. The values of ΔH_m^o used for PLA and PCL are 93.7 J/g and 139 J/g, respectively (Patrício and Bártolo, 2013). DSC results for neat PLA and neat PCL, their blends, and their blend nanocomposites with 1, 3, and 5 wt.% CNCs are presented in Figures 4.2 and 4.3 and Table 4.4.

Figures 4.2a and 4.3a show the cooling and second heating scans for the neat polymers and their blends. Neat PLA exhibits a T_g at 59.6 °C, a T_{cc} at 113.3°C, and a T_m at 149.1 °C, with a degree of crystallinity of 7.5%. The presence of a cold crystallization peak reflects the slow crystallization of PLA, and during cooling, it cannot crystallize completely. Therefore, PLA finishes the crystallization process during heating. In contrast, neat PCL shows two distinct melting peaks at 45.6 °C and 52.2°C, suggesting the coexistence of crystals with different levels of perfection, which might be due to the crystallization process (Lattimer et al., 1992; Xu et al., 2018). The measured ΔH_m of 56 J/g closely matches the ΔH_c of 54 J/g, with a T_c of 18,4 °C and crystallinity of 40.3%.

For PLA/PCL blends, DSC curves (Figures 4.2a and 4.3a) reveal transitions dominated by the major component. The PLA/PCL (70/30) blend retains dominant PLA thermal features, while the (30/70) blend is PCL-dominated. The ΔH_m of PCL in the 30/70 blend (30 J/g) far exceeds that in the 70/30 blend (8 J/g), reflecting the influence of PCL on the overall thermal behavior. The T_c of the PLA/PCL blends slightly enhanced to higher temperatures due to the presence of PLA (Motloung et al., 2020a). The unchanged T_m values support phase immiscibility, consistent with SEM-observed phase separation. However, the improved dispersion in PLA/PCL (70/30) blend suggests partial compatibility, since T_c shows broad and suppressed peak while T_{cc} slightly shifted to higher temperatures, in line with SEM findings. Theoretical scans and experimental scans DSC for 70/30 and 30/70 PLA/PCL blends are presented in the appendix Figure A2. Experimental scans follow theoretical scans, and they evidence immiscibility.

The incorporation of CNCs into PLA/PCL blends affects crystallinity, depending on the concentration and matrix ratio. In the PLA/PCL (30/70) system (Figures 4.2b and 4.3b),

the incorporation of CNCs slightly increased T_c, suggesting nucleation of PCL crystallization for all samples. The incorporation of CNCs increases the degree of crystallinity of PCL for PCL-rich nanocomposites with the increasing CNCs content, while it only increased the degree of crystallinity of PLA only at 1 wt.% CNCs loading (Figure 4.4a). For PLA-rich nanocomposites (Figure 4.4b), the degree of crystallinity of PCL significantly increased at 1 and 3 wt.% CNCs loading and decreased it at 5 wt.% CNCs, but not below that of the blend, while PLA degree of crystallinity only increased at 1 wt.% CNCs loading.

Double melting peaks for PLA were observed from the curves with 3 and 5 wt.% CNCs loading. Melting temperatures vs CNCs content plots are presented in the appendix Figure A3 for clear understanding of the impact of CNCs on the melting temperatures of each polymer in the nanocomposite. This suggests that CNCs disrupt the order of PLA crystals, which is in agreement with SAXS results where no long order (L) peak was observed at 3 and 5 wt.% CNCs loading. In the PLA/PCL (70/30) system (Figures 4.2c and 4.3c), CNCs enhance crystallinity of PCL, notably at 1 and 3 wt.% loading (Figure 4.2b). Five wt.% CNCs reduces T_c, which might be due to CNCs agglomeration. Quantitatively, the cold crystallization temperature (T_{cc}) of PLA decreased from 113.3°C in neat PLA to 91.4°C in PLA/PCL (70/30)/5 wt.% CNCs (Table 4.4), confirming the role of CNCs as nucleating agents for PLA. Incorporations of 3 and 5 wt.% CNCs shifted T_{cc} of PLA to lower temperatures, which suggests that it is acting as a nucleating agent for PLA, for both PLA-rich and PCL-rich systems. The assumption is that there is poor interacting between CNCs and both PLA and PCL phases, since CNCs is highly hydrophilic while PLA and PCL are hydrophobic (Motloung et al., 2020a).

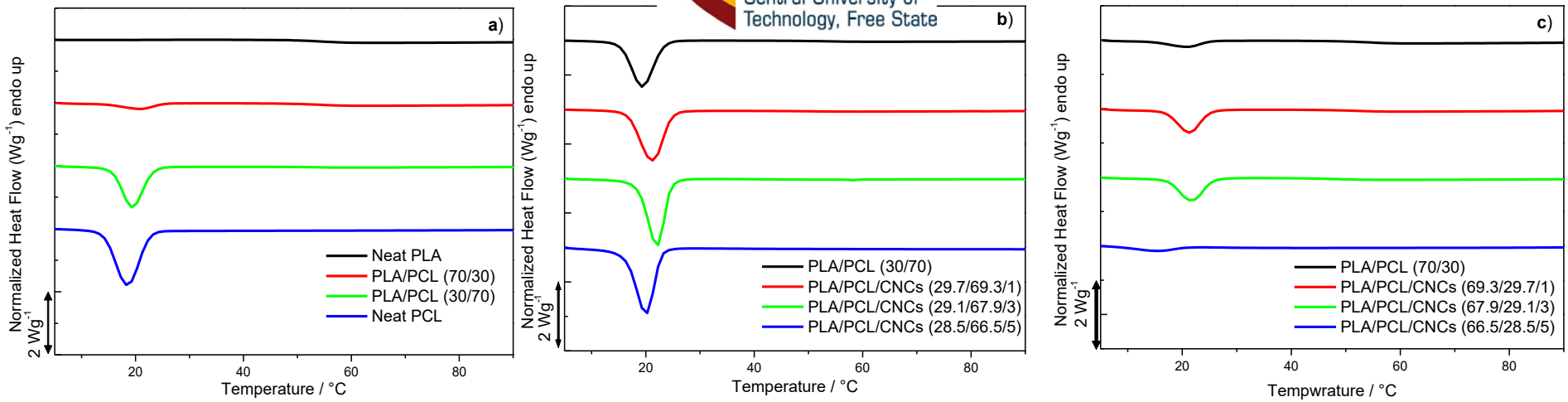

Figure 4.2 **Differential scanning calorimetry cooling curves for (a) neat PLA, neat PCL, 70/30 and 30/70 PLA/PCL blends; (b) 30/70 PLA/PCL blend and 30/70 PLA/PCL blend nanocomposites with CNCs at 1, 3 and 5 wt.%; (c) 70/30 PLA/PCL blend, and 70/30 PLA/PCL blend nanocomposites with CNCs at 1, 3 and 5 wt.% .**

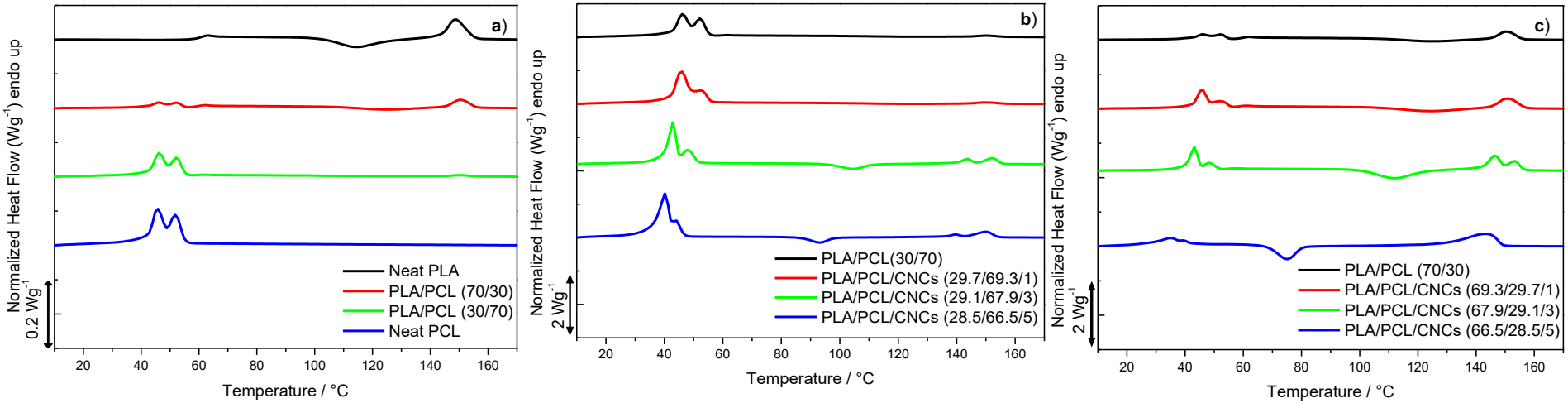

Figure 4.3 **Differential scanning calorimetry second heating curves for (a) neat PLA, neat PCL, 70/30 and 30/70 PLA/PCL blends; (b) 30/70 PLA/PCL blend and 30/70 PLA/PCL blend nanocomposites with CNCs at 1, 3 and 5 wt.%; (c) 70/30 PLA/PCL blend, and 70/30 PLA/PCL blend nanocomposites with CNCs at 1, 3 and 5 wt.% .**

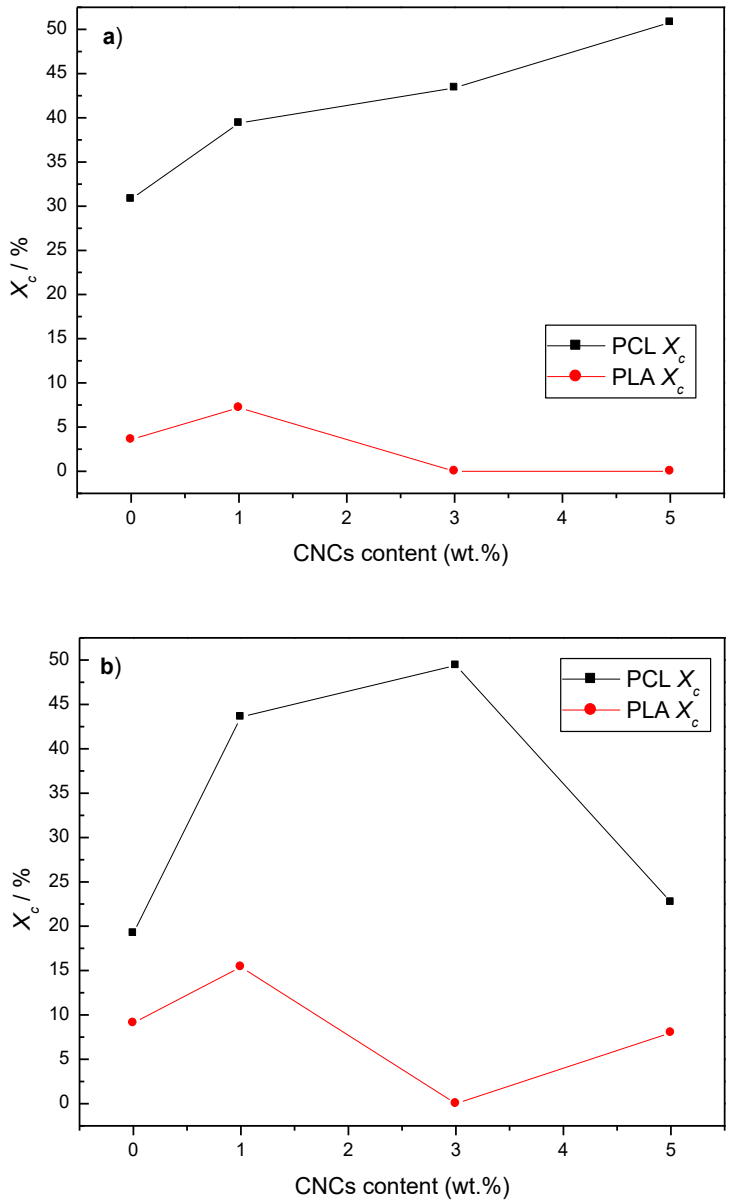

Figure 4.4 Degree of crystallinity of PCL and PLA in (a) 30/70 and (b) 70/30 PLA/PCL nanocomposites with 1, 3 and 5 wt.% CNCs content.

Table 4.4 Differential scanning calorimetry results for [illegible]caprolactone) neat polymers, their blends, and their blend nanocomposites with 1, 3 and 5 wt.% cellulose nanocrystals loading.

Sample	PCL T_c and ΔH_c		PCL T_m and ΔH_m			PCL X_c	PLA T_g	PLA T_{cc} and ΔH_{cc}		PLA T_m & ΔH_m			PLA X_c
	T_c	ΔH_c	T_{m1}	T_{m2}	ΔH_m		T_g	T_{cc}	ΔH_{cc}	T_{m1}	T_{m2}	ΔH_m	
Neat PLA	–	–	–	–	–	–	59.6±0.1	113.3±0.5	14±1.5	149.1±0.1	–	21±0.2	7.5
PLA/PCL (70/30)	21.2±0.0	6±0.1	46.6±0.0	52.5±0.2	8±0.3	19.2	59.0±0.0	126.0±0.5	2±1.0	150.6±0.0	–	8±0.2	9.1,
PLA/PCL (30/70)	19.4±0.0	36±0.1	45.7±0.4	52.3±0.0	30±0.2	30.8	59.3±0.3	–	–	150.4±0.1	–	1±0.1	3.6
Neat PCL	18.4±0.0	54±0.1	45.6±0.2	52.2±0.1	56±0.4	40.3	–	–	–	–	–	–	–
PLA/PCL/CNCs (29.7/69.3/1)	20.7±0.5	43±1.3	45.6±0.3	52.4±0.3	38±2.2	39.4	–	–	–	150.7±0.5	–	2±0.4	7.2
PLA/PCL/CNCs (29.1/67.9/3)	22.2±0.1	42±4.5	43.0±0.3	48.0±0.2	41±4.3	43.4	–	103.8±0.8	9±2.1	143.8±0.2	152.5±0.4	9±2.3	0
PLA/PCL/CNCs (28.5/66.5/5)	19.9±0.1	47±3.0	40.3±0.1	43.4±0.5	47±2.9	50.8	–	91.4±1.6	4±2.7	139.0±0.6	149.5±0.5	4±5.3	0
PLA/PCL/CNCs (69.3/29.7/1)	21.4±0.1	20±0.4	45.7±0.2	51.5±0.3	18±2.1	43.6	48.4±0.2	123.9±0.5	1±0.4	151.0±0.0	–	11±0.1	15.4
PLA/PCL/CNCs (67.9/29.1/3)	21.8±0.0	21±0.3	42.9±0.3	47.7±0.3	20±0.6	49.4	–	109.6±1.5	19±3.8	146.0±0.5	153.2±0.1	19±1.8	0.0
PLA/PCL/CNCs (66.5/28.5/5)	15.6±0.7	5±0.6	36.0±0.7	40.2±0.6	9±1.5	22.7	–	75.8±0.9	18±1.4	143.9±0.2	–	23±1.4	8

Note: PCL = poly(ε-caprolactone); PLA = poly(lactic acid) and CNCs = cellulose nanocrystals; T_m – melting peak temperature, ΔH_m – melting enthalpy, T_c – crystallization temperature, ΔH_c – crystallization enthalpy, T_{cc} – cold crystallization temperature, ΔH_{cc} – cold crystallization enthalpy, T_g – glass transition temperature and X_c – degree of crystallinity.

4.5.2 Morphological analysis

Scanning electron microscopy

Figures 4.5, 4.6, and 4.7 present SEM micrographs illustrating the morphological characteristics of neat polymers, blends, CNCs, and nanocomposites. SEM analysis provides complementary insights into phase compatibility, dispersion, and interfacial interactions discussed in DSC, FTIR and X-ray scattering sections. In Figure 4.5a, neat PLA displays a rough fractured surface, indicative of its brittle nature and amorphous morphology. Neat PCL (Figure 4.5b), in contrast, exhibits a smooth and homogeneous surface, characteristic of its ductile and semicrystalline nature. These morphological features align with WAXS and SAXS results, where PLA showed less crystallinity and no stack, while PCL exhibited broader but distinct crystalline reflections.

Blends of PLA/PCL (Figures 4.5c and 4.5d) demonstrate phase separation, confirming their immiscibility, as supported by DSC results where the melting temperatures of the polymers in the blends correspond to that of neat polymers. In the PLA/PCL (70/30) blend (Figure 4.5c), PCL microspheres with a diameter range from 250 nm to 1.5 µm are dispersed within the PLA matrix, suggesting restricted compatibility but effective dispersion. Although no quantitative droplet size analysis (e.g., via Image J) was performed, the approximate ranges observed (250 nm–1,5 µm in PLA-rich blends, versus ~5 µm PLA domains in PCL-rich blends) indicated reduced phase size upon CNCs addition. This qualitative observation supports improved miscibility, consistent with crystallinity increases from DSC/WAXS. This morphology supports the findings of Botlhoko et al. (2018) and Motloung et al. (2020a), who noted PCL domains well dispersed on the PLA matrix at this 70/30 PLA/PCL blend ratio. Conversely, the PLA/PCL (30/70) blend (Figure 4.5d) exhibits a large PLA sphere with a diameter of 5,25 µm embedded within a continuous PCL matrix, which suggests increased phase separation and reduced interfacial interaction (Zhu et al., 2020).

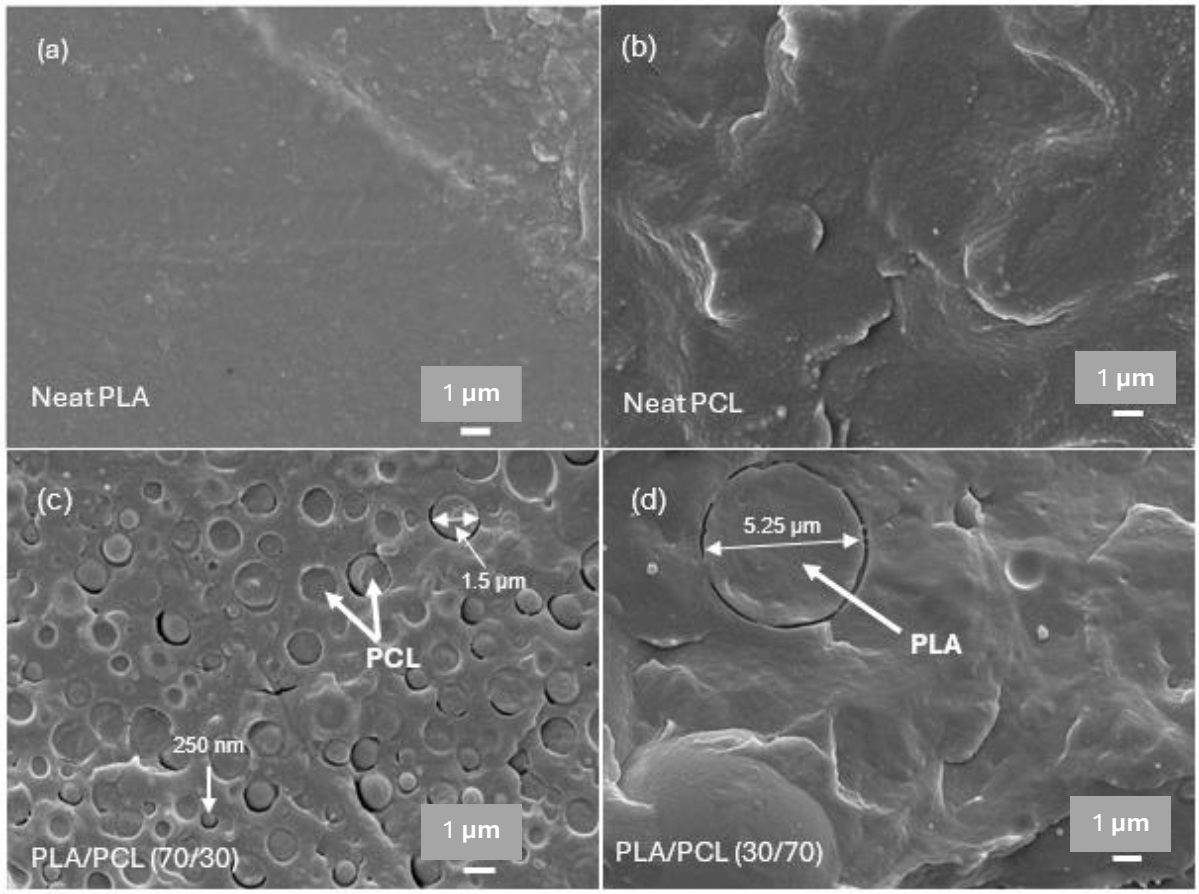

Figure 4.5 Morphological features of (a) neat PLA, (b) neat PCL, (c) PLA/PCL (70/30) blend, and (d) PLA/PCL (30/70) blend, captured at a scale of 1 µm

Figure 4.6 shows the morphology of PLA/PCL (30/70) nanocomposites with CNCs at 1, 3, and 5 wt.% loading. Neat CNCs (Figure 4.6b) appear as rod-like nanoparticles with length ranges from 230 nm to 850 nm, consistent with their known geometry. At 1 wt.% CNCs (Figure 4.6c), the phase boundary between PLA and PCL becomes less distinct, and dispersion appears improved compared to the PLA/PCL (30/70) blend, suggesting enhanced interfacial adhesion (Zhu et al., 2020). At 3 and 5 wt.% CNCs (Figures 4.6d and 4.6e), surfaces appear rougher with blurred phase boundaries, indicative of possible plastic deformation due to the flexibility of PCL. These results are in line with WAXS results showing increased crystallinity with increasing CNCs content.

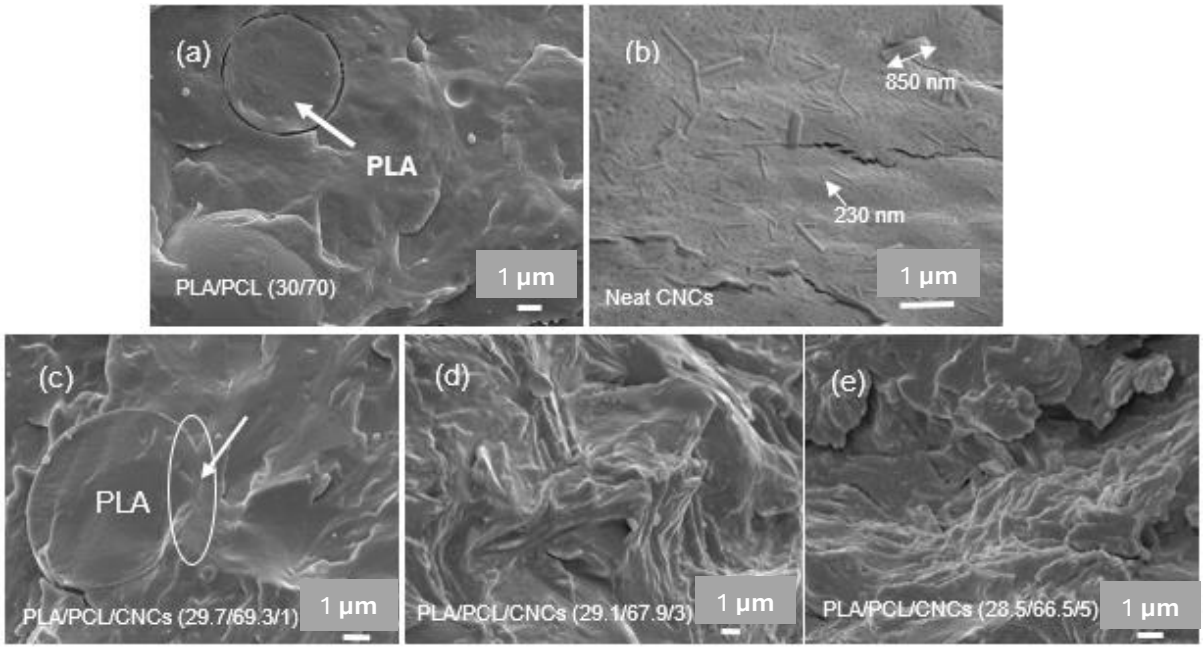

Figure 4.6 Scanning electron microscopy morphological features of (a) PLA/PCL (30/70) blend, (b) neat CNCs, (c) PLA/PCL/CNCs (29,7/69,3/1), (d) PLA/PCL/CNCs (29,1/67,9/3), and PLA/PCL/CNCs (28,5/66.5/5)

Figure 4.7 illustrates PLA/PCL (70/30) nanocomposites with CNCs. At 1 wt.% CNCs (Figure 4.7c), the morphology shows dispersed PCL domains within the PLA matrix, but with slightly reduced droplet size compared to the blend alone. At 3 wt.% CNCs (Figure 4.7d), surface morphology becomes smoother at the interface, suggesting enhanced interfacial adhesion in PLA and PCL, reflecting optimal CNCs distribution. These results correspond with the WAXS findings of increased crystallinity. At 5 wt.% CNCs (Figure 4.7e), phase boundaries are vanishing, suggesting that CNCs are localized in the minor PCL phase (Motloung et al., 2020a). This observation corroborates SAXS data, where high CNCs loadings led to diminished structural ordering.

In summary, SEM confirms that CNCs at 1–3 wt.% enhance dispersion and interfacial adhesion in PLA/PCL blends, leading to improved compatibility and crystallinity. At higher loadings (5 wt.%), surface irregularities dominate, reducing structural homogeneity. These morphological observations reinforce the complementary findings of WAXS and SAXS.

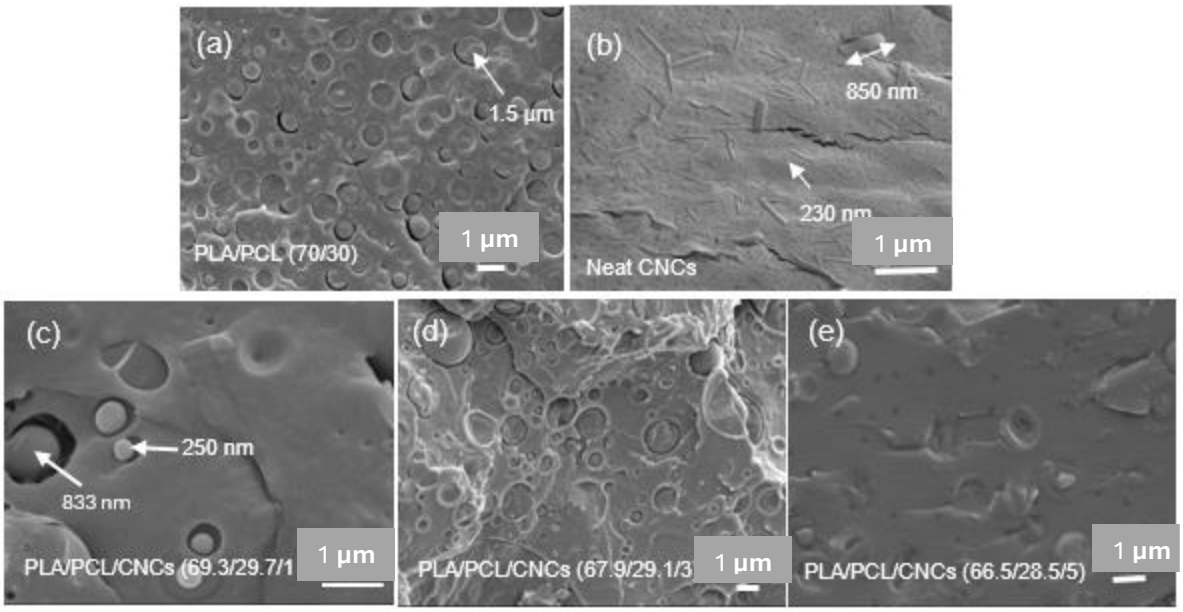

Figure 4.7 Scanning electron microscopy morphological features of (a) PLA/PCL (70/30) blend, (b) neat CNCs, (c) PLA/PCL/CNCs (69,3/29,7/1), (d) PLA/PCL/CNCs (67,9/29,1/3), and PLA/PCL/CNCs (66.5/28,5/5)

4.5.3 Structural analysis

Wide angle X-ray scattering

The WAXS patterns (Figure 4.8) provide insight into the crystalline structures of neat polymers, CNCs, their blends and nanocomposites. Table 4.5 presents their crystallinity (X_{cx}) which was calculated by Equation 4.2:

$$X_{cx} = \frac{I_c}{I_c + I_a} \qquad 4.2$$

where I_c and I_a are respectively the integrated intensities of the crystalline and amorphous phases. Illustrative example is presented in the appendix Figure A4.

Figure 4.8a presents the WAXS spectra of neat PLA, neat PCL and the PLA/PCL blends. Neat PLA exhibits a broad halo in the q range of 7.0 –15.0 nm^{-1}, reflecting reduced long-range order and a more amorphous character. Two sharp PLA crystalline peaks at q values of 11.6 and 13.3 nm^{-1} with a crystallinity of 8,9%, correspond to the 110/200 and 203 planes of the α-form crystal structure (Sun et al., 2014). In contrast, neat PCL presents broader peaks at q = 15.0 and 17.0 nm^{-1}, with a crystallinity of 17.9%, assigned to its 110 and 200 planes (Gumede et al., 2017a; Sun et al., 2014). Minor peaks around

27.0 and 31.0 nm^{-1} in both polymers indicate a long-range crystalline order (Motloung et al., 2020b).

In the PLA/PCL (70/30) blend, only a broad halo appears in the q range of 7.0–15.0 nm^{-1}, no PLA crystalline peaks, which is unusual since PLA is a dominant component. This suggests that PLA lack long-range order detectable crystals due to the presence of PCL in a blend. This might be in line with the DSC results where X_c of PLA in a blend is lower compared to that of neat PLA. The suppressed intensity of the PCL peaks at 15.5 and 17.5 nm^{-1} further suggests that PLA inhibits PCL crystallization in the blend. The crystallinity (Table 4.5) of PLA/PCL (70/30) blend is 3.5%, which is much lower than that of neat polymers. This suppression corresponds with the dominance of PLA bands in FTIR for this blend, indicating phase separation but physical compatibility (Motloung et al., 2020b; Salmani et al., 2024). Conversely, the PLA/PCL (30/70) blend shows clearer PCL peaks at 15.6 and 17.3 nm^{-1}, alongside a shoulder at 16.1 nm^{-1} (assigned to the 111 plane), confirming the structural dominance of PCL in this formulation (Gumede et al., 2017b; Dodda et al., 2023). These results corroborate with the FTIR data, showing PCL peak dominance in this composition.

Figure 4.8b shows the WAXS patterns of neat CNCs and PLA/PCL (30/70)/CNCs nanocomposites with varying CNCs content. Neat CNCs reveal sharp, intense peaks at q = 26.8, 31.0, 44.1, 51.2, and 53.8 nm^{-1}, indicating high crystallinity (53.7%). The CNCs peaks are deviated to higher q values compared to the q values reported in literature which might be due to the source and processing of CNCs (Islam et al., 2025; Motloung et al., 2020a; Salmani et al., 2024). For example, Motloung et al., 2020a, presented WAXS results for spray dried CNCs with q = 10.6, 14.6, 15.8 and 24.1 nm^{-1}. The shift is due to the decreased interplanar spacing (d) in the CNCs. The decrease in d-spacing may be caused by thicker packing of crystals or a modification process such as drying methods (Kádár et al., 2021). When 1 wt.% CNCs is incorporated into the PLA/PCL (30/70) blend, the WAXS pattern retains the PCL peaks at 14.9 and 17.1 nm^{-1}, with minor additional peaks around 26.8 and 31.0 nm^{-1} resembling CNCs. This suggests the successful dispersion of CNCs and increased crystallinity by 66.6%. However, in the 3 and 5 wt.% CNCs loading nanocomposites, the intensity of polymer (PLA and PCL)-related peaks diminished, and only CNCs peaks remained. This suggests that high CNCs loading

irregulate crystal ordering, as observed from the SEM results. However, the crystallinity of the nanocomposites increased due to the increasing of high crystalline CNCs content in the nanocomposites.

Figure 4.8c presents patterns for the PLA/PCL (70/30) blend and its CNCs nanocomposites. At a 1 and 3 wt.% CNC loading, WAXS scans reveal peaks for both polymers and CNCs; even PLA crystal peaks that are not present in the PLA/PCL 70/30 blend. This suggests that the incorporation of CNCs increases the crystallinity of the blend. Although at 1 wt.% CNCs, the amorphous halo is still present. At higher CNCs loadings (3 and 5 wt.%), peak intensity declines, and amorphous halos disappear, further indicating increased crystallinity but possibly at the cost of homogeneity. The 5 wt.% sample retains only the PLA peak at 11,6 nm^{-1}, with no detectable PCL signal, implying suppressed PCL crystallization due to excessive CNCs content. This is consistent with the DSC degree of crystallinity.

Notably, PLA crystalline peaks that were absent in the PLA/PCL (70/30) blend, reappeared upon the addition of CNCs, confirming their role as effective nucleating agents (Figure 4.8c). Similar effects have been reported by (Sessini et al., 2018) for CNCs-grafted PLA/PCL systems, reinforcing that CNCs enhance crystallinity when optimally dispersed.

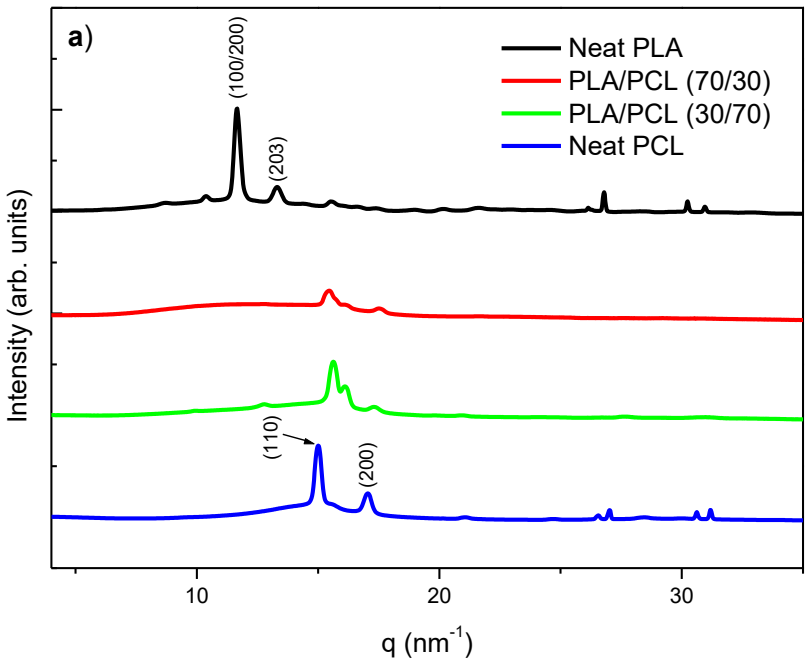

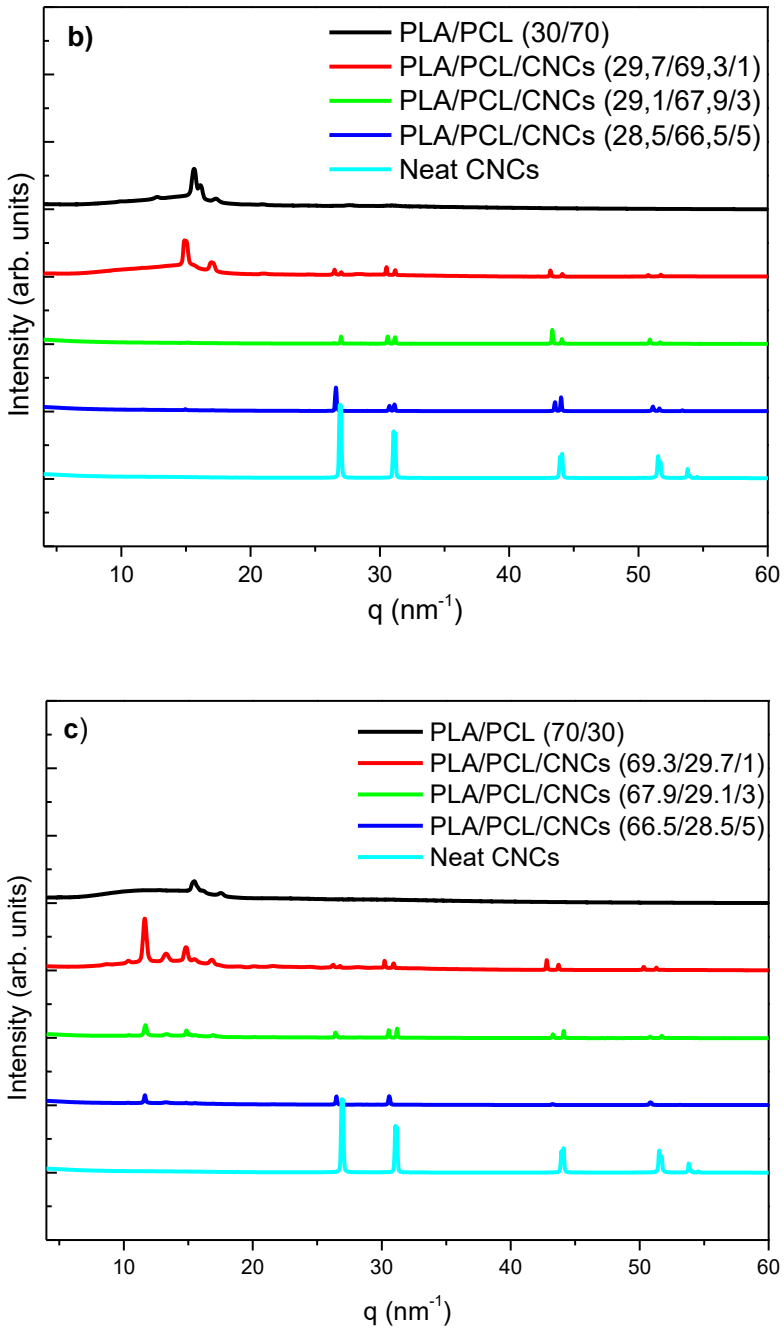

Figure 4.8 WAXS patterns of (a) neat PLA, neat PCL, 70/30 and 30/70 PLA/PCL blends (b) neat CNCs, 30/70 PLA/PCL blend and 30/70 PLA/PCL blend nanocomposites with CNCs at 1, 3 and 5 wt.%; (c) neat CNCs, 70/30 PLA/PCL blend, and 70/30 PLA/PCL blend nanocomposites with CNCs at 1, 3 and 5 wt.%. (Results taken from second heating at 25 °C)

Table 4.5 Crystallinity of neat polymers, their blends, cellulose nanocrystals and their nanocomposites

Sample	I_c	(I_c+I_a)	X_{cx}%
Neat PLA	0.00349	0.0392	8.9
PLA/PCL (70/30)	0.00232	0.0666	3.5
PLA/PCL (30/70)	0.00659	0.0640	10.2
Neat PCL	0.00756	0.0422	17.9
PLA/PCL/CNCs (29.7/69.3/1)	0.00731	0.0477	15.3
PLA/PCL/CNCs (29.1/67.9/3)	0.00176	0.00962	18.3
PLA/PCL/CNCs (28.5/66.5/5)	0.00295	0.0113	26.2
PLA/PCL/CNCs (69.3/29.7/1)	0.01090	0.0538	20.3
PLA/PCL/CNCs (67.9/29.1/3)	0.00308	0.01667	18.5
PLA/PCL/CNCs (66.5/28.5/5)	0.00165	0.01326	12.4
Neat CNCs	0.01265	0.02357	53.7

Note: PCL = poly(ε-caprolactone); PLA = poly(lactic acid) and CNCs = cellulose nanocrystals

Small angle X-ray scattering

Figure 4.9 presents SAXS profiles for neat PLA, neat PCL, PLA/PCL blends, and their nanocomposites with various CNCs loadings. SAXS provides insights into nanoscale morphology by analyzing periodicities of crystalline and amorphous layers. Table 4.5 presents the long period (L), representing the average spacing of lamellar structures, calculated using Equation 4.3, and lamella thickness (l_c) calculated using Equation 4.4:

$$L = \frac{2\pi}{q_{max}} \qquad 4.3$$

where q_{max} is the position of the peak maximum in nm^{-1}.

$$l_c = L.X_{cx} \qquad 4.4$$

where L is long period in nm and X_{cx} is the crystallinity.

In Figure 4.9a, neat PLA shows a very weak or absent SAXS peak, indicating a mostly amorphous structure, supported by the broad, less intense peaks in WAXS. This is also in agreement with DSC results that indicated a minimal degree of crystallinity. In contrast, neat PCL exhibits a broader and more intense SAXS peak, with an L value of approximately 16.5 nm, suggesting the presence of semicrystalline lamellae with limited order (Gumede et al., 2017b).

Both PLA/PCL 70/30 and 30/70 blends exhibit broader and less intense peaks compared to neat PCL. This reduction in intensity and peak clarity correlates with the decrease in PCL content and supports the partial immiscibility observed in SEM and DSC. The absence of new peaks also supports the notion that PLA and PCL phases remain distinct, without significant co-crystallization or interpenetration.

In Figure 4.9b, the PLA/PCL (30/70) nanocomposites with CNCs are presented. Neat CNCs, as expected, do not show any peak in the SAXS range due to their small particle size and high crystallinity revealed in WAXS. Among the nanocomposites, only the 1 wt.% CNCs sample shows a broad SAXS peak, indicative of some degree of nanoscale ordering. The long period (L) of nanocomposite with 1 wt.% CNCs slightly decreases compared to that of the blend, this means the spacing between crystalline lamellae (crystal + amorphous thickness) is smaller. This suggests that at low loadings, CNCs may facilitate lamellar organization. At 3 and 5 wt.% CNCs, no SAXS peaks are observed, implying disruption of long-range ordering, possibly due to CNCs incorporation, consistent diminished peak intensity in WAXS.

Figure 4.9c shows SAXS data for the PLA/PCL (70/30) nanocomposites. Similar to the 30/70 system, only the 1 wt.% CNCs sample exhibits a weak SAXS peak, suggesting some lamellar order. The peak is less intense than the corresponding PLA/PCL (70/30) blend, indicating possible interference with lamellar packing. The 3 and 5 wt.% CNCs samples show no observable peaks in this region, further confirming the absence of nanoscale periodicity at high CNCs content. SAXS profiles of intensity (I) vs scattering vector (q) are presented in the appendix Figure A6, and they provide information similar to that presented in Figure 4.9. These findings are supported by WAXS data indicating increased crystallinity but reduced homogeneity.

In summary, SAXS analysis confirms that CNCs influence nanoscale structural ordering, depending on their concentration. At 1 wt.%, CNCs enhance lamellar alignment, especially in PCL-rich systems, while higher loadings disrupt this order. These observations support and extend the crystalline trends observed in WAXS, highlighting the importance of CNCs loading in tuning nanocomposite structure.

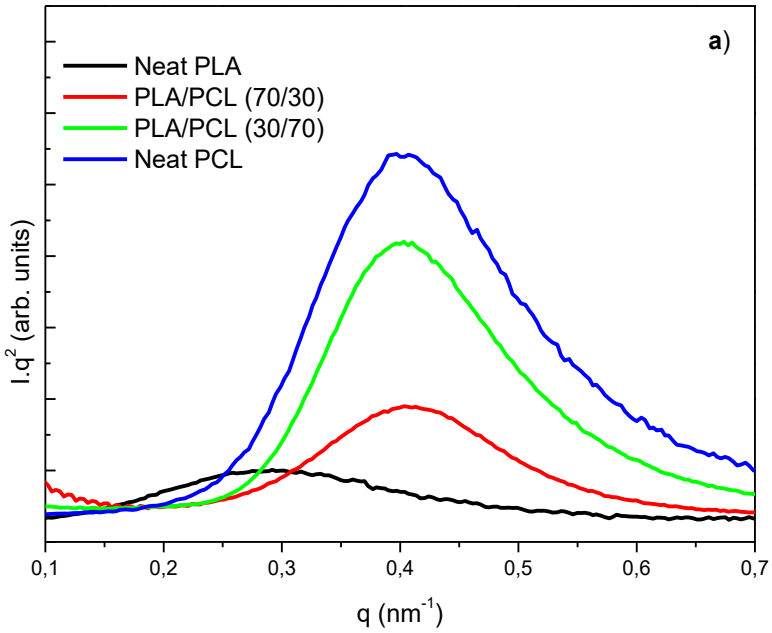

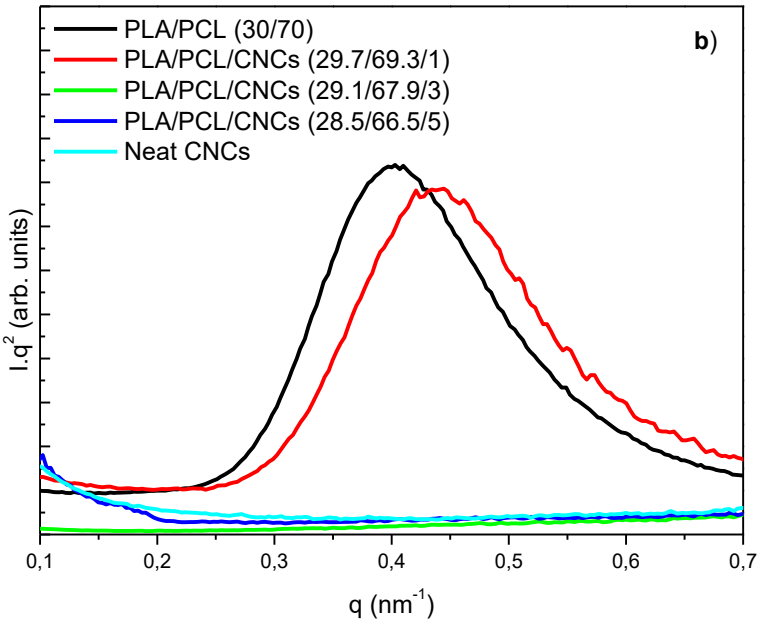

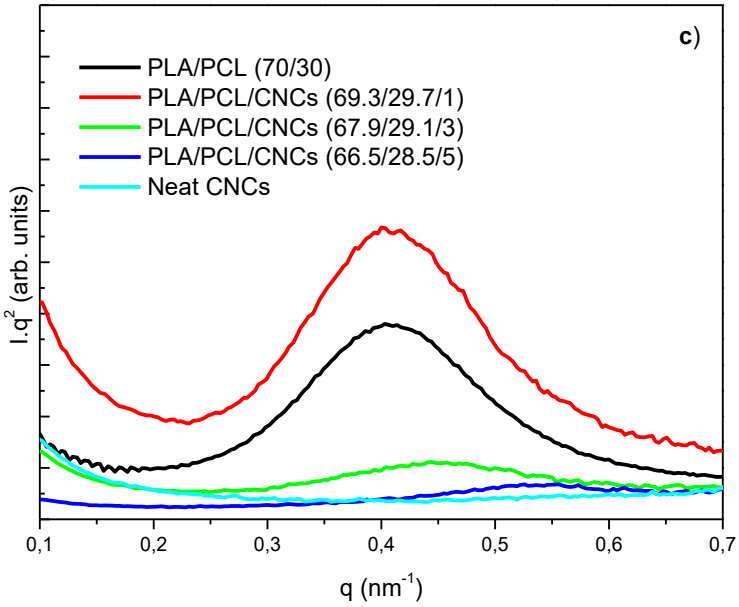

Figure 4.9 SAXS patterns of (a) neat PLA, neat PCL, 70/30 and 30/70 PLA/PCL blends; (b) neat CNCs, 30/70 PLA/PCL blend and 30/70 PLA/PCL blend nanocomposites with CNCs at 1, 3 and 5 wt.%; (c) neat CNCs, 70/30 PLA/PCL blend, and 70/30 PLA/PCL blend nanocomposites with CNCs at 1, 3 and 5 wt.%. (Results taken from second heating at 25 °C)

Table 4.6 summarizes the SAXS parameters obtained from neat polymers, blends, and nanocomposites. Neat PCL, PLA/PCL (70/30), and PLA/PCL (30/70) all displayed a long period (L) of ~16.5 nm, confirming the presence of semicrystalline lamellar structures. When CNCs were introduced, only the 1 wt.% nanocomposites retained a measurable SAXS peak, with a reduced L value of 15.0 nm in the 30/70 system. This suggests that low CNCs loading promotes tighter lamellar packing, while higher CNCs contents (3 and 5 wt.%) disrupted nanoscale periodicity, eliminating SAXS peaks. These results complement the WAXS analysis, where CNCs acted as nucleating agents at low loading but interfered with crystal organization at higher loadings.

Table 4.6 Small angle X-ray scattering parameters obtained from neat polymers, blends, and nanocomposites

Sample	q_{max}	L	l_c
Neat PLA	0.29	21.7	193.1
PLA/PCL (70/30)	0.40	15.7	55.0
PLA/PCL (30/70)	0.40	15.7	160.1

Sample	q_{max}	L	l_c
Neat PCL	0.40	15.7	281.0
PLA/PCL/CNCs (29.7/69.3/1)	0.44	14.3	218.8
PLA/PCL/CNCs (29.1/67.9/3)	–	–	–
PLA/PCL/CNCs (28.5/66.5/5)	–	–	–
PLA/PCL/CNCs (69.3/29.7/1)	0.40	15.7	318.7
PLA/PCL/CNCs (67.9/29.1/3)	0.45	14.0	259.0
PLA/PCL/CNCs (66.5/28.5/5)	0.54	11.6	143.8
Neat CNCs	–	–	–

Note: PCL = poly(ε-caprolactone); PLA = poly(lactic acid) and CNCs = cellulose nanocrystals; q_{max}= peak maximum ; L = Long period.

Fourier transform infrared spectroscopy

The FTIR spectra shown in Figure 4.10 presents the characteristic functional groups of neat PLA, neat PCL, CNCs, their blends, and nanocomposites with varying CNCs compositions. As shown in Figure 4.9a, neat PLA exhibits a medium-intensity C=O stretching peak at 1 753 cm^{-1}, associated with ester carbonyl groups. Additionally, C–H stretching vibrations are observed at 2 960 and 2 882 cm^{-1}, and a prominent C–O–C asymmetric stretching peak appears around 1 188 cm^{-1}, along with a symmetric stretching peak near 1 086 cm^{-1}. Neat PCL, on the other hand, shows its own distinctive features, including a strong C=O stretching band at 1 730 cm^{-1}, and prominent C–O–C peaks at 1 263 cm^{-1} (asymmetric) and 1 173 cm^{-1} (symmetric).

When PLA and PCL are blended, the FTIR spectra shows the superimposition of neat PLA and PCL bands. For example, in PLA/PCL (70/30) and (30/70) blends, the characteristic ester carbonyl peaks at 1 753 and 1 730 cm^{-1} are still observed with no significant shift, suggesting the absence of chemical interactions. However, their relative intensities vary based on composition. The PLA/PCL (30/70) blend shows stronger C–H and PCL-related

C–O–C peaks (1 263 and 1 173 cm^{-1}), confirming PCL dominance. Conversely, the PLA/PCL (70/30) blend shows more pronounced PLA spectral features. These results confirm the immiscibility of PLA and PCL, which align with literature findings(Coates, 2000; Motloung et al., 2020a; Nandiyanto et al., 2019).

Figures 4.10b and 4.10c show the FTIR spectra for nanocomposites incorporating CNCs. Cellulose nanocrystals exhibit a broad O−H stretching band at 3 330 cm^{-1} due to intra- and intermolecular hydrogen bonding between hydroxyl groups, characteristic C–H stretching from 2 977 to 2 892 cm^{-1}, and a sharp peak near 1 040 cm^{-1} due to C–O stretching and C–H rocking of the pyranose ring. Additional bands at 1 437 and 1 326 cm^{-1} correspond to CH_2 bending and polysaccharide ring vibrations, respectively (Kargarzadeh et al., 2012; Sikhosana et al., 2023; Sirviö et al., 2016). Incorporation of CNCs into the PLA/PCL (30/70) blends (Figure 4.10b) results in notable changes in C–O–C peak intensities at 1 173 cm^{-1} for all nanocomposites. The increase in C–O–C intensity is attributed to CNCs, indicating their presence in the matrix. However, no new peaks emerge, affirming the absence of covalent bonding. For PLA/PCL (70/30)/CNCs nanocomposites (Figure 4.10c), notably nanocomposite with 3 wt.% CNCs show increased peak intensities, while 1 wt.% CNCs suppressed the peak intensities. This might be influenced by the amount of the sample analyzed, hydrogen bonding between the hydroxyl groups of CNCs and the ester carbonyls of PLA or PCL which can reduce the number of free hydroxyl groups, thereby decreasing the intensity of the O–H stretching band. Crystallinity also plays an important role, as CNCs display intensity variations in crystallinity-sensitive bands. In addition, the broadening of the O–H stretching band at ~3 330 cm^{-1} and subtle shifts in the C=O stretching peaks (1 753 → 1 749 cm^{-1}) suggest hydrogen bonding between CNCs hydroxyl groups and PLA/PCL ester carbonyls. No new covalent bonds formed, but hydrogen bonding between CNCs hydroxyl groups and PLA/PCL carbonyls contributed to improved compatibility. The results suggest that CNCs influence the intensity of the peaks but not the position of characteristic peaks (Dadras Chomachayi et al., 2020; Kalita et al., 2020c).

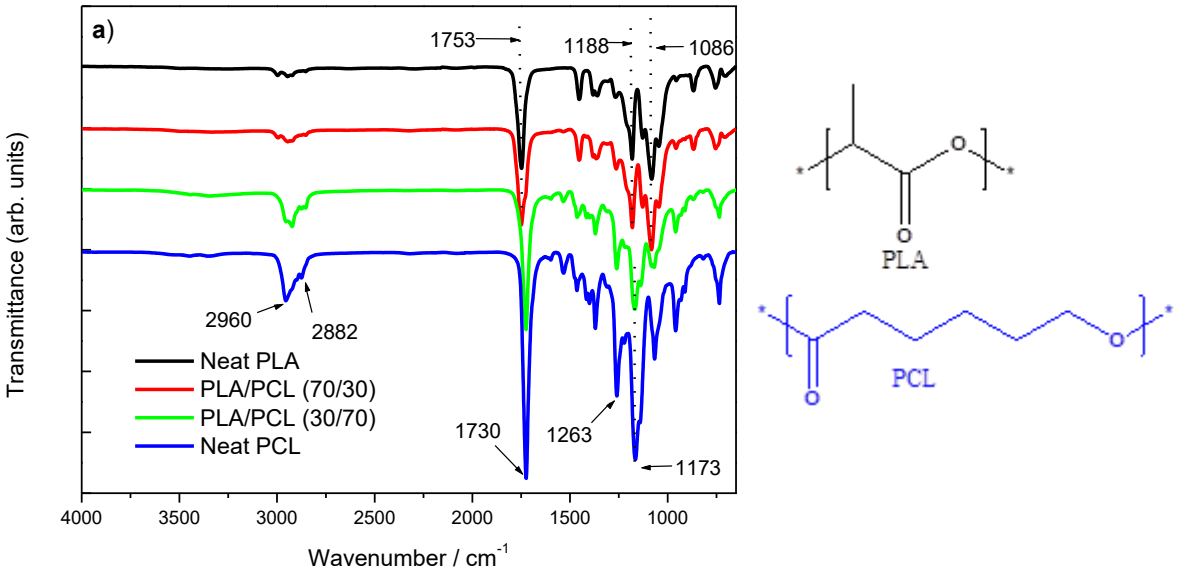

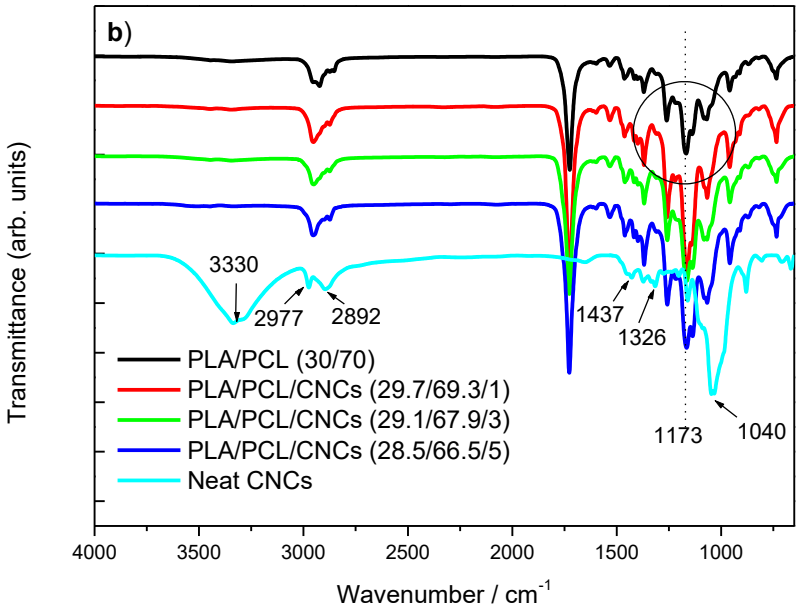

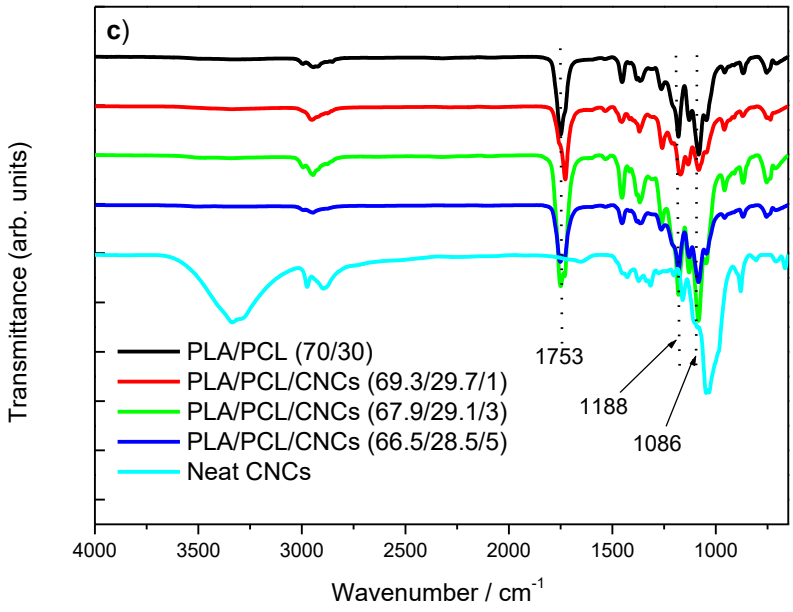

Figure 4.10 FTIR spectra of (a) neat PLA, neat PCL, 70/30 and 30/70 PLA/PCL blends; (b) neat CNCs, 30/70 PLA/PCL blend and 30/70 PLA/PCL blend nanocomposites with CNCs at 1, 3 and 5 wt.%; (c) neat CNCs, 70/30 PLA/PCL blend, and 70/30 PLA/PCL blend nano-composites with CNCs at 1, 3 and 5 wt.%.

4.5.4 Thermal stability

Thermogravimetric analysis

Thermal stability was assessed using TGA, as shown in Figures 4.11 to 4.13 and Tables 4.6 and 4.7. For neat polymers (Figure 4.11a and 4.11b), neat PLA exhibits a single degradation step with an onset temperature (T_{onset}) of 305.8°C and a maximum degradation temperature (T_{max}) of 369.0°C. In contrast, neat PCL demonstrates higher thermal stability, with a T_{onset} of 310.3°C and a T_{max} of 418.0°C. These findings correlate with DSC results, where PCL showed higher crystallinity and thermal resistance compared to PLA.

For PLA/PCL blends, the TGA and DTG curves (Figures 4.11a and 4.11b) exhibit two-step degradation patterns, representing the individual decomposition of PLA and PCL phases. The onset temperatures (T_{onset}) of PLA/PCL (70/30) and (30/70) blends shift to lower temperatures compared to that of neat PLA. The thermal stability of PLA was expected to increase, but that did not happen probably due to immiscibility of the two polymers leading to no improvement in the thermal stability of PLA. This corresponds to findings

by Motloung et al. (2020a). The blend of PLA/PCL (30/70) shows higher thermal stability compared to the PLA/PCL (70/30) blend, consistent with the larger PCL fraction. These outcomes support the immiscibility observed via SEM and the dominant thermal transitions seen in DSC data.

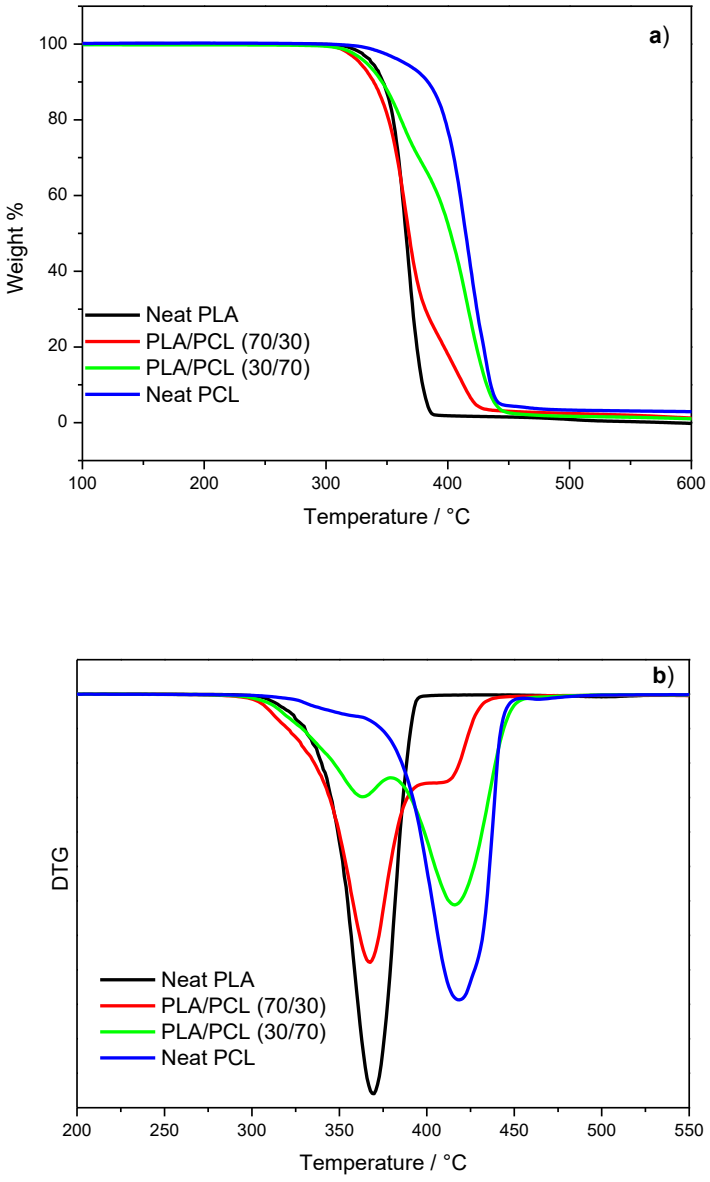

Figure 4.2 (a) TGA and (b) DTG curves for neat PLA, neat PCL, 70/30 and 30/70 PLA/PCL blends

Figures 4.12 and 4.13 show the thermal degradation behavior of PLA/PCL/CNCs nanocomposites. Onset degradation temperature (T_{onset}), maximum degradation temperature (T_{max}), and residual weight ($W_{residue}$) for neat CNCs, neat polymers, their blends, and the nanocomposites of their blends, are presented in Tables 4.7 and 4.8. The neat CNCs spectrum presented in both Figures 4.12 and 4.13, and Table 4.7 shows the

initial weight loss around 100 °C due to the evaporation of moisture. Neat CNCs exhibit a two-step degradation process. The first degradation step corresponds to the degradation of sulphated cellulose (sulphate-containing CNCs), and the second degradation process is ascribed to the breakdown of the interior of non-sulphated crystalline cellulose (Wang et al., 2019; Xing et al., 2018). The char residue of CNCs is higher compared to that of the blends and nanocomposites. This is due to strong intra- and intermolecular hydrogen bonding between cellulose chains that stabilize the structure during heating, so instead of volatilizing completely, the cellulose undergoes dehydration and carbonization, leaving a stable char.

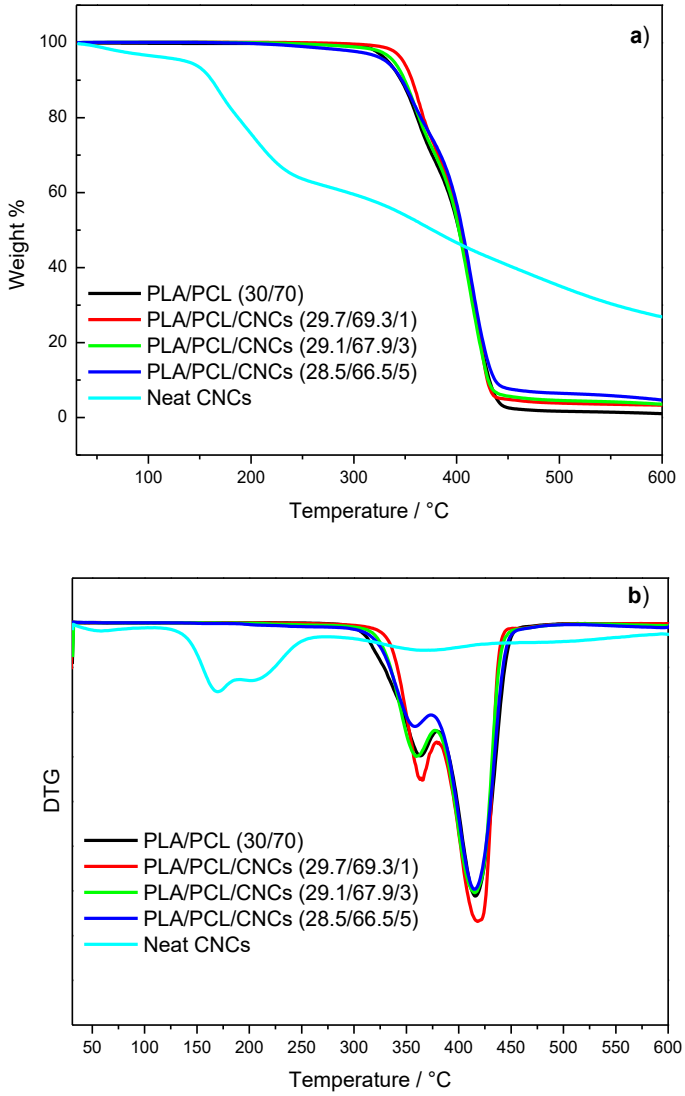

Figure 4.12 (a) TGA and (b) DTG curves for neat CNCs, 30/70 PLA/PCL blend, and 30/70 PLA/PCL blend nanocomposites with CNCs at 1,3 and 5 wt.%.

In the PLA/PCL (30/70) blend (Figure 4.12), the addition of 1 wt.% CNCs slightly enhances thermal stability, as reflected in increased T_{onset} and T_{max} values, reported in Table 4.8. However, higher CNCs loadings (3 and 5 wt.%) reduce thermal stability. In PLA/PCL (70/30) nanocomposites (Figure 4.13), 1 wt.% CNCs only increases T_{onset}, while 3 and 5 wt.% lead to thermally unstable nanocomposites. For example (Table 4.8), neat PLA exhibited T_{onset} = 305.8°C, while PLA/PCL (30/70)/5 wt.% CNCs degraded earlier at 261.1°C, showing that sulphated CNCs catalyze polymer decomposition at high loadings. These results show that there is no significant thermal stability enhancement in the blends, due to the incorporation of less thermally stable CNCs which degrade before the polymers. These results can also confirm the immiscibility/incompatibility between the two polymers since two degradation steps are observed from the nanocomposites which are assigned to individual polymers.

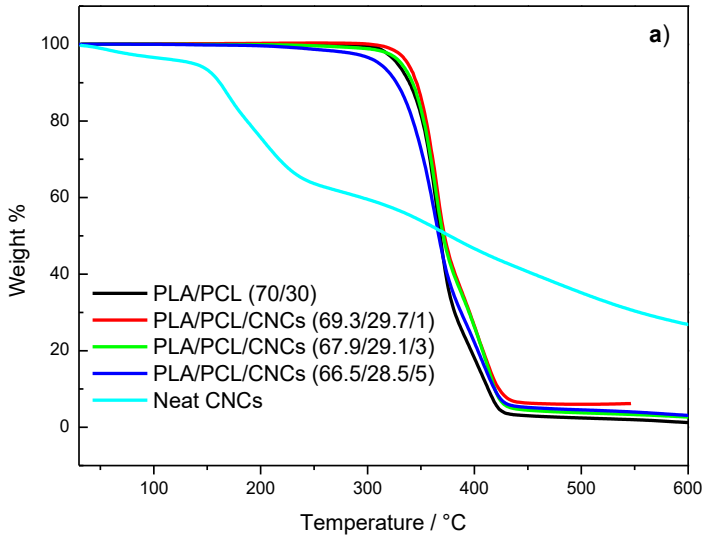

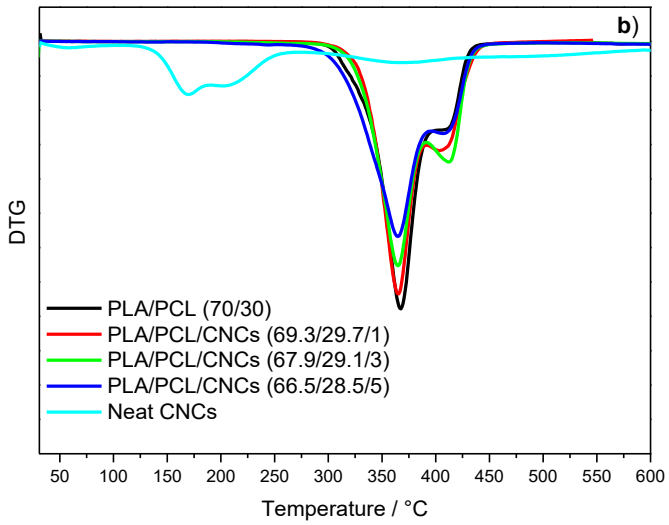

Figure 4.13 (a) TGA and (b) DTG curves for neat CNCs, 70/30 PLA/PCL blend, and 70/30 PLA/PCL blend nanocomposites with CNCs at 1,3 and 5 wt.%

Table 4.7 Thermal characteristics of cellulose nanocrystals, including onset temperatures, peak temperatures, and residual weight

Sample	T_{1onset} / °C	T_{1max} / °C	T_{2onset} / °C	T_{2max} / °C	$W_{residue}$ / %
Cellulose nanocrystals	128.4	168.8	299.4	368.8	26.9

Note: T_{onset} = onset temperatures; T_{max} = peak temperatures; $W_{residue}$ = Residual weight

Table 4.8 Thermal stability for neat polymers, their blends and nanocomposites

Sample	PLA T_{onset} / °C	PLA T_{max} / °C	PCL T_{onset} / °C	PCL T_{max} / °C	$W_{residue}$ / %
Neat PLA	305.8	369.0	–	–	0,0
PLA/PCL (70/30)	293.1	367.0	402.1	411.0	1.4
PLA/PCL (30/70)	299.5	362.5	380.4	416.1	1.3
Neat PCL	–	–	310.3	418.0	3.1
PLA/PCL/CNCs (29.7/69.3/1)	302.6	364.7	379.2	418.7	3.4

PLA/PCL/CNCs (29.1/67.9/3)	287.0	360.6	376.1	415.4	3.6
PLA/PCL/CNCs (28.5/66.5/5)	261.1	363.7	373.0	415.4	4.8
PLA/PCL/CNCs (69.3/29.7/1)	302.1	365.7	390.6	405.1	6.0
PLA/PCL/CNCs (67.9/29.1/3)	282.9	364.7	390.6	413.4	2.5
PLA/PCL/CNCs (66.5/28.5/5)	256.9	364.7	395.8	407.2	3.1

Note: PCL = poly(ε-caprolactone); PLA = poly(lactic acid) and CNCs = cellulose nanocrystals; T_{onset} = onset temperatures; T_{max} = peak temperatures; $W_{residue}$ = Residual weight

4.5.5 Mechanical properties

Tensile testing

The tensile behavior of neat PLA, neat PCL and their blends (70/30 and 30/70 PLA/PCL) is presented in Table 4.9 and Figure 4.14. In a graph of strain (%) versus stress (N/mm^2) presented in Figure 4.14, and maximum values of strain and stress presented in Table 4.9, neat PLA exhibited the highest tensile strength and modulus but fractured at very low elongation, confirming its brittle nature. In contrast, neat PCL displayed lower strength but very high elongation at break, consistent with its ductile behavior. These differences can be attributed to their morphology, where SEM fracture surfaces further supported these observations, with PLA showing smooth, brittle fracture features and PCL displaying rougher, fibrillated surfaces typical of ductile failure. These findings are consistent with a previous report by (Botlhoko et al., 2018), where PLA exhibited high stiffness but fractured at low strains, while PCL showed high ductility at the expense of strength.

The 70/30 PLA/PCL blend exhibited reduced tensile strength compared to neat PLA but slightly improved elongation at break. This indicates that PCL acted as a toughening agent, imparting ductility to the otherwise brittle PLA matrix. DSC confirmed partial miscibility between PCL and PLA, which may have facilitated stress transfer across

phases. SEM images revealed phase-separated morphology, explaining why the strength did not fully match that of neat PLA. The 30/70 PLA/PCL blend exhibited reduced tensile strength but slightly improved elongation at break compared to neat PLA and PLA-rich blend. These results align with SEM features where a large PLA sphere was observed in the PCL matrix, which confirms the incompatibility of the two polymers at this ratio and contribute to poor tensile strength. Similar phase-separated morphologies have been observed in PLA/PCL blends by other researchers (Zhu et al., 2020), and this has been identified as a key factor limiting stress transfer and reducing tensile strength.

Tensile testing could not be performed on the CNCs-reinforced nanocomposites (1, 3, and 5 wt.%), as the samples fractured during specimen preparation. The brittle nature of these materials prevented reliable measurements. This limitation reflects the inherent fragility of the material, rather than a shortcoming in experimental design. Previous studies on PLA/PCL/CNCs (Motloung et al., 2020a; Salmani et al., 2024), also did not report tensile testing results, which might be due to these challenges. Nevertheless, thermal (DSC, TGA) and structural (WAXS, SAXS) analyses revealed that the incorporation of CNCs influenced crystallinity and thermal stability, suggesting that their mechanical properties may have been enhanced but at the expense of reduced toughness. Future work should employ alternative testing methods (e.g., micro-tensile or DMA) to quantify these effects.

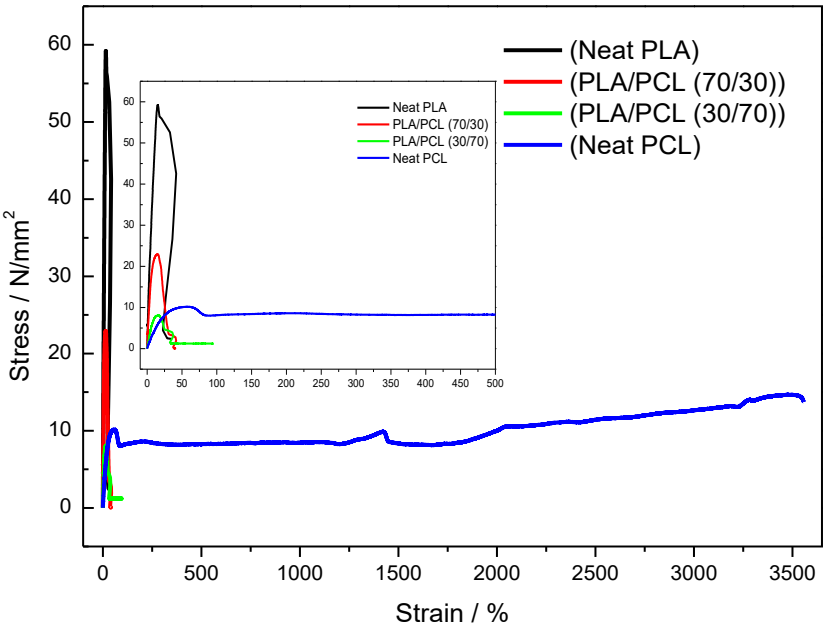

Figure 4.14 Tensile testing for neat PLA, neat PCL, 70/30, 30/70 PLA/PCL blend

Table 4.9 Maximum strain and stress of poly(lactic acid), poly(ε-caprolactone) and their blends

Sample	Maximum strain / %	Maximum stress / N/mm²
Neat PLA	12.96±2.2	58.72±0.9
PLA/PCL (70/30)	13.65±1.6	31.57±7.7
PLA/PCL (30/70)	19.51±4.4	9.45±1.2
Neat PCL	3 593.82±314.3	15.85±1.6

Note: PLA = poly(lactic acid), PCL = poly(ε-caprolactone)

4.5.6 Biodegradation response and functional integration

Soil burial

The biodegradation test for neat polymers, their blends and nanocomposites were conducted by soil burial and reported in Figures 4.15, Table 4.10 and 4.11. Degradation patterns for neat polymers and their blends are presented in Figure 4.15a. Neat PLA and PLA-rich blends did not degrade at all in a period of 84 days while the neat PCL and PCL-rich blend lost a weight of about 4% in the same period. In a period of 112 days, the neat

PLA and PLA-rich blend only lost a weight of 0,3%, while the neat PCL and PCL-rich blend lost 5,5 and 4,5%, respectively. This concludes that the PCL and PCL-rich blend degrade faster compared to a PLA and PLA-rich blend. Factors such as temperature, moisture, pH, and microbial activity all impact the degradation rates. PLA typically requires higher temperature and humidity, as found in industrial composting conditions (Muniyasamy *et al.*, 2016; Kalita *et al.*, 2020), while PCL degrades faster in soil because of its flexibility, enzyme-accessible structure, low T_g, more permeable crystallinity, and direct susceptibility to microbial attack (Al Hosni, Pittman and Robson, 2019). Consequently, the soil conditions in this study favored faster degradation of PCL.

For a PLA/PCL (30/70) blend with 1, 3 and 5 wt.% CNCs (Figure 4.15b). The presence of CNCs sped up the biodegradation and the high percentage of each composite degraded compared to the blend. The degradation rate and weight loss increase with the increasing CNCs content in the composites, as seen in Figure 4.15b and Table 4.10. For the PLA/PCL (70/30) blend with 1, 3 and 5 wt.% CNCs (Figure 4.15c). Low (1 and 3 wt.%) CNCs loading does not show significant impact on the biodegradation of the composites, while 5 wt.% sped up the degradation and degraded completely on Day 112. These results conclude that the addition of CNCs to PLA/PCL blend improved the biodegradability of a blend, especially for the PCL-rich blend, while for the PLA-rich blend, only 5 wt.% CNCs improved the biodegradability. The most striking result is the complete degradation of PLA/PCL (70/30)/5 wt.% CNCs within 112 days, compared to only 0,3% weight loss in neat PLA over the same period. This highlights the dual role of CNCs in improving crystallinity and enhancing water uptake/microbial colonization, thereby accelerating biodegradation.

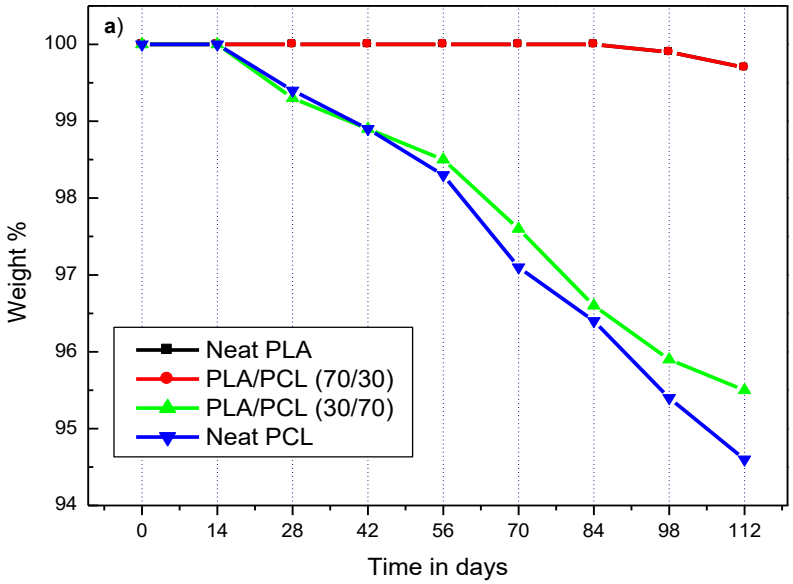

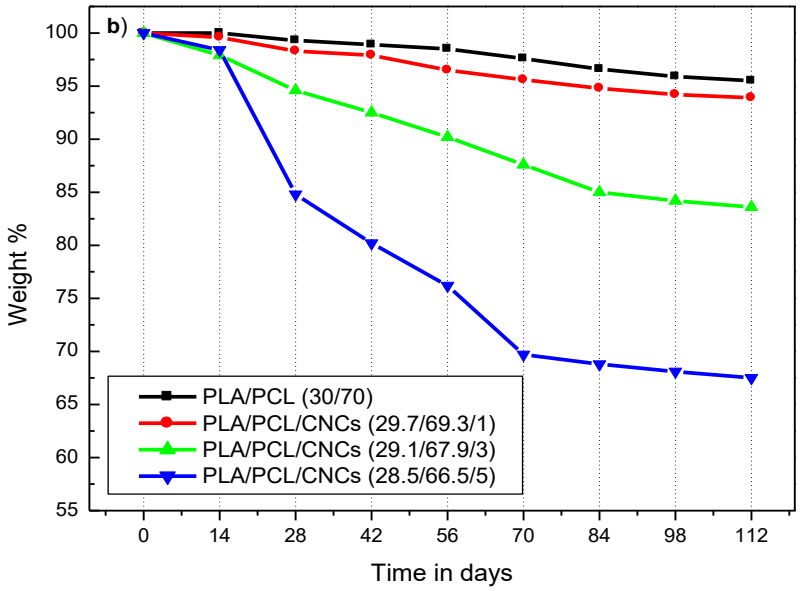

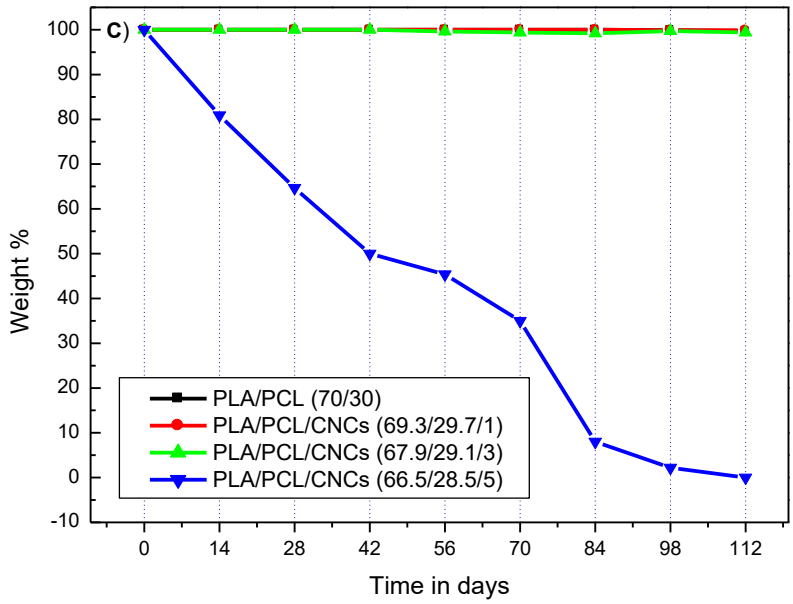

Figure 4.15 Weight percentage as a function of time in days for (a) neat PLA, neat PCL, 70/30 and 30/70 PLA/PCL blends; (b) 30/70 PLA/PCL blend and 30/70 PLA/PCL/CNC blend nanocomposites with CNCs at 1, 3 and 5 wt.%; (c) 70/30 PLA/PCL blend, and 70/30 PLA/PCL/CNCs blend nanocomposites with CNCs at 1, 3 and 5 wt.%

Table 4.10 Weight percentage versus time in days for neat PLA, neat PCL, 70/30 and 30/70 PLA/PCL blends; and 30/70 PLA/PCL/CNC blend nanocomposites with CNCs at 1, 3 and 5 wt.%.

Sample	Day 0	Day 14	Day 28	Day 42	Day 56	Day 70	Day 84	Day 98	Day 112
Neat PLA	100	100	100	100	100	100	99.9	99.9	99.7
PLA/PCL (70/30)	100	100	100	100	100	100	99.9	99.9	99.7
PLA/PCL (30/70)	100	100	99.3	98.9	98.5	97.6	96.6	95.9	95.5
Neat PCL	100	100	99.4	98.9	98.3	97.1	96.4	95.4	94.6
PLA/PCL/CNCs (29.7/69.3/1)	100	99.6	98.3	97.9	96.5	95.6	94.8	94.2	93.9
PLA/PCL/CNCs (29.1/67.9/3)	100	97.9	94.6	92.5	90.2	87.6	85.0	84.2	83.6
PLA/PCL/CNCs (28.5/66.5/5)	100	98.4	84.8	80.2	76.2	69.7	68.8	68.1	67.5
PLA/PCL/CNCs (69.3/29.7/1)	100	100	100	100	100	100	99.9	99.9	99.9
PLA/PCL/CNCs (67.9/29.1/3)	100	100	100	100	99.8	99.7	99.7	99.7	99.4
PLA/PCL/CNCs (66.5/28.5/5)	100	80.9	64.7	50.0	45.4	35.0	8.0	2.2	0.00

Table 4.11 Biodegradation analysis images for neat PLA, neat PCL 30/70 and 70/30 PLA/PCL blends, and their nanocomposites with 1, 3 and 5 wt.% CNCs, taken at days 0, 42, 84 and 112

Day 0		Day 42		Day 84		Day 112	
 Neat PLA	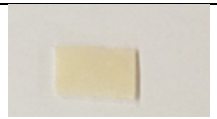 Neat PCL	 Neat PLA	 Neat PCL	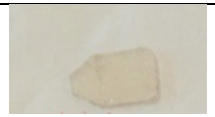 Neat PLA	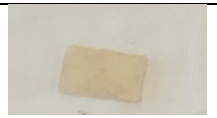 Neat PCL	 Neat PLA	 Neat PCL
 PLA/PCL (70/30)	 PLA/PCL (30/70)	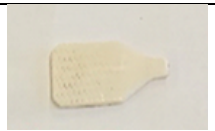 PLA/PCL (70/30)	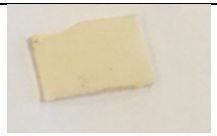 PLA/PCL (30/70)	 PLA/PCL (70/30)	 PLA/PCL (30/70)	 PLA/PCL (70/30)	 PLA/PCL (30/70)
 PLA/PCL/CNCs (69.3/29.7/1)	 PLA/PCL/CNCs (29.7/69.3/1)	 PLA/PCL/CNCs (69.3/29.7/1)	 PLA/PCL/CNCs (29.7/69.3/1)	 PLA/PCL/CNCs (69.3/29.7/1)	 PLA/PCL/CNCs (29.7/69.3/1)	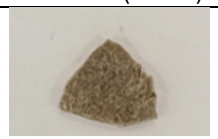 PLA/PCL/CNCs (69.3/29.7/1)	 PLA/PCL/CNCs (29.7/69.3/1)
 PLA/PCL/CNCs (67.9/29.1/3)	 PLA/PCL/CNCs (29.1/67.9/3)	 PLA/PCL/CNCs (67.9/29.1/3)	 PLA/PCL/CNCs (29.1/67.9/3)	 PLA/PCL/CNCs (67.9/29.1/3)	 PLA/PCL/CNCs (29.1/67.9/3)	 PLA/PCL/CNCs (67.9/29.1/3)	 PLA/PCL/CNCs (29.1/67.9/3)
 PLA/PCL/CNCs (66.5/28.5/5)	 PLA/PCL/CNCs (28.5/66.5/5)	 PLA/PCL/CNCs (66.5/28.5/5)	 PLA/PCL/CNCs (28.5/66.5/5)	 PLA/PCL/CNCs (66.5/28.5/5)	 PLA/PCL/CNCs (28.5/66.5/5)	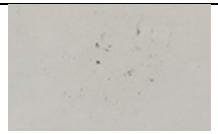 PLA/PCL/CNCs (66.5/28.5/5)	 PLA/PCL/CNCs (28.5/66.5/5)

4.6 Conclusion

This study demonstrated the fabrication and characterization of PLA/PCL biodegradable nanocomposites reinforced with CNCs extracted from sugarcane bagasse. The incorporation of CNCs influenced the thermal, morphological, and structural behavior of PLA/PCL blends in a composition-dependent manner. The incorporation of CNCs improved the biodegradation rate, crystallinity, interfacial adhesion, and slightly (only at 1 wt.% CNCs) thermal stability. Tensile testing confirmed that PLA exhibited higher strength compared to PCL and PLA/PCL blends, whereas mechanical testing of CNCs-reinforced nanocomposites could not be performed due to premature sample fracture, reflecting their brittle nature. The enhancements observed in the thermal behavior, morphology, structure, and biodegradation were supported by DSC, SEM, FTIR, WAXS, SAXS, TGA, and soil burial biodegradation test results. In general, the findings confirmed that sugarcane bagasse-derived CNCs can enhance the performance of PLA/PCL systems, providing a sustainable approach to developing high-performance biodegradable materials for diverse applications such as food packaging and biomedical.

Acknowledgements

This research was funded by the National Research Foundation (NRF) of South Africa through the Thuthuka Programme (Grant No. TTK2204264865) and the NRF postgraduate student support fund (Grant No. PMDS22062125350), and DSI-NRF Innovation Postdoctoral Fellowship (Grant No. PSTD2205057154). Additional financial support was provided by the postgraduate student fund of the Central University of Technology, Free State, and Future Coal Mining (Chelmsford Colliery). ALBA synchrotron facility for SAXS/WASX analysis.

References

Alokika, Anu, Kumar, A., Kumar, V. and Singh, B. (2021) “Cellulosic and hemicellulosic fractions of sugarcane bagasse: Potential, challenges and future perspective,” *International Journal of Biological Macromolecules*. Elsevier B.V., pp. 564–582. Available at: https://doi.org/10.1016/j.ijbiomac.2020.12.175.

Asadnia, M. and Sadat-Shojai, M. (2025) “Recent perspective of synthesis and modification strategies of cellulose nanocrystals and cellulose nanofibrils and their

beneficial impact in scaffold-based tissue engineering: A review," *International Journal of Biological Macromolecules*. Elsevier B.V. Available at: https://doi.org/10.1016/j.ijbiomac.2024.139409.

Botlhoko, O.J., Sinha Ray, S. and Ramontja, J. (2018) *A new insight into morphological, thermal, and mechanical properties of melt-processed polylactide/poly(ε-caprolactone) blends*. Available at: https://doi.org/https://doi.org/10.1016/j.polymdegradstab.2018.05.025.

Chaka, K.T. (2022) "Extraction of cellulose nanocrystals from agricultural by-products: a review," *Green Chemistry Letters and Reviews*. Taylor and Francis Ltd., pp. 582–597. Available at: https://doi.org/10.1080/17518253.2022.2121183.

Chen, Y., Lu, T., Li, L., Zhang, H., Wang, H. and Ke, F. (2023) "Fully biodegradable PLA composite with improved mechanical properties via 3D printing," *Materials Letters*, 331(November 2022), p. 133543. Available at: https://doi.org/10.1016/j.matlet.2022.133543.

Coates, J.P. (2000) Interpretation of infrared spectra: A practical and systematic approach. In: Meyers, R.A. (Ed.), Encyclopedia of *analytical* chemistry*: Applications, theory and instrumentation*, 10815-10837. Wiley. https://doi.org/10.1002/9780470027318.a5606

Dabhi, M., Dange, H., Bonde, C. and Bonde, S. (2025) "A comprehensive review on sustainable production of nano crystalline cellulose from sugarcane bagasse and its applications," *Chemical Engineering Communications* [Preprint]. Taylor and Francis Ltd. Available at: https://doi.org/10.1080/00986445.2025.2469588.

Dadras Chomachayi, M., Jalali-Arani, A., Beltrán, F.R., De La Orden, U. and Urreaga, J.M. (2020) "Biodegradable Nanocomposite Developed from the PLA/PCL Blends and Silk Fibroin Nanoparticle: Study on the Microstructure, Thermal Behavior, Crystallinity, and Performance," *Journal of Polymers and the Environment*, 28, pp. 1252–1264. Available at: https://doi.org/10.1007/s10924.

Dodda, J.M., Azar, M.G., Bělský, P., Šlouf, M., Gajdošová, V., Kasi, P.B., Anerillas, L.O. and Kovářík, T. (2023) "Bioresorbable films of polycaprolactone blended with poly(lactic acid) or poly(lactic-co-glycolic acid)," *International Journal of Biological Macromolecules*, 248. Available at: https://doi.org/10.1016/j.ijbiomac.2023.126654.

Fernández-Tena, A., Otaegi, I., Irusta, L., Sebastián, V., Guerrica-Echevarria, G., Müller, A.J. and Aranburu, N. (2023) "High-Impact PLA in Compatibilized PLA/PCL Blends: Optimization of Blend Composition and Type and Content of Compatibilizer," *Macromolecular Materials and Engineering*, 308(12). Available at: https://doi.org/10.1002/mame.202300213.

Fitch-Vargas, P.R., Camacho-Hernández, I.L., Rodríguez-González, F.J., Martínez-Bustos, F., Calderón-Castro, A., Zazueta-Morales, J. de J. and Aguilar-Palazuelos, E. (2023) "Effect of compounding and plastic processing methods on the development of bioplastics based on acetylated starch reinforced with sugarcane bagasse cellulose fibers," *Industrial Crops and Products*, 192. Available at: https://doi.org/10.1016/j.indcrop.2022.116084.

Gan, I. and Chow, W.S. (2019) "Synthesis of phosphoric acid-treated sugarcane bagasse cellulose nanocrystal and its thermal properties enhancement for poly(lactic acid) nanocomposites," *Journal of Thermoplastic Composite Materials*, 32(5), pp. 619–634. Available at: https://doi.org/10.1177/0892705718772866.

Gumede, T.P., Luyt, A.S., Pérez-Camargo, R.A., Tercjak, A. and Müller, A.J. (2017a) "Morphology, nucleation, and isothermal crystallization kinetics of poly(ε-caprolactone) mixed with a polycarbonate/MWCNTs masterbatch," *Polymers*, 9, p. 709. Available at: https://doi.org/10.3390/polym912070.

Gumede, T.P., Luyt, A.S., Pérez-Camargo, R.A., Tercjak, A. and Müller, A.J. (2017b) "Morphology, nucleation, and isothermal crystallization kinetics of poly(ε-caprolactone) mixed with a polycarbonate/MWCNTs masterbatch," *Polymers*, 9, p. 709. Available at: https://doi.org/10.3390/polym912070.

Al Hosni, A.S., Pittman, J.K. and Robson, G.D. (2019) "Microbial degradation of four biodegradable polymers in soil and compost demonstrating polycaprolactone as an ideal compostable plastic," *Waste Management*, 97, pp. 105–114. Available at: https://doi.org/10.1016/j.wasman.2019.07.042.

Islam, M.M., Islam, M.A., Rahman, A.N.M.M., Xuepeng, Z., Li, J. and Liu, L. (2025) "Development of hybrid nanocellulose-reinforced PLA biocomposites from waste jute bags and ramie fabric with enhanced mechanical and thermal properties," *Biomass Conversion and Biorefinery* [Preprint]. Available at: https://doi.org/10.1007/s13399-025-06577-7.

Kádár, R., Spirk, S. and Nypelö, T. (2021) "Cellulose Nanocrystal Liquid Crystal Phases: Progress and Challenges in Characterization Using Rheology Coupled to Optics, Scattering, and Spectroscopy," *ACS Nano*. American Chemical Society, pp. 7931–7945. Available at: https://doi.org/10.1021/acsnano.0c09829.

Kalita, N.K., Bhasney, S.M., Mudenur, C., Kalamdhad, A. and Katiyar, V. (2020a) "End-of-life evaluation and biodegradation of Poly(lactic acid) (PLA)/Polycaprolactone (PCL)/Microcrystalline cellulose (MCC) polyblends under composting conditions," *Chemosphere*, 247, p. 125875. Available at: https://doi.org/10.1016/j.chemosphere.2020.125875.

Kalita, N.K., Bhasney, S.M., Mudenur, C., Kalamdhad, A. and Katiyar, V. (2020b) "End-of-life evaluation and biodegradation of Poly(lactic acid) (PLA)/Polycaprolactone (PCL)/Microcrystalline cellulose (MCC) polyblends under composting conditions," *Chemosphere*, 247. Available at: https://doi.org/10.1016/j.chemosphere.2020.125875.

Kalita, N.K., Bhasney, S.M., Mudenur, C., Kalamdhad, A. and Katiyar, V. (2020c) "End-of-life evaluation and biodegradation of Poly(lactic acid) (PLA)/Polycaprolactone (PCL)/Microcrystalline cellulose (MCC) polyblends under composting conditions," *Chemosphere*, 247. Available at: https://doi.org/10.1016/j.chemosphere.2020.125875.

Kargarzadeh, H., Ahmad, I., Abdullah, I., Dufresne, A., Zainudin, S.Y. and Sheltami, R.M. (2012) "Effects of hydrolysis conditions on the morphology, crystallinity, and thermal stability of cellulose nanocrystals extracted from kenaf bast fibers," *Cellulose*, 19(3), pp. 855–866. Available at: https://doi.org/10.1007/s10570-012-9684-6.

Kurakula, M., Rao, G.S.N.K. and Yadav, K.S. (2020) "Fabrication and characterization of polycaprolactone-based green materials for drug delivery," in *Applications of Advanced Green Materials*. Elsevier, pp. 395–423. Available at: https://doi.org/10.1016/B978-0-12-820484-9.00016-7.

Lattimer, M.P., Hobbs, J.K., Hill, M.J. and Barham, P.J. (1992) *On the origin of the multiple endotherms in PEEK*.

Luyt, A.S. and Malik, S.S. (2018) *Can biodegradable plastics solve plastic solid waste accumulation?*, *Plastics to Energy: Fuel, Chemicals, and Sustainability Implications*. Elsevier Inc. Available at: https://doi.org/10.1016/B978-0-12-813140-4.00016-9.

Melesse, G.T., Hone, F.G. and Mekonnen, M.A. (2022) "Extraction of Cellulose from Sugarcane Bagasse Optimization and Characterization," *Advances in Materials Science and Engineering*, 2022. Available at: https://doi.org/10.1155/2022/1712207.

Motloung, M.P., Ojijo, V., Bandyopadhyay, J. and Ray, S.S. (2020a) "Morphological characteristics and thermal, rheological, and mechanical properties of cellulose nanocrystals-containing biodegradable poly(lactic acid)/poly(ε-caprolactone) blend composites," *Journal of Applied Polymer Science*, 137(19). Available at: https://doi.org/10.1002/app.48665.

Motloung, M.P., Ojijo, V., Bandyopadhyay, J. and Ray, S.S. (2020b) "Morphological characteristics and thermal, rheological, and mechanical properties of cellulose nanocrystals-containing biodegradable poly(lactic acid)/poly(ε-caprolactone) blend composites," *Journal of Applied Polymer Science*, 137(19). Available at: https://doi.org/10.1002/app.48665.

Muniyasamy, S., Ofosu, O., John, M.J. and Anandjiwala, R.D. (2016) "Mineralization of poly(lactic acid) (PLA), Poly(3-hydroxybutyrate-co-valerate) (PHBV) and PLA/PHBV blend in compost and soil environments," *Journal of Renewable Materials*, 4(2), pp. 133–145. Available at: https://doi.org/10.7569/JRM.2016.634104.

Nandiyanto, A.B.D., Oktiani, R. and Ragadhita, R. (2019) "How to read and interpret ftir spectroscope of organic material," *Indonesian Journal of Science and Technology*, 4(1), pp. 97–118. Available at: https://doi.org/10.17509/ijost.v4i1.15806.

Padhi, S., Singh, A. and Routray, W. (2023) "Nanocellulose from agro-waste: a comprehensive review of extraction methods and applications," *Reviews in Environmental Science and Biotechnology*. Springer Science and Business Media B.V., pp. 1–27. Available at: https://doi.org/10.1007/s11157-023-09643-6.

Patrício, T. and Bártolo, P. (2013) "Thermal stability of PCL/PLA blends produced by physical blending process," in *Procedia Engineering*. Elsevier Ltd, pp. 292–297. Available at: https://doi.org/10.1016/j.proeng.2013.05.124.

Salmani, M.R., Shirazi, F., Goodarzi, K., Noormohammadi, F. and Nourany, M. (2024) "Improving Phase Compatibility of PLA-PCL Matrix-Droplet Blend Using CNC/PCL-PEG-PCL Triblock Copolymer to Prepare Porous 3D Osteoinductive Scaffolds," *Journal of Polymers and the Environment* [Preprint]. Available at: https://doi.org/10.1007/s10924-024-03392-5.

Sessini, V., Navarro-Baena, I., Arrieta, M.P., Dominici, F., López, D., Torre, L., Kenny, J.M., Dubois, P., Raquez, J.M. and Peponi, L. (2018a) "Effect of the addition of polyester-grafted-cellulose nanocrystals on the shape memory properties of biodegradable PLA/PCL nanocomposites," *Polymer Degradation and Stability*, 152, pp. 126–138. Available at: https://doi.org/10.1016/j.polymdegradstab.2018.04.012.

Sessini, V., Navarro-Baena, I., Arrieta, M.P., Dominici, F., López, D., Torre, L., Kenny, J.M., Dubois, P., Raquez, J.M. and Peponi, L. (2018b) "Effect of the addition of polyester-grafted-cellulose nanocrystals on the shape memory properties of biodegradable PLA/PCL nanocomposites," *Polymer Degradation and Stability*, 152, pp. 126–138. Available at: https://doi.org/10.1016/j.polymdegradstab.2018.04.012.

Sikhosana, S.T., Gumede, T.P., Malebo, N.J., Ogundeji, A.O. and Motloung, B. (2023) " The influence of cellulose content on the morphology, thermal, and mechanical properties of poly(lactic acid)/ Eucomis autumnalis cellulose biocomposites ," *Polymer Engineering & Science* [Preprint]. Available at: https://doi.org/10.1002/pen.26293.

Sirviö, J.A., Visanko, M., Heiskanen, J.P. and Liimatainen, H. (2016) "UV-absorbing cellulose nanocrystals as functional reinforcing fillers in polymer nanocomposite films," *Journal of Materials Chemistry A*, 4(17), pp. 6368–6375. Available at: https://doi.org/10.1039/c6ta00900j.

Sun, H., Yu, B., Han, J., Kong, J., Meng, L. and Zhu, F. (2014) "Microstructure, thermal properties and rheological behavior of PLA/PCL blends for melt-blown nonwovens," *Polymer (Korea)*, 38(4), pp. 477–483. Available at: https://doi.org/10.7317/pk.2014.38.4.477.

Wachirahuttapong, S., Thongpin, C. and Sombatsompop, N. (2016) "Effect of PCL and Compatibility Contents on the Morphology, Crystallization and Mechanical Properties of PLA/PCL Blends," *Energy Procedia*, 89, pp. 198–206. Available at: https://doi.org/10.1016/j.egypro.2016.05.026.

Wang, W., Niu, B., Liu, R., Chen, H., Fang, X., Wu, W., Wang, G., Gao, H. and Mu, H. (2023) "Development of bio-based PLA/cellulose antibacterial packaging and its application for the storage of shiitake mushroom," *Food Chemistry*, 429. Available at: https://doi.org/10.1016/j.foodchem.2023.136905.

Wang, Z., Yao, Z., Zhou, J., He, M., Jiang, Q., Li, S., Ma, Y., Liu, M. and Luo, S. (2019) "Isolation and characterization of cellulose nanocrystals from pueraria root residue," *International Journal of Biological Macromolecules*, 129, pp. 1081–1089. Available at: https://doi.org/10.1016/j.ijbiomac.2018.07.055.

Wani, A.K., Rahayu, F., Fauziah, L. and Suhara, C. (2023) "Advances in safe processing of sugarcane and bagasse for the generation of biofuels and bioactive compounds," *Journal of Agriculture and Food Research*, 12. Available at: https://doi.org/10.1016/j.jafr.2023.100549.

Xing, L., Gu, J., Zhang, W., Tu, D. and Hu, C. (2018) "Cellulose I and II nanocrystals produced by sulfuric acid hydrolysis of Tetra pak cellulose I," *Carbohydrate Polymers*, 192, pp. 184–192. Available at: https://doi.org/10.1016/j.carbpol.2018.03.042.

Xu, C., Chen, C. and Wu, D. (2018) "The starch nanocrystal filled biodegradable poly(ε-caprolactone) composite membrane with highly improved properties," *Carbohydrate Polymers*, 182, pp. 115–122. Available at: https://doi.org/10.1016/j.carbpol.2017.11.001.

Ye, G., Yong, Q., Hu, L., Rosqvist, E., Peltonen, J., Hu, Y., Xu, W. and Xu, C. (2025) "Molecular engineering of nanocellulose-poly(lactic acid) bio-nanocomposite interface by reactive surface grafting from copolymerization," *International Journal of Biological Macromolecules*, 306. Available at: https://doi.org/10.1016/j.ijbiomac.2025.141371.

Zhao, Z., Yan, H., Zheng, R., Khan, M.S., Fu, X., Tao, Z. and Zhang, Z. (2018) "Anthocyanins characterization and antioxidant activities of sugarcane (Saccharum officinarum L.) rind extracts," *Industrial Crops and Products*, 113, pp. 38–45. Available at: https://doi.org/10.1016/j.indcrop.2018.01.015.

Zhu, B., Wang, Y., Liu, H., Ying, J., Liu, C. and Shen, C. (2020) “Effects of interface interaction and microphase dispersion on the mechanical properties of PCL/PLA/MMT nanocomposites visualized by nanomechanical mapping,” *Composites Science and Technology*, 190. Available at: https://doi.org/10.1016/j.compscitech.2020.108048.

Zhu, H., Han, Z., Cheng, J.H. and Sun, D.W. (2022) “Modification of cellulose from sugarcane (Saccharum officinarum) bagasse pulp by cold plasma: Dissolution, structure and surface chemistry analysis,” *Food Chemistry*, 374. Available at: https://doi.org/10.1016/j.foodchem.2021.131675.

Chapter 5

CONCLUSIONS

This thesis investigated the fabrication, characterization, and performance of biodegradable nanocomposites based on poly(lactic acid) (PLA), poly(ε-caprolactone) (PCL), and their blends reinforced with cellulose nanocrystals (CNCs) derived from sugarcane bagasse. The research was driven by the need to address the limitations of individual biodegradable polymers and to explore sustainable reinforcements from agro-waste resources.

The first part of the study focused on CNCs-reinforced PLA and PCL systems. CNCs were shown to influence thermal, morphological, and structural properties in a composition-dependent manner. While CNCs incorporation enhanced crystallinity and significantly improved biodegradation, it also reduced the thermal stability of PLA at higher loadings and disrupted crystal ordering. In PCL, CNCs accelerated biodegradation progressively with increasing content, with little effect on thermal stability. These findings highlighted the polymer-specific effects of CNCs and their potential as functional reinforcements.

The second part of the study examined PLA/PCL blends and their CNCs-reinforced nanocomposites. Blending PLA with PCL improved flexibility compared to neat PLA, although mechanical strength remained lower. The addition of CNCs improved interfacial adhesion, crystallinity, and biodegradation, with 5 wt.% CNCs achieving complete mass loss within 112 days, compared to negligible degradation in neat PLA. However, CNCs offered only limited thermal stability benefits, with improvements observed at a 1 wt.% loading but reductions at higher concentrations. Tensile testing confirmed superior mechanical strength of neat PLA compared to PCL and PLA/PCL blends, while CNCs-reinforced nanocomposites could not be tested due to premature failure during specimen preparation.

For PCL/CNCs and PLA/CNCs, the effect of CNCs is mainly in the biodegradation. Properties such as thermal stability were not significantly affected by the incorporation of CNCs to PLC or PLA, this might be due to the undispersed CNCs. However, when a second polymer is used, PLA/PCL/CNCs, it seems that the CNCs effect is bigger, not only impacting the biodegradation but also other properties, and this might be related to the CNCs located at the interphase or acting as compatibilizing agent and therefore exploiting the properties of both polymeric matrices.

Taken together, the findings demonstrate that sugarcane bagasse-derived CNCs are effective reinforcements for biodegradable polymer systems, capable of enhancing crystallinity, morphology, and biodegradation performance. The outcomes provide clear evidence of the potential of agro-waste-derived nanocellulose in advancing sustainable polymer research and applications.

Future work should focus on optimizing processing strategies to overcome the brittleness of CNCs-reinforced nanocomposites, enabling the evaluation of reliable mechanical performance. Additionally, exploring surface modifications of CNCs and compatibilization strategies could further enhance their dispersion, interfacial adhesion, and property balance within PLA/PCL matrices.

This thesis confirms the viability of integrating nanocellulose from agricultural residues into biodegradable polymer systems and contributes valuable insights toward the development of next-generation sustainable materials for packaging, biomedical, and environmental applications.

APPENDIX

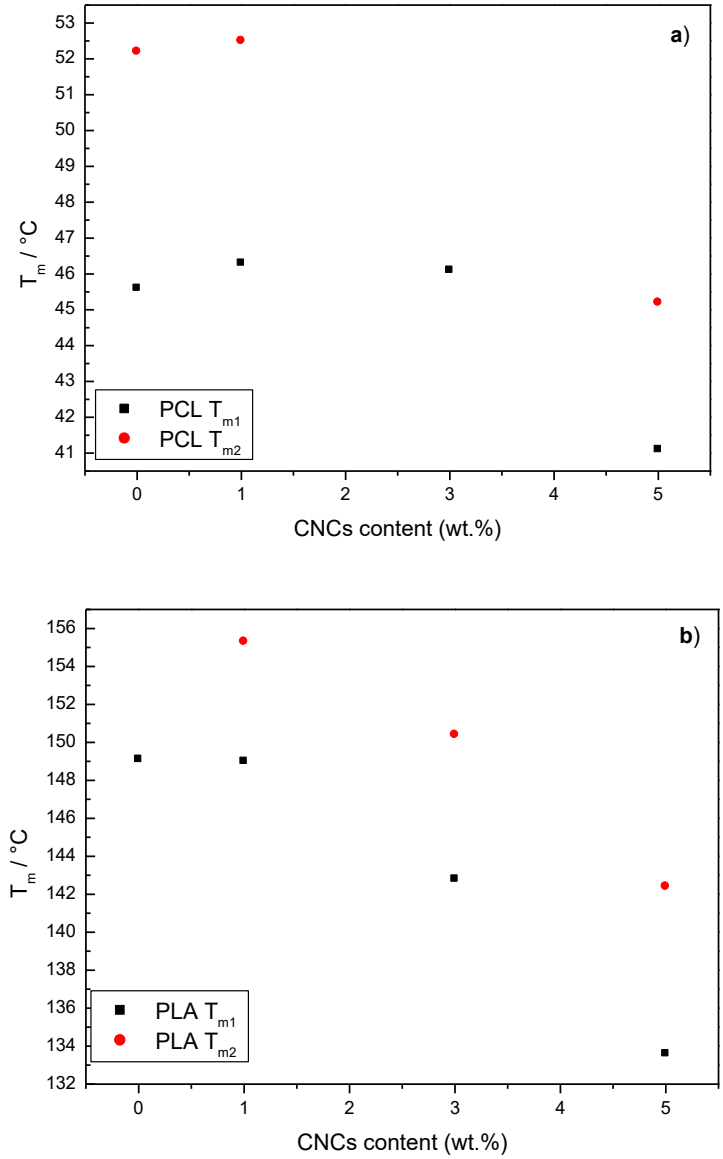

Figure A1 Melting temperatures for (a) PCL and (b) PLA with 1, 3 and 5 wt.% CNCs content.

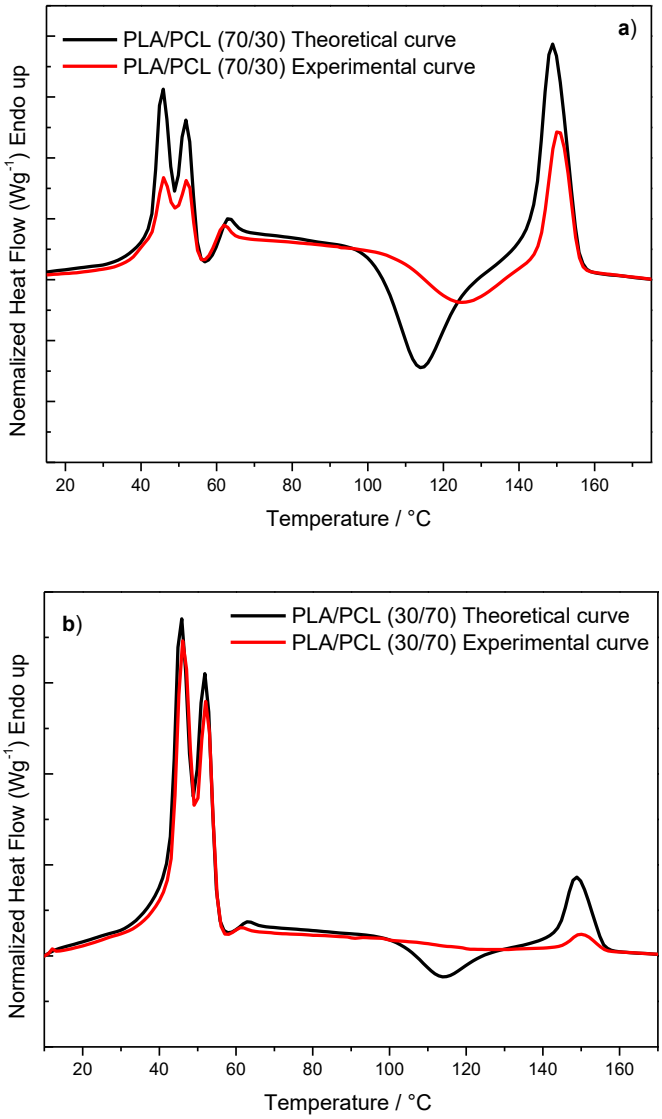

Figure A2 **DSC theoretical and experimental curves for (a) PLA/PCL (70/30), and (b) PLA/PCL (30/70).**

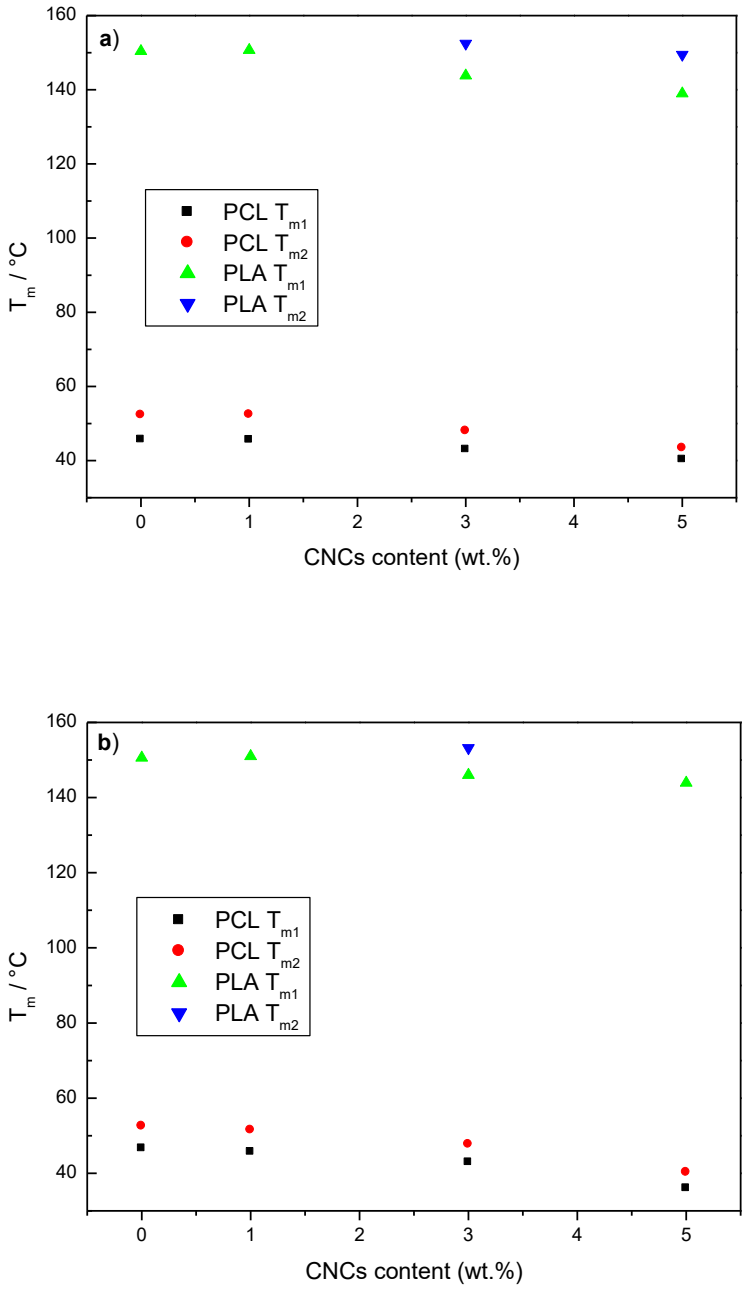

Figure A3 **Melting temperatures for PCL and PLA in (a) 30/70 and (b) 70/30 PLA/PCL nanocomposites with 1, 3 and 5 wt.% CNCs content.**

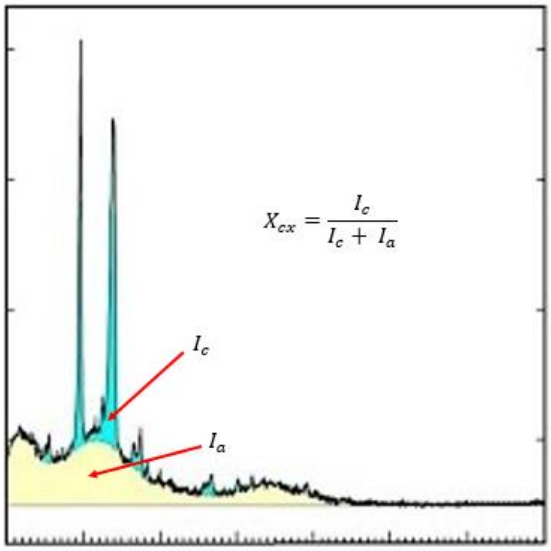

Figure A4 Concept of calculating crystallinity from WAXS curve on origin.

Source: Physical concept (2021)

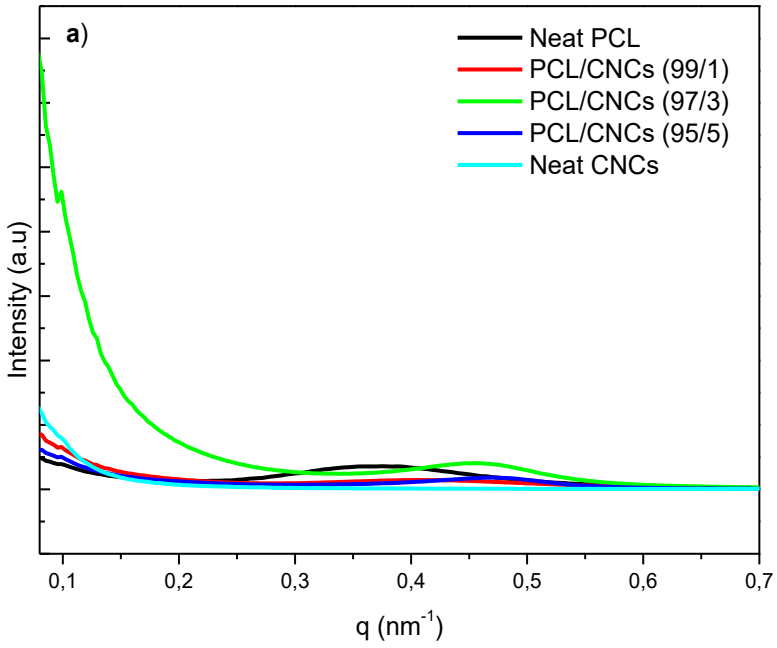

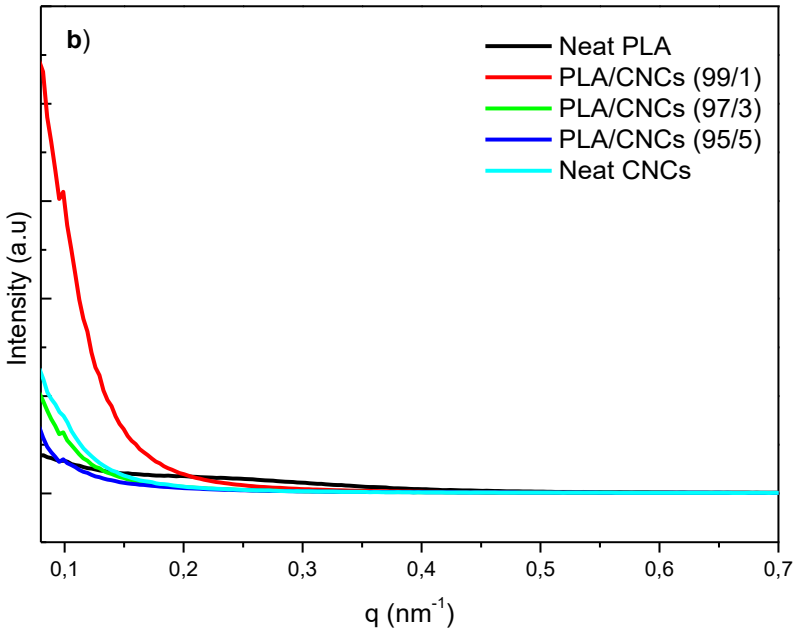

Figure A5 **SAXS plots for I vs q of (a) neat PCL, neat CNCs and their nanocomposites with 1, 3 and 5 wt.% CNCs; (b) neat PLA, neat CNCs and their nanocomposites with 1, 3 and 5 wt.% CNCs.** Results taken from second heating at 25 °C

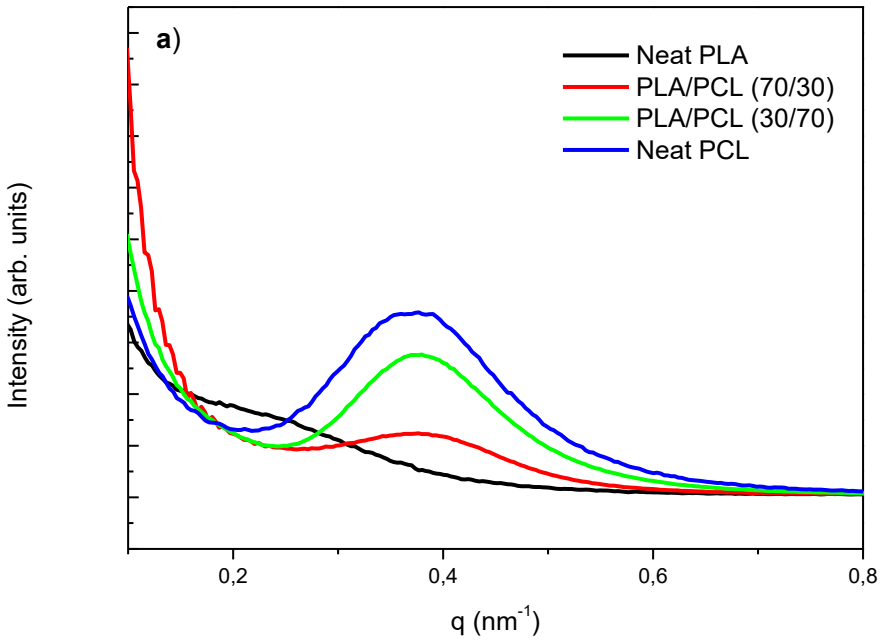

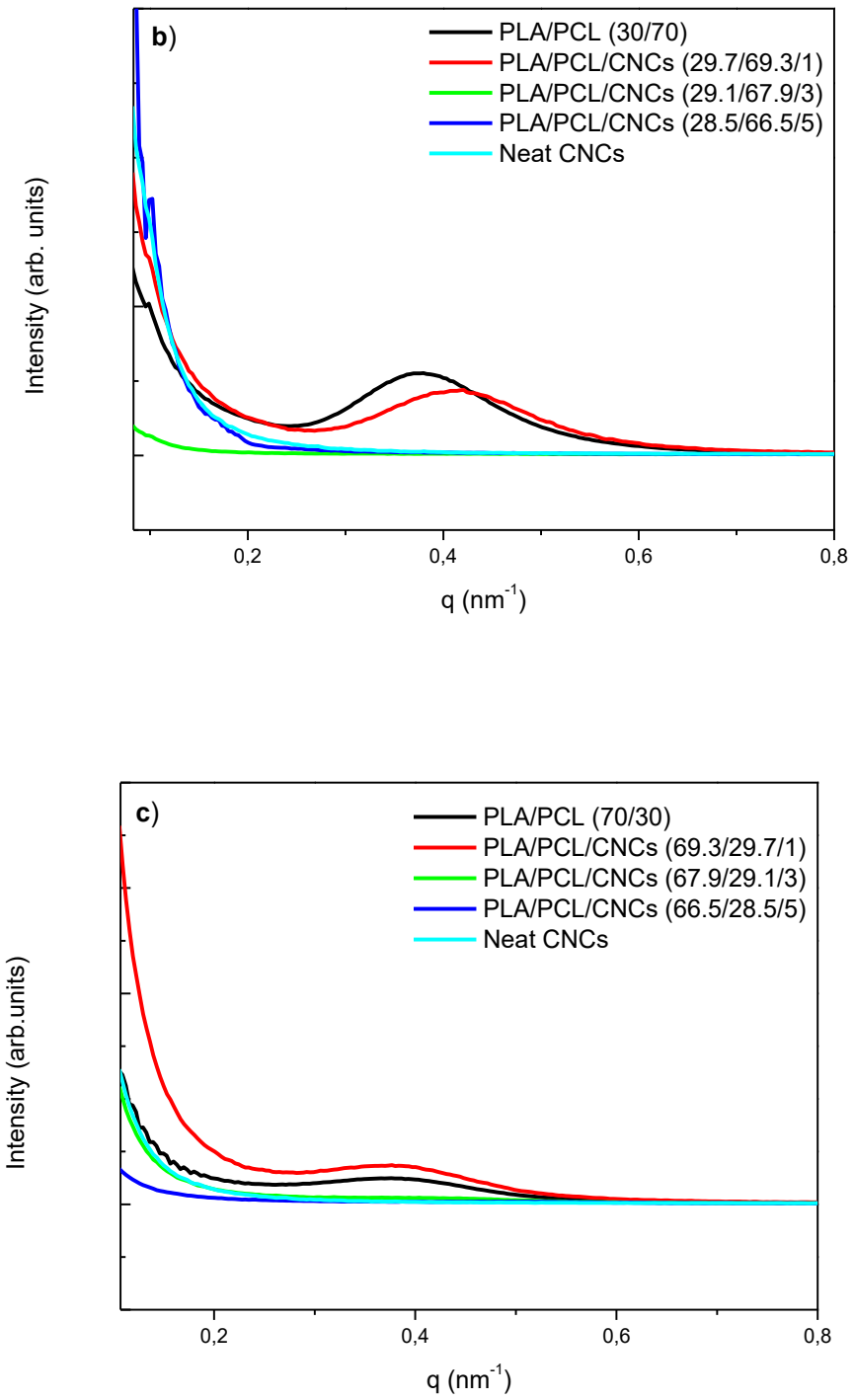

Figure A6 **SAXS plots for I vs q of (a) neat PLA, neat PCL, 70/30 and 30/70 PLA/PCL blends; (b) neat CNCs, 30/70 PLA/PCL blend and 30/70 PLA/PCL blend nanocomposites with CNCs at 1, 3 and 5 wt.%; (c) neat CNCs, 70/30 PLA/PCL blend, and 70/30 PLA/PCL blend nanocomposites with CNCs at 1, 3 and 5 wt.%.** (Results taken from second heating at 25°C)